VILNIUS UNIVERSITY

LINA MIKOLIŪNAITĖ

APPLICATION OF POLYPYRROLE FOR BIOSENSOR DESIGN AND MODIFICATION OF LIVING CELLS

Doctoral dissertation

Physical sciences, Chemistry (03 P)

Vilnius, 2015

The dissertation was prepared at Vilnius University Faculty of Chemistry and Technical University of Chemnitz in the period of 2010 – 2014.

Scientific supervisor - Prof. habil. dr. Arūnas Ramanavičius (Vilnius University, Physical Sciences, Chemistry – 03 P).

VILNIAUS UNIVERSITETAS

LINA MIKOLIŪNAITĖ

POLIPIROLO TAIKYMAS BIOLOGINIAMS JUTIKLIAMS IR GYVŲ LĄSTELIŲ MODIFIKAVIMUI

Daktaro Disertacija

Fiziniai mokslai, Chemija (03 P)

Vilnius, 2015

Disertacija parengta 2010 – 2014 metais Vilniaus universitete, Chemijos fakultete ir Chemnitso technikos universitete.

Mokslinis vadovas – prof. habil. dr. Arūnas Ramanavičius (Vilniaus universitetas, Fiziniai mokslai, chemija – 03 P).

ACKNOWLEDGMENTS

Firstly, I would like to express my gratitude to my supervisor Head of Department of Physical Chemistry, Faculty of Chemistry Prof. Dr. Arūnas Ramanavičius for the great possibility to work in his laboratory under his guidance as well as for his encouraging conversations and positive view of the world.

I am thankful to all Vilnius University, Faculty of Chemistry staff members for the provided possibility to study doctoral studies and for the granted Erasmus Training courses at Semiconductor Physics research group, Physics Department, Technological University of Chemnitz, Germany.

My warmest thanks are directed to Dr. Raul D. Rodriguez, Dr. Evgeniya Sheremet from Semiconductor Physics research group, Technological University of Chemnitz for the kind invitation, positive experience and warm atmosphere during my stay in Germany.

I am grateful to Assoc. Prof. Dr. Deivis Plaušinaitis, Dr. Vilma Ratautaitė, Dr. Aida Vaitkuvienė and Dr. Andrius Garbaras for their work with EQCM device and electrochemical equipment, experiments with bone marrow stem cells and measurements with isotope ratio mass spectrometry respectively, and for the possibility to work together.

For the friendly atmosphere, supply of yeast cells and novel ideas I would like to thank to the heart of Bio-Nanotechnology laboratory at Center for Physical Sciences and Technology Dr. Arūnas Stirkė and all the team working there. I would also like to acknowledge head of Department of Material Science and Electrical Engineering Prof. Dr. Saulius Balevičius for many valuable conversations and optimistic view of life.

I would like to express my thanks to the staff and students of Center of Nanotechnology and Material Science “NanoTechnas”, especially Prof. Dr. Almira Ramanavičienė, Dr. Jaroslav Voronovič, PhD students Anton Popov and Asta Makaravičiūtė for the friendly atmosphere and valuable discussions.

My heartly thanks are dedicated to Assoc. Prof. Dr. Simas Šakirzanovas and Assoc. Prof. Dr. Artūras Katelnikovas for their critical view of the world and moral encouragement.

Finally, I would like to sincerely thank my family for their trust and belief in me as well as for the manifold support.

Table of Contents

List of abbreviations

AcB – acetate buffer;
AFM – atomic force microscopy;
AuNP – gold nanoparticle;
AuNP/Ppy – polypyrrole/(gold nanoparticle) composite;
BM – bone marrow;
BOD – biochemical oxygen demand;
CFU – colony-forming unit;
CV – cyclic voltammetry;
DI – distilled water;
DLS – dynamic light scattering;
DMEM – Dulbecco's Modified Eagle's medium;
DNA – deoxyribonucleic acid;
DPV – differential pulse voltammetry;
(ds)-DNA – double stranded deoxyribonucleic acid;
EA – elemental analyser;
EDTA – Ethylenediaminetetraacetic acid;
EDX – energy-dispersive X-ray spectroscopy;
EQCM – electrochemical quartz crystal microbalance;
FCS – fetal bovine serum;
FEM – finite element method;
GA – glutar aldehyde;
GOx – enzyme Glucose oxidase;
HOMO – highest occupied molecular orbital;
HOPG – highly oriented pyrolytic graphite;
HPLC – high-performance liquid chromatography;
IAEA – International Atomic Energy Agency;
INDO/CNDO – Intermediate Neglect of Differential Overlap/ Complete Neglect of Differential Overlap calculation methods;
IR – infrared;
IRMS – isotope ratio mass spectrometry;
IUPAC – International Union of Pure and Applied Chemistry;
k_a – association rate constant;
k_d – dissociation rate constant;
K_D – equilibrium dissociation constant;
LLD – lowest limit of detection;
LUMO – lowest unoccupied molecular orbital;
MIP – molecular imprints;
MIPpy – molecularly imprinted polypyrrole;
$MIPpy_{caff}$ – caffeine molecularly imprinted polypyrrole

MIPpy-CV – molecularly imprinted polypyrrole obtained by cyclic voltammetry;
MIPpy-PPS – molecularly imprinted polypyrrole obtained by potential pulse sequence;
MSC – mesenchymal stem cells;
NAD(P)H – reduced form of nicotinamide adenine dinucleotide phosphate;
$NAD(P)^+$ – oxidized form of nicotinamide adenine dinucleotide phosphate;
NIP – non-imprinted layer;
NIPpy – non-imprinted polypyrrole;
NIPpy-CV – non-imprinted polypyrrole obtained by cyclic voltammetry;
NIPpy-PPS – non-imprinted polypyrrole obtained by potential pulse sequence;
NP – nanoparticle;
PAA – 3-pyrrolylacrylic acid;
PBS – phosphate buffer saline;
PDB – Vienna Pee Dee Belemnite;
PGE – pencil graphite electrode;
PLL – poly-L-lysine;
PMOR – plasma membrane oxido-reductases;
PPS – potential pulse sequence;
Ppy – polypyrrole;
Ppy/GOx – biocomposite composed from polypyrrole and enzyme Glucose oxidase;
PVA – polyvinyl alcohol;
Py – pyrrole;
RMS – roughness, calculated by root mean square;
RNA – ribonucleic acid;
RS – Raman spectroscopy;
s/n – signal to noise ratio;
SEM – scanning electron microscopy;
SERS – surface enhanced Raman scattering;
SPR – surface plasmon resonance;
ssDNA – single stranded deoxyribonucleic acid;
TCP – tissue culture polystyrene plates;
TERS – tip enhanced Raman scattering;
UV – ultraviolet;
VB – valence band;
YPD – yeast extract peptone dextrose.

Introduction

According to the IUPAC biosensor is a ‘device that uses specific biochemical reactions mediated by isolated enzymes, immunosystems, tissues, organelles or whole cells to detect chemical compounds usually by electrical, thermal or optical signals’. These devices have wide application possibilities in many fields, such as environmental monitoring, food industry, medicine, safety and defence. Biosensor usually consists of two parts: bioreceptor (containing biological component) and signal transducer, which converts chemical signal to a detectable one. According to chosen receptor biosensors could be divided into enzymatic, immunosensors or whole cell sensors while to the respect of signal transducer the biosensors could be sorted to optical, electrochemical, piezoelectrical, thermal, acoustic and others.

Polypyrrole is a conjugated polymer, which dependently on the doping and synthesis conditions could obtain different conductivity (in all range from insulator to conductor), colour and other properties. Since its discovery this polymer was successfully applied in a wide variety of fields: electronics, photovoltaic cells, membranes, surface protective layers, sensors and biosensors. In sensorics it was chosen for several reasons. First of all, due to its conductivity polypyrrole could be used as an electrode or signal transducer from a sensing element to a registration device. Secondly, it could be used as semipermeable protective layer, which preserves the sensing element from harmful environmental effect and allows analyte to reach the receptor at the same time. What is more, during the synthesis procedure, polypyrrole could be obtained in different shapes and structures. For this reason it was decided to apply polypyrrole as a matrix for DNA and caffeine molecular imprints, in which structured polypyrrole was used as a receptor and a signal transducer towards the electrode. It was tested, if such a system could provide a detectable electrochemical signal. Yeast cells used for biosensoric have some drawbacks. One of them is the signal transfer if it starts inside the cell. The modification of the cell wall with conducting polymer could provide a possibility to increase the conductivity of the cell and to improve the signal transfer.

Substrate is also important for the other kind of sensors. Single cell sensors is used in various essential research fields from pharmaceutical screening to environmental monitoring. In this kind of sensors the properties of the cell itself are registered instead

of analyte or product. For the detection and analysis of single cell various techniques could be used: ultrasensitive flow cytometry, potentiometry, as well as atomic force microscopy (AFM) and Raman Spectroscopy (RS). In both latter techniques the substrate plays an important role. For AFM measurements the substrate should be flat and the cells should adhere firmly that they would not be brushed off with the AFM tip. For RS measurements every Raman photon should be collected and reach the detector, as Raman signal is usually very low. Since the cells are relatively thin the laser, used for Raman excitation, usually interacts with the substrate as well. For this reason the choice of the substrate is of high importance and should be selected very carefully. In our experiments several substrates were proposed for Raman measurements. The ones giving the best results are emphasized and some possible explanations on the related mechanisms are suggested.

The aim of the study:

to explore some properties of polypyrrole and its applicability in biosensor design, in modification of living cells and in preparation of polypyrrole and AuNPs or enzyme based composites, to investigate the impact of the substrate to the efficiency of Raman spectroscopy applied for yeast cell evaluation.

The objectives of the study:

1. To investigate the electrochemical formation of polypyrrole layer on gold electrode and to evaluate the stability and surface morphology of formed Ppy layer.
2. To synthesize the molecularly imprinted polypyrrole layer on a graphite electrode using potential cycle and potential pulse sequences and to investigate the applicability of such system for DNA determination.
3. To synthesize the caffeine molecularly imprinted polypyrrole layer on a gold electrode and to evaluate such sensor selectivity for caffeine and theophylline molecules.
4. To analyse the polypyrrole polymerization induced by chemical synthesis using tetrachloroauric(III) acid at time frame up to 147 h and to evaluate dimensions of formed composites.
5. To calculate the stoichiometry of enzyme – Glucose oxidase (GOx) – and pyrrole in the biocomposite (GOx/Ppy), obtained after 337 h of the GOx induced

chemical polymerization and to determine the formation dynamics of GOx/Ppy composite structures.

6. To compare the bone marrow-derived stem cell proliferation on polypyrrole layers formed on gold by chemical synthesis using different initial concentrations of pyrrole monomer.

7. To investigate the suitability of glass, gold, silicon, silicon oxide, highly oriented pyrolytic graphite and structured silver substrates for the Raman spectroscopy of yeast cells.

8. To compare cell wall roughness of yeasts modified with some chemicals or by polypyrrole using atomic force microscopy, and to evaluate viability of polypyrrole modified yeast cells.

Scientific novelty:

1. It was shown that Ppy, synthesized using potential pulse or potential cycle sequences, is suitable for the design of DNA or caffeine molecular imprints.

2. It was demonstrated that stable isotope ratio mass spectrometry is applicable for the determination of stoichiometry between compounds forming biocomposites: enzyme Glucose oxidase and polypyrrole.

3. It was determined that polypyrrole is biocompatibile with mouse bone marrow-derived stem cells and the cells attach and proliferate on this polypyrrole surface.

4. It was observed that there is significant impact of chemically different substrates to the Raman signal of yeast cells and the simulation of the laser light distribution inside and around the cell depends on the substrate used for cell deposition.

5. New yeast cell wall and/or periplasm modification with conducting polymer polypyrrole was elaborated and evaluated.

Statements for defense

1. The electrochemical formation of polypyrrole layer proceeds by forming islands of polymer on the golden disk electrode. This layer is stable in aqueous media and could be used for the formation of caffeine or DNA molecular imprints.

2. Tetrachloroauric (III) acid in polypyrrole/(gold nanoparticle) composites could be used for the polymerization of pyrrole and enlargement of gold seeds.

3. Pyrrole and enzyme stoichiometry in the biocomposite, obtained by GOx induced chemical polymerization of polypyrrole, could be precisely determined using the stable isotope ratio mass spectrometry method.

4. Polypyrrole layer formed chemically on the gold electrode is biocompatible with mouse bone marrow-derived stem cells and does not strongly affect cell attachment and proliferation. Yeast cells could be modified by Ppy synthesized inside the cell wall or periplasm; after this modification cells remains viable.

5. Intensity of Raman signal and the place of the highest laser intensity inside the yeast cell depend on the substrate, on which the cells are deposited.

6. The AFM method provides much better resolution for yeast cell wall morphology imaging in comparison with optical microscopy, AFM enables to visualize small features, such as bud scars or polypyrrole agglomerates.

1. Literature review

1.1. Biosensors

A biosensor is a device that detects, transmits and records information regarding a physiological or biochemical change (Figure 1). Technically, it is a probe that integrates a biological component with an electronic transducer thereby converting a biochemical signal into an electrical response. A wide variety of transducers could be used, such as electrochemical, optical, acoustic and electronic [1-3].

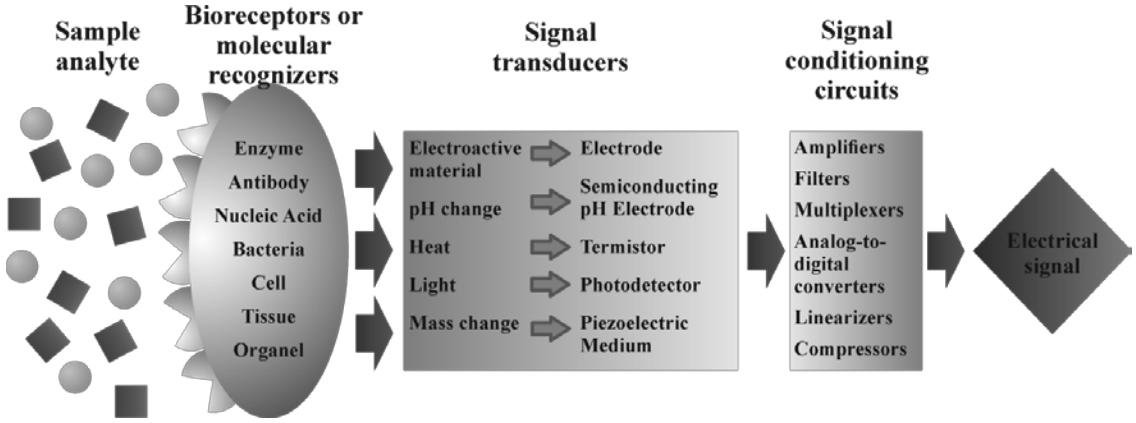

Figure 1 *Biosensor operating principle: main subsystems. Adapted from [4].*

The function of a biosensor depends on the biochemical specificity of the biologically active material. The specificity, storage, operational and environmental stability will determine the choice of the biological material. Selection also depends on the analyte to be detected such as chemical compounds, antigens, microbes, hormones, nucleic acids or any subjective parameters like smell and taste. Enzymes, antibodies, DNA, receptors, organelles and microorganisms as well as animal and plant cells or tissues have been used as biological sensing elements. Some of the major attributes of a good biosensing system are its specificity, sensitivity, reliability, portability, (in most cases) ability to function even in optically opaque solutions, real-time analysis and simplicity of operation [5]. Biosensors are mostly applied for environmental monitoring, food and pharmaceutical industry, defense, and safety.

1.2. Polypyrrole

Polypyrrole (Ppy) is an organic polymer formed by polymerization of pyrrole (Py) molecules (Figure 2). Together with polythiophene, polyaniline, polyacetilene, and

others it belongs to the conducting polymers (CP). The major aspect of these conducting polymers is not the metal-like electrical property itself, but the combination of electrical conductivity and polymeric properties such as flexibility, low density, and ease of structural modification that suffice for many commercial applications. Among the conducting polymers known to date, ones based upon Ppy have attracted special interest because of their high conductivity [6-8], ease and high flexibility in preparation [9], stability [10, 11], biocompatibility [12, 13] and good mechanical properties. However, like most conducting polymers, it is also intractable. Although initially the most important factor was the chemical and thermal stability of the polymer in severe environmental conditions [14], ease of synthesis is also an advantage. The possibility of modifying the electrical and physical properties with derivatives, copolymers, or specific counter anions in order to achieve the desired polymer properties is another advantage [15]. In general, electrical, electrochemical, mechanical and morphological properties of Ppy films strongly depend on the preparation conditions and any post treatments. Among different factors, the counterion or dopant anion plays the most important role [16, 17].

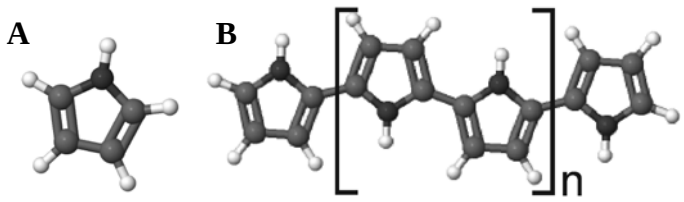

Figure 2 *A) monomer of pyrrole; B) structural formula of polypyrrole. Here bubbles refer to atoms: white – hydrogen, grey – carbon, black – nitrogen.*

Polypyrrole is usually fabricated in its oxidized conducting state. Through a simultaneous polymerization and oxidation of the π system of the final polymer, the Ppy film can be electrochemically or chemically reduced to give the neutral polymer. The Ppy conducting polymers, unlike polythiophenes, which are stable in air even in the undoped state, are less stable in their reduced or undoped form due to its low oxidation potential. Autoxidation in the undoped state proceeds very fast and irreversibly to produce a dark film [18, 19].

1.2.1. Historical Review

Polypyrrole as a polymer was known and investigated for a long time. In 1963 D.E. Weiss group reported a series of papers where they presented iodine doped Ppy and

thoroughly examined its chemical structure, charge-transfer complex and electronic properties resulted by doping [20]. However, the conductivity firstly was noticed in other polymers. In 1973 V.V. Walatka et al. discovered the conductivity of the inorganic polymer polysulfurnitride. The key property of this material is one unpaired electron for each S-N unit, which results in no forbidden gap between the highest occupied and lowest unoccupied levels, therefore, electrons can readily move under the application of an electric field giving rise to electrical conductivity. In 1977 it was found that when a variety of halogens, such as bromine, was incorporated into the structure of the $(SN)_x$ lattice, conductivity at room temperature could be increased by an order of magnitude [21]. Also in 1977, polyacetylene $(CH)_x$ film was demonstrated to exhibit metallic and semiconducting properties through partial oxidation or reduction with electron acceptors or donors [22, 23]. In 1979 A.F. Diaz et al. manufactured free-standing Ppy films with excellent electrical and mechanical properties using an electrochemical method, proving electrochemical synthesis to be more suitable for the deposition of thin films at specific oxidation states than chemical one [24]. From that date the era of conducting polymers begun and it resulted in the Nobel Prize in chemistry at 2000 where Alan Heeger, Alan MacDiarmid and Hideki Shirakawa were awarded for their discoveries in polyacetilene conductivity.

1.2.2. Optical properties

Pyrrole molecule itself has several absorption bands in UV region; they are attributed to intra-valence transition (at 210 nm) or excitation to the 1^1B_1 and 2^1B_2 states (at 165 nm) [25]. After the polymerization, the bandgap of neutral form of polypyrrole is 3.2 eV, representing HOMO-LUMO transition (Figure 3 D). However, this state of the polymer is very unstable and is changed dependently on the storage conditions or presence of the counterion. Most absorption changes are attributed to the doping process when a charge is introduced to the polymer chain.

Usually, when a charge is moving through a crystal, it is permanently surrounded by a polarized region of lattice. Therefore, when the charge carries are moving through dielectric crystal, they distort the lattice. The moving charge together with the accompanying self-consistent polarization field can be treated as a quasiparticle, which is called a ‘polaron’, with its own particular characteristics, such as effective mass, total

momentum, energy and spin of ½. In the presence of such polaron the localized electronic states in the gap appears due to a local upward shift of the HOMO and downward shift of the LUMO (Figure 3 B, E) [26]. This polaron in chemical terminology is called a radical ion. Figure 3 B shows a polaron spread over four pyrrole units. If the second electron is removed from the polaron a spinless bipolaron is formed (Figure 3 C). Bipolaron is defined as a pair of charge-like particles (such as dication) associated with a strong local lattice distortion. The formation of a bipolaron implies that the energy gained by the interaction with the lattice is larger than the Coulomb repulsion between the two charges of same sign, which are confined in a very close proximity.

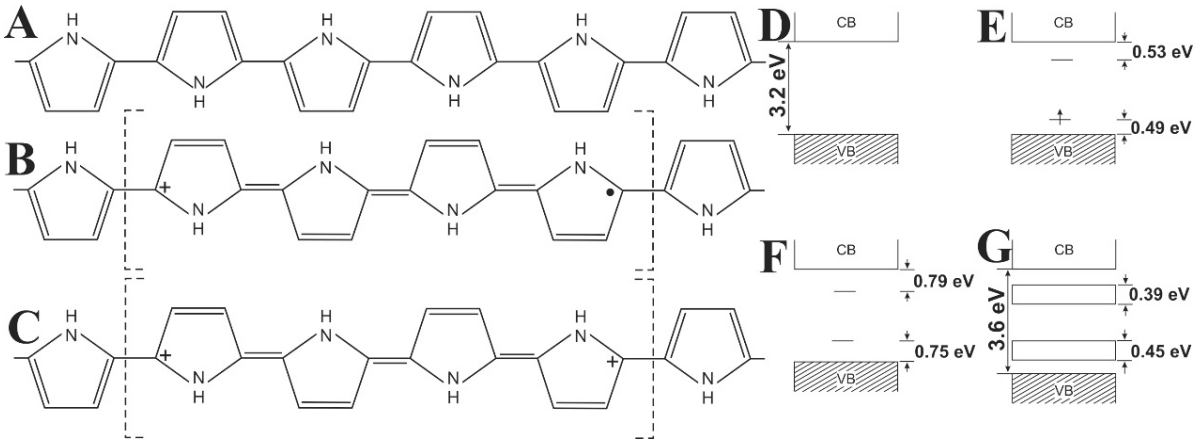

Figure 3 *The structures of A) neutral polypyrrole chain; B) polaron; C) bipolaron. Evolution of the polypyrrole band structure upon doping: D) neutral polymer; E) low doping level, formation of polaron; F) moderate doping level, formation of bipolaron; G) high (33 mol %) doping level, the bands of bipolarons. Adapted from [27].*

Aside with the bandgap of 3.2 eV (388 nm) the partly oxidized state of Ppy possesses three additional features at 0.7 eV (1771 nm), 1.4 eV (885 nm) and 2.1 eV (590 nm) within the gap region which are referred to polaron formation. The 0.7 and 2.1 eV absorptions are interpreted as transitions from the valence band (VB) to, the lower and the upper polaron levels, respectively, whereas the 1.4 eV absorption corresponds to a transition between the two polaron levels (Figure 3 E) in the gap [28]. However, as the level of oxidation increases the middle 1.4 eV absorption disappears and the other transitions shift to higher energy. In the fully oxidized sample, two intense, broad absorption bands are present at 1.0 eV (1240 nm) and 2.7 eV (460 nm) and the interband transition appears as a shoulder at 3.6 eV (344 nm) [29]. This suggests that polarons recombine to form spinless bipolarons. The bipolaron levels are either

completely empty (p-type doping) or filled (n-type doping), therefore, no optical transition between the bipolaron levels is possible [27].

Electronic conduction occurs by movement of the charged polarons or bipolarons along (or hopping between) the polymer chains. It is widely accepted that the bipolaronic structure is predominant in the fully oxidized Ppy, while the polaronic structure is predominant in the partially reduced Ppy. The polaronic structure can be formed by the partial oxidation of a neutral Ppy or the injection of an electron into a bipolaronic structure. It is, however, obvious that the as-prepared soluble Ppy cannot consist of only bipolarons, but some polarons must also coexist at the same time.

1.2.3. Electrochemical properties

The very first electrochemical studies showed that Ppy is sufficiently stable and can be used as a non-metallic electrode material [24, 30]. Neutral polypyrrole, like most plastics, has a filled valence band and is a poor conductor. When the polymer is oxidized (p-doped), electrons are withdrawn from the valence band and then the polymer becomes conducting. Since the π-electrons have a low ionization potential due to the extended conjugated π-electron system along the chains, they can be relatively easily removed from the valence band to switch the polymer to the conducting state [31]. In air, at room temperature, the electrochemical properties of polypyrrole are stable only for some time [32]. The conductivity of unprotected films at standart laboratory conditions after one year decreases by about 20%. Under appropriate protection, considerable improvement in the stability of Ppy properties can be expected. When the temperature is elevated to 100-200 °C, the stability of Ppy depends on the nature of the anion. Polypyrrole is also quite stable in acidic conditions, but basic conditions can cause temporarily reversible loss of conductivity.

1.2.4. The mechanism of polymer formation

Through chemical oxidation or electrochemical polymerization, electrons are removed from the backbone of the conducting polymer resulting in the synthesis of cationic salts of conjugated polymers. Chemical reduction is achieved with reagents such as sodium naphthalide or electrochemical reduction. Electrons are added to the backbone of the conducting polymer what results in the anionic salts of conjugated polymers. In solid-

state physics terminology, the use of an oxidizing agent corresponds to p-type doping and that of a reducing agent to n-type doping. In general, there are two basic synthesis methods of conducting polymers: chemical polymerization [33-35] and electrochemical polymerization [24], or the combination of both [36]. Among chemical polymerization types enzyme induced chemical polymerization sometimes could be excluded [37, 38]. However, an alternate synthesis routs could also be executed, such as UV polymerization [39], plasma polymerization [40, 41] and others.

Scheme 1 *The oxidative coupling mechanism of polypyrrole formation. Adapted from [42]*.

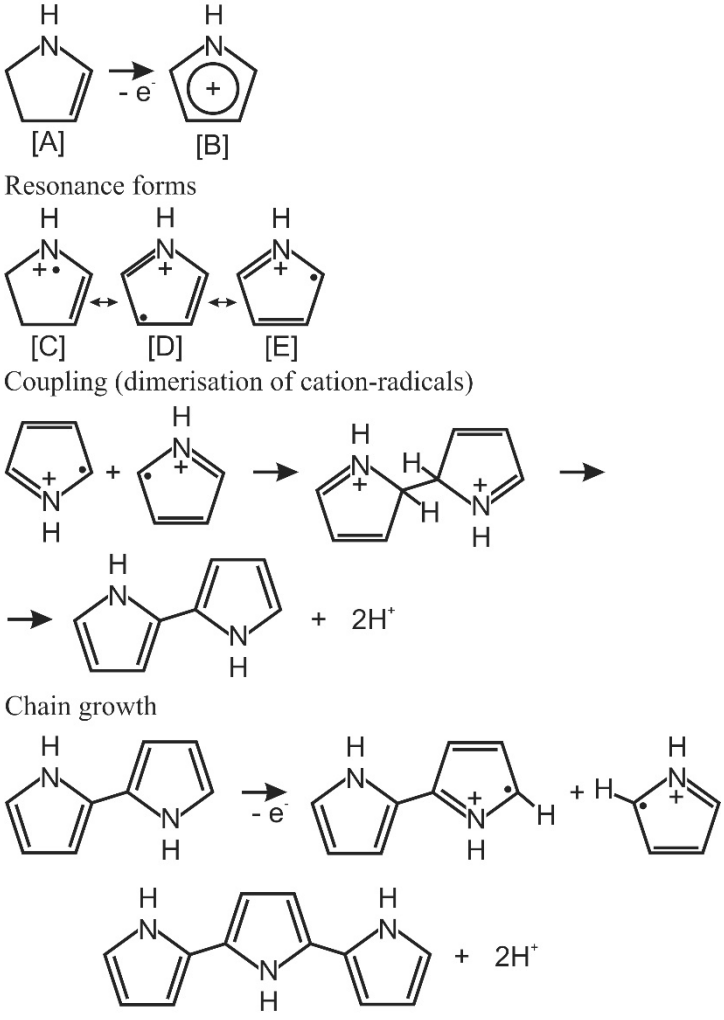

Among the scientists two polymerization mechanisms of the polypyrrole are proposed. One is called oxidative coupling (Scheme 1) [43]. First of all the oxidation of the monomer takes place and the cation-radical is formed with the radical delocalized over the pyrrole ring (Scheme 1 B). According to the INDO/CNDO calculations [44] the maximum spin density for the monomer is at α-position. Thus among three possible

resonant states (Scheme 1 C, D, E) the E shows the highest stability. If the second similar radical is nearby the radical dimerization occurs discarding two protons, as confirmed by C.P. Andrieux et al. [45].

Under the given reaction conditions, the dimer is easier oxidized in comparison with the monomer due to a stronger conjugation, therefore, the oxidation potential of oligomeric or polymeric pyrrole species is lower than that of the monomer [46]. The formed oligomer radical grows by attaching the new radical cations [42]. In the propagation step, reoxidation, coupling, and deprotonation continue to form oligomers and finally long polymeric chains of Ppy. Once the chain length of the oligomers exceeds the solubility limit in the solvent, then the precipitation of Ppy occurs. The termination step has not been fully elucidated but it is presumed, that it involves a nucleophilic attack on the polymer chain [47].

The second route of polymerization (Scheme 2) is called the free radical reaction. During this process the cation-radical is formed by the loss of electron as it was in the previous explanation and then it is followed by the loss of proton. In this way a very active radical is formed, which can attack any monomer molecule nearby and form a radical dimer, but this explanation is not generally accepted [48, 49].

Scheme 2 *The mechanism of polypyrrole formation, called free radical reaction. Adapted from [42].*

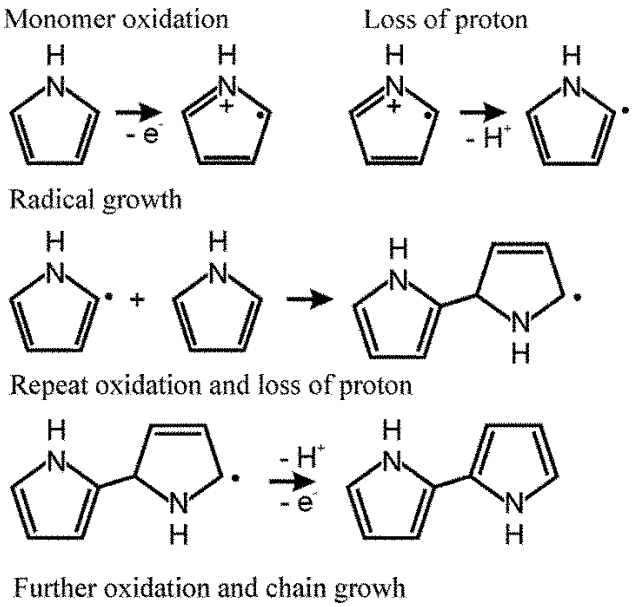

The resulting polymer is produced in the oxidized state with incorporation of counterions [43]. It is calculated that the level of oxidation of Ppy is 0.25-0.32 per

pyrrole unit, depending on the type and the charge of the incorporated anion [50], corresponding to one anion for every 3-4 pyrrole units in order to achieve electroneutrality, and this makes up 30-40% of the final weight of the polymer [51].

1.2.4.1. Chemical synthesis of polypyrrole

Chemical polymerization is a simple and fast process with no need for special instruments. Bulk quantities of Ppy can be obtained as fine powders using oxidative polymerization of the monomer by chemical oxidants in aqueous or non-aqueous solvents [52-55] or by chemical vapour deposition [56]. In the chemical oxidation method, an oxidizing agent such as lead dioxide, quinones, aqueous or anhydrous $FeCl_3$ or other iron(III) and cooper(II) salts (chlorides or persulfates) are added to the pyrrole and a dopant is dissolved in a suitable solvent, resulting in the precipitation of doped Ppy powder. The Ppy synthesis using halogens and organic electron acceptors as oxidants has also been reported [57, 58]. It has been found that factors such as solvent, reaction temperature, time, nature and concentration of the oxidizing agent, affect the oxidation potential of the solution. These, in turn, influence the final conductivity and other properties of the chemically synthesized polypyrrole [52, 53]. Elemental analysis data has shown [59] that the composition of polypyrrole when it is prepared chemically is almost identical with that formed by electrochemical methods.

The yield of Ppy was close to 100% when the optimal ratio of Fe(III)/monomer, which is 2.4, was chosen [54]. The enhanced conductivity of the polymer was achieved using lower temperatures and shorter polymerization times [53]. Among various solvents (water, alcohols, benzene, tetrahydrofuran, chloroform, acetone, acetonitrile, dimethylformamide) the highest conductivity was achieved for Ppy obtained by monomer oxidation with $FeCl_3$ in methanol solution (190 S/cm) [52]. The Ppy conductivity was also enhanced by varying of the oxidation potential: changing the ratio of $FeCl_3$ and $FeCl_2$ the conductivity of 220 S/cm was reported [52] and using binary acetonitrile/methanol solvent 328 S/cm was achieved [60].

However, the use of chemical polymerization limits the range of conducting polymers that can be produced since only a limited number of counterions can be incorporated. The chemical polymerization of pyrrole appears to be a general and useful

tool for the preparation of conducting composites [54, 61] and dispersed particles in aqueous media [62, 63].

1.2.4.2. Electrochemical synthesis of polypyrrole

The oxidation potential of Py is 0.8 V, which is lower than that of other heterocyclic monomers and lower than the oxidation potential of water (1.2 V). Consequently, Ppy is readily to be synthesized from a range of aqueous and non-aqueous solvents [47]. In fact, Ppy is one of the few electrically conducting polymers that can be prepared in aqueous solutions [51]. The flexible film with conductivity of 100 S/cm by electrolysis of an aqueous solution of pyrrole was prepared by A.F. Diaz et al. [6, 30] in 1979. This work gave a start to the extensive use of electrochemical synthesis of Ppy and other conducting polymers up to now. The Ppy films are obtained in doped (conducting) form directly in the course of synthesis. They can be transferred to neutral (insulating) form by means of electrochemical reduction [42].

When a positive potential is applied at the electrode, the Py monomer is oxidized to a delocalized radical cation. The electrochemical polymerization is proceeded according the same scheme, presented earlier (Scheme 1). The electrochemical oxidation and radical coupling process is repeated continuously and finally results in a polymer film on anodic electrode. A central point of electrochemical research is the analysis of the doping mechanism [64].

Electropolymerization of pyrrole can be performed in various regimes, in particular, potentiostatic [46, 65], galvanostatic [16, 66, 67], potentiodynamic [68, 69] and pulsed one [70]. Out of all polymerization methods studied, the potential cycling method is the simplest one and it is especially useful to test whether a new monomer can be polymerized. The formation of a conducting polymer film is clearly indicated by monotonically increasing redox peaks due to the electroactive polymer film accumulating on the support electrode during potential cycling. The number of potential cycles can be used as a rough control of the thickness of the polymer film. The oxidation potentials of the monomer and the formal potential of the polymer can be estimated from the cyclic voltammograms. Too small current density lowers the polymerization efficiency, while too large current density causes the polymer to be overoxidized. Overoxidation occurs when the electrode potential rises too high, and consequently the

polymer becomes non-conducting. In extreme cases, overoxidation terminates the polymerization process.

In choosing an electrode material for support of the polymer film, criteria that are usually considered include electronic conductivity and electrochemical stability over the applied potential range. However, the observed change of the monomer oxidation potential with the nature of the electrode material indicates that the electrode's catalytic effect towards the oxidation of the monomer and/or nucleation of the polymer is also an important factor. It has been observed that some properties of the polymer, such as conductivity and morphology [71], can be affected by the electrode material especially during the early stages of polymer formation. The lowest monomer oxidation potential is found on its own polymer and is independent of the nature of the electrode material underneath the polymer film. A wide variety of the electrodes were used as working electrodes for polymerization reaction: Pt, Au, Pd, Rh, Ir [72, 73] conducting In_2O_3-SnO_2 glases [30, 74, 75], carbonaceous materials (graphite, vitreous carbon) [16, 73, 76]. The polymerization of conducting polymers was also reported on Al, Ta, Fe, Cu, Ti, Ni, Cr, Nb and stainless steel. It was found that the nature of metal substrate does not virtually affect the kinetics of Ppy synthesis. However, the effect may appear using Ta, Ti, Nb and Al due to the metal oxide layer between the electrode and the polymer.

The electrochemical approach for the formation of electroactive/conducting films is very versatile and provides a facile way to vary the film properties by simple variation the electrolysis conditions (e.g. electrode potential, current density, solvent, and electrolyte) in a controlled way. The nature and concentration of monomer/electrolyte, cell conditions, the solvent, electrode, applied potential and temperature, pH all have a strong effect on the electro-oxidation reaction and quality of the film [77].

Electropolymerisation of Ppy could be performed in both aqueous and non-aqueous media, such as acetonitrile, propylene carbonate and dichloromethane [16, 72, 73, 78], but higher nucleophilisity of the solvent do inhibit the film growth due to the interaction of solvent with monomer. The polymer layer does not form in such nucleophilic solvents as dimethylformamide, dimethyl sulfoxide, hexamethylphosphoroamide, unless the nucleophilicity of solvent is reduced by addition of protic acid. In considering the effect of solvent, it has been found that traces of water in organic solvents (e.g. CH_3CN) have a substantial influence on the polymerization process and the structure of the films

prepared [79]. The mechanical properties of Ppy films are also improved when the electropolymerization is carried out in the presence of slight amount of water (e.g. 1%).

1.2.4.3. Comparison of chemical and electrochemical synthesis

The chemical polymerization of pyrrole was reported in 1916 by an Italian chemist A. Angeli [80], who discovered that oxidation of pyrrole, from an acidic pyrrole/H_2O_2 solution, forms a black conducting powder. The first electrochemical polymerization of pyrrole was reported in 1968 by A. Dall'Olio et al. [81]. They found that when pyrrole was anodically oxidized in sulphuric acid a conducting polypyrrole film was formed on the electrode.

Comparing chemical polymerization to electrochemical, it is considered that the polymers have more regular structure and higher crystallinity than those produced electrochemically [42]. Chemical and electrochemical polymerizations have been widely applied in industry and academic research. When mass production is needed, chemical polymerization is the best choice, but the introduction of reactant reagents and byproducts may sometimes affect the properties of the conducting polymers. Electrochemical polymerization is desirable for conducting polymer thin film and nanostructure fabrication. The fine control of conducting polymer film thickness and nanostructure morphology can be achieved by monitoring electropolymerization time, applied potential and total charge [82].

Compared to chemical polymerization, the electrochemical route offers several advantages for electrochemical studies. Most chemical oxidations form polypyrrole powders. Although films can be prepared by oxidizing pyrrole at a solid or liquid interface [83, 84], these films are of poor quality and sometimes even non-conducting [83]. In electrochemical polymerization, an adhering polymer film is formed on the electrode and is ready to be characterized with a variety of electrochemical techniques. Yield in charge terms is close to 100%; this provides a possibility of controlling the mass and thickness of the film. Electrochemical methods give the researcher much better control over the polymerization process. The film thickness can be controlled by monitoring the charge density, and the electrode potential can be adjusted, in this way the overoxidation of the polymer film could be significantly reduced. The electrochemical polymerization method also allows the formation of various

polypyrrole/electrolyte anion composites by simply changing the electrolyte in the monomer solution. Since the formal potential of the polymer is lower than the oxidation potential of the monomer, the freshly formed polymer is in its oxidized state and electrolyte anions are incorporated to reach electroneutrality. A study by R. John and G.G. Wallace [85] showed that polypyrrole is formed by the continual precipitation of oligomers onto the electrode surface and not by addition of pyrrole monomers to the ends of polymer chains in the growing film. Consequently, polypyrrole has a densely packed space filling appearance. The electrode potential has a profound effect on the quality of the final polymer obtained. In a study of the electrochemical polymerization of another very similar conducting polymer – polythiophene, the molecular weight distribution has been found to be a function of the electrode potential [86]. This may also be true for polypyrrole. Also, since the oxidation potential of the monomer is much higher than the polymer redox potential, overoxidation can easily occur during the polymerization process, especially in the presence of nucleophiles such as OH^-, CN^-, CH_3O^-, and Br^-.

Conformational and chemical changes

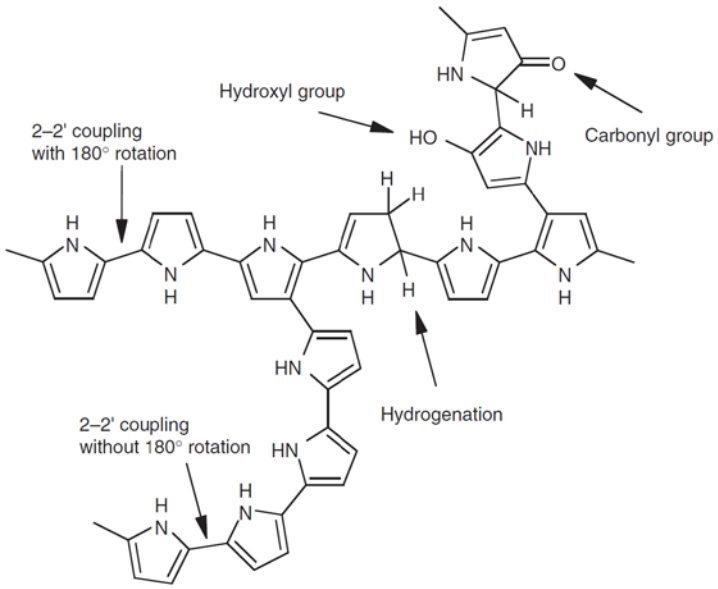

Figure 4 *Chemical and conformational defects in Ppy [88].*

Conformational and chemical defects in the Ppy chain structure can be formed during the polymerization process despite the fact that the chains are intrinsically planar and linear [87]. The defects break the planarity and linearity of the Ppy chain and reduce the extent of π-orbital overlaps. Such distortions include conformational defects such as 2-2’

coupling with nonregular 180° rotation of the alternating pyrrole unit, chemical defects such as 2-3’ or 2-4’ coupling and non-aromatic bonding and formation of carbonyl or hydroxyl groups in Ppy chain due to overoxidation (Figure 4).

1.2.5. Applications

Electrochemical switching between the oxidized and reduced state of polypyrrole is accompanied by a color change what makes polypyrrole a possible candidate for electrochromic display material [89-91]. Furthermore, Ppy and other conducting polymers are developed for such potential technological applications as transistors [92, 93] and switches, counterelectrode in electrolytic capacitors [94], supercapacitors [9], sensors [95, 96] and biosensors [97-99], chromatographic stationary phases [100], light-weight batteries [101] and photovoltaic cells [102], membrane separation [103], surface protection [104] and others.

Ppy has received a special attention in cell research due to its biocompatibility *in vitro* and *in vivo* [105, 106], ease of synthesis [63], low cost, and electrical conductivity. Ppy is considered a good material for tissue engineering [107-109]. *In vitro* studies have proved that polypyrrole supports the adhesion and growth of various kinds of cells, such as neuronal cells [110, 111], endothelial cells [112], keratinocytes [113], skeletal muscle cells [114] and rat pheochromocytoma cells [115]. It was found that the Ppy-coated nanowire surfaces facilitates *in vitro* C17.2 neural stem cell line adhesion, proliferation and differentiation [116]. Lundin et al. have shown that Ppy can be tailored to promote cell survival and maintenance of rat fetal neural stem cells, and the biocompatibility of polypyrrole with neural stem cells depend on the counterion incorporated in the polymer [117]. It was shown, that Ppy due to its electrical conductivity is very suitable for the construction of scaffolds for nerve tissue engineering [115, 118].

1.2.5.1. Nanoparticles

The polymer nanoparticles are now widely used in various experimental fields such as electronics and photonics [119-121], sensors and medicine [122], biology and biotechnology [123], also for the pollution and environmental control [124]. The first method to prepare the polymer nanoparticles was solvent evaporation [125]. By now polymers could be obtained using a number of techniques including solvent evaporation,

salting-out, dialysis, supercritical fluid technology, micro-emulsion, mini-emulsion, surfactant-free emulsion, and interfacial polymerization [126]. The obtained nanoparticles could be of various chemical compositions (e.g. a mixture of inorganic and organic materials, different polymers and various biomaterials) and forms (e.g. nanospheres, tubes, rods, fibers or pellets).

Polymer nanocomposites with metal nanoparticles

The formation of composite nanomaterials based on seed-mediated approach recently becomes increasingly popular in the production of ordered morphologies AuNPs in aqueous solutions [127]. In a seed-mediated method, firstly small metal NPs are prepared and later they are used as seeds (nucleation centers) for a systematic growth of larger NPs. However, difficulties arising in order to determine the appropriate growth condition, which inhibits additional nucleation, generally limits the application of here mentioned methods [128]. Weak reducing conditions are required for a systematic growth of AuNPs [129]. The formation of gold nanoparticles might be controlled by the overall molecular weight and relative block length of the block copolymer if the polymer is used in the reaction solution as stabilizer [130-133]. Also the stability of the gold nanoparticles was greater when the block copolymer was used instead of the homopolymer. Size and shape of NPs are generally controlled by external factors such as reaction duration, temperature, and precursor or surfactant concentration. Lack of external influence may eventually lead to uncontroled growth of NPs and possibly to the loss of their unique properties. On the other hand, polypyrrole offers excellent biocompatibility [12, 13] and could be doped by various biologically active compounds. The release of such compounds in a controlled manner could be induced by infrared irradiation based heating of trapped metal nanoparticles [134]. Therefore, the development of metal nanoparticle and polypyrrole composites could be important strategy in creation of new targeted drug delivery systems as well as for biosensors [135].

1.2.5.2. Polypyrrole layers

Ppy layers are usually obtained using electrochemical synthesis or plasma polymerization [40, 41]. However, chemical synthesis and precipitation can be used as well [136]. The resulted properties of the layer depend on a vast number of preparation

conditions: solvent, temperature, current density, nature of dopant and its concentration. Among all the properties the dopant is considered to have the highest impact [79]. Furthermore, the impact of the ion could be changed even after the polymerization process is finished. By changing the solvent and voltage of the electrode the polymer film could be redoped with the other ion and thus possesses the greatly changed properties.

Next to the pure Ppy coatings, nowadays the quality of the layer is improved by adding different materials to the formed Ppy structure: multi and single walled carbon nanotubes [137, 138], nanodiamonds [139], nanoparticles [140, 141] or organometallic compounds [142], polysaccharides [143], and other materials. Obtained composites could be applied in different fields, such as sensors for gases, drugs, glucose or metal ions [137, 143], tissue engineering [144, 145], as a protective coating against corrosion [146, 147] or could be used as a matrix for other materials [140, 141].

1.3. Molecularly imprinted polymers

The interest in molecularly imprinted polymers (MIPs) arises from their potential to recognize selected molecules. The principle of MIP-based technology was inspired by mimicking of some native processes, e.g.: antigen-antibody interaction, which is based on selective recognition. In the typical synthesis of the MIPs, monomers and template molecules are involved. The template molecules that are used for MIP preparation usually are similar to the target molecules or in many cases they are the same type of molecules. Hence, after polymerization three-dimensional polymer networks with entrapped template molecules are formed. For different MIP applications polymerization of one or copolymerization of more different types of monomers are used [148-151]. After polymerization the template molecules are removed, leaving cavities, which are complementary to the target molecules, therefore they can be involved into selective recognition of target molecules (Figure 5).

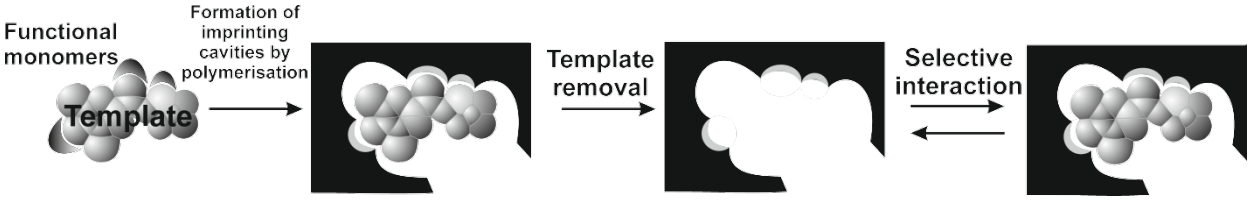

Figure 5 *The basic principle of molecular imprinting.*

It has been demonstrated that the effect of the nucleic acid as a dopant upon the redox activity of the resulting Ppy-modified electrode imparts a high degree of discrimination between synthetic oligonucleotides and chromosomal DNA [152]. The behavior of Ppy films, prepared in the oligonucleotides and DNA mixtures has been mostly influenced by oligodinucleotides molecules, which are smaller. Hence, the recognition of oligonucleotides has been a result of discrimination of oligonucleotides and DNA molecules by size. Application of polypyrrole as a linker between a substrate and oligonucleotide probes has been demonstrated by S. Szunerits et al. [153]. The modification step has been based on the electrochemical copolymerization of pyrrole and oligonucleotides bearing a pyrrole group on its 5' end. This strategy has been employed for the immobilization of oligonucleotides on millimeter-sized electrodes, microelectrode arrays, as well as for the local structuring of homogeneous gold surfaces [153]. It has been found, that localized immobilization could be achieved by using an electrospotting technique, where a micropipette has been served as an electrochemical cell. In this case formation of Ppy was performed by cyclic voltammetry. This electrochemical procedure allowed the formation of a copolymer, which was a mixture of polypyrrole and a polypyrrole bearing covalently linked oligonucleotides [153]. From study describing an electrochemical DNA sensor based on polypyrrole and 3-pyrrolylacrylic acid (PAA) copolymer it was concluded that it is possible to detect DNA hybridization using this not imprinted copolymer [154]. In this study electrochemical impedance spectroscopy supported by redox couple was used as detection method. Other study describes the application of poly[pyrrole-*co*-(*N*-pyrrolyl)-caproic acid] copolymer for the detection of DNA by cyclic voltammetry [155]. There was reported that on such copolymer functionalized with carboxyl groups exhibit the efficient hybridization of DNA double helix. However, until recently, no reports on application of polymers with DNA molecular imprints were published.

The Ppy is preferable for sensor development because of some advantages including rapid electrochemical response time, low cost, wide dynamic range, low detection limits, and operation at physiological pH [156]. The application of MIP modified polypyrrole for the determination of low molecular weight molecules like caffeine [149, 157], ascorbic acid [148, 158], paracetamol [159] and high molecular weight molecules including proteins [160] has been reported.

1.4. Bone-marrow stem cells

Mesenchymal stem cells (MSCs) were selected as a model system for investigations of biocompatibility because they are attractive for regenerative medicine. Castano et al. have evaluated the attachment, proliferation, and differentiation of rat MSCs toward the osteoblastic phenotype seeded on polypyrrole thin films made by admicellar polymerization [161]. They have demonstrated that the polypyrrole thin films support the osteogenic differentiation of rat mesenchymal stem cells and can induce absolutely different cellular events: from excellent cell attachment, to the complete inability to adhere.

1.5. Yeast cells for biosensorics

Among yeasts, the well-known baker's yeast, *Saccharomyces cerevisiae*, is an excellent organism for evaluating genetic functions of more complex eukaryotic organisms, including toxic effects on human cells and tissues [162]. Like most yeasts, *S. cerevisiae* is easy to cultivate, manipulate genetically and, furthermore, is inexpensive [163]. Several possible applications of the yeast cells for the biosensors are presented in the Table 1.

Table 1 *Examples of various yeast cells used for the whole cell biosensors. LLD – lowest limit of detection; BOD – biochemical oxygen demand.*

Species	**Type of transducer**	**Analyte**	**LLD**	**Technique of immobilization**	**Ref.**
Specially constructed mutant of the methyl-trophic yeast *Hansenula polymorpha A3-11*	Potentiometry	formaldehyde	0.5 mM	Entrappment in a calcium alginate membrane placed on the gate of a pH-sensitive field effect transistor	[164]
Succharomyces Uvarum	Clark-type oxygen electr.	Vitamin B_6	0.5 ng/mL	Immobilization in cellulose nitrate membrane via filtration	[165]
The yeast *Saccharomyces cerevisiae*, genetically modified to express firefly luciferase	luminometer	Any toxic chemical that interfere cell metabolism (copper, mecoprop, diuron)	Not determined	Spread in the solution	[166]
Saccharomyces cerevisiae	Oxygen electr.	Cyanide	1.5 µM (cel. mem.) 0.15 µM (glass b.)	Two types of immobilization on: 1) cellulose membrane 2) glass beads	[167]
Yeast cells	Oxygen microelectr.	Bioavailable organic carbon	Micro-scale	Polyvinylalcohol	[168]

		in oxic sediments			
The yeast *Arxula adeninivorans* (two types of biosensor: budding cells and mycelia)	Oxygen electr.	Waste water with a large range of analytes	2.61 mg/L	The capillary membranes "RoTrac"	[169]
Saccharomyces cerevisiae with a modified luciferase gene	Luminescence	5,6-benzoflavone, rapamycin, nystatin and cycloheximide	Not indicate	Growth on agar plates or in the solution	[163]
Gluconobacter Oxdans together with *Saccharo-myces cerevisiae*	Clarc type oxygen electr.	Sucrose, glucose, lactose	1mM sucrose	Gelatin membrane	[170]
Yeast cells	Amperometry	BOD	1 mg/L	A porous inorganic Al_2O_3 sol–gel matrix	[171]
Yeast SPT1 and SPT2	Amperometry	BOD	2 mg/L	Adsorption on glassy carbon electrode	[172]
Saccharomyces cerevisiae	Clark-type oxygen electr., potentiometry	Sucrose	3.2 µM	Nitrocelulose membrane	[173]
Saccharomyces cerevisiae	Oxygen electr., amperometry	Cyanide	0-15 µM	On glass beads	[174]
Saccharomyces cerevisiae	Oxygen electr., amperometry	Cyanide	0.3-150 µM	Trapped between two porous membranes	[175]
Recombinant *Saccharomyces cerevisiae*	Oxygen electr., amperometry	Cu^{2+}	0.5-2 mM	Dried in PVA onto a capillary membrane	[176]

1.6. Raman Spectroscopy for the cell characterization

Various techniques could be employed for the registration of the signal from the cells. If a signal from many cells in one time is expected potentiometry or the registration of fluorescence is usually employed (Table 1). However, other optical techniques could provide a possibility to obtain signal from a single cell and thus detect the changes inside the cell. Several optical bio-compatible methods are known for the investigation of cellular behaviour in culture: infrared spectroscopy [177], surface plasmon resonance [178], optical coherence tomography [179], and bioluminescence imaging [180]. In addition, there is progress in non-optical methods such as electron tomography [181]. However, complementary methods are required for the investigation of cells under different conditions with minimal external perturbations. Raman spectroscopy appears to be one of the most popular, informative, contactless, non-invasive, and non-destructive methods with applications from bioanalysis [182-184] to novel materials such as graphene [185]. Contrary to fluorescence microscopy, RS does not require any dyes or molecular probes to induce image contrast. RS demands minimal sample preparation and

is sensitive to structural, chemical, and conformational changes of proteins and molecules. The sub-micrometric spatial resolution given by the diffraction limit of light allows the identification of different cell components. This was illustrated in various kinds of cell lines including the investigation of different cell components, highlighting the versatility of RS for biological investigations [186, 187]. RS and RS imaging [188] were used to observe the cell life-cycle [186], including cell death [189-192], differentiation, and mitosis [193]. Despite several advantages of this method, the Raman scattering process is very inefficient; the intensity of the Raman signal is considerably lower than the intensities of other optical processes, such as IR absorption, fluorescence, or photoluminescence. In order to deal with this limitation the use of intense light sources, such as lasers is required. However, if one is not careful, the intense and focused laser light may have a negative effect in cell investigations due to the degradation of the analyzed specimen. There are a few ways to address this situation: 1) lowering the laser intensity and compensating by increasing the acquisition time; 2) using laser wavelengths in resonance with the molecular groups of interest; and 3) using plasmon-enhanced RS methods (surface-enhanced Raman scattering (SERS) [194] and tip-enhanced Raman scattering (TERS) [195, 196]). Due to the enhanced signal to noise ratio (s/n), RS together with hierarchical cluster analysis made it possible to distinguish different kinds of yeast cells [197]. The influence of the cell fixation was investigated by anchoring the inner cell arrangement with ethanol, formaldehyde, heating, and by poly-L-lysine treatment. The signal of the heated cells was found to be less intense in comparison to control or ethanol-fixed samples, while poly-L-lysine had the most negative effect on the RS signal [198]. Even though the consideration of the substrate has received little attention, in the work of F. Draux et al. several materials including quartz, calcium fluoride, and zinc selenide were investigated [199]. They showed that different substrates preserve cell integrity and viability allowing direct Raman spectroscopy analysis at the single-cell level. In addition to other substrates, a glass substrate was improved for optical microscopy and a better image contrast was obtained by adding a gold film on the opposite side of the glass supporting the cells [200]. However, no effect on the RS response from the cells on substrates with and without gold was reported.

2. Materials and methods

In this chapter the chemicals, preparation technology and instrumentation, that were used for the chemical and electrochemical synthesis of polypyrrole and its composites, are presented as well as the cultivation, preparation and measurements of the living cells and molecular imprints.

2.1. Chemicals

Chemicals of analytical grade and deionized water were used, if not otherwise stated. Tetrachloroauric acid ($HAuCl_4 \cdot 3H_2O$), tannic acid ($C_{76}H_{52}O_{46}$), disodium hydrogen phosphate dodecahydrate ($Na_2HPO_4 \cdot 12H_2O$), potassium ferrocyanide trihydrate ($K_4[Fe(CN)_6] \cdot 3H_2O$), glutar aldehyde ($C_5H_8O_2$) (GA) and D-(+)-glucose ($C_6H_{12}O_6$) were obtained from Carl Roth (Germany), sodium citrate ($C_6H_5Na_3O_7 \cdot 2H_2O$) and potassium chloride (KCl) were recieved from Scharlau Chemie S.A. (Spain). Glucose was prepared in deionized water at least 24 h before use in order to allow glucose to mutarotate. Fish sperm double stranded (ds)-DNA, which was used as target-DNA during MIPpy preparation and DNA template during evaluation of specific or non-specific interaction, and pyrrole, used for molecular imprints formation and modification of yeast cells, were obtained from Sigma-Aldrich Chemie GmbH (Germany). Glucose oxidase (GOx(2)) from *Aspergillus niger* (100 – 250 U/mg), theophylline ($C_7H_8N_4O_2$), potassium hexacyanoferrate(III) ($K_3[Fe(CN)_6]$) and hydrogen peroxide (H_2O_2) (30%) were also received from Sigma–Aldrich Chemie GmbH (Germany). Pyrrole monomer for the other experiments and caffeine ($C_8H_{10}N_4O_2$) were purchased from Alfa Aesar GmbH & Co (Germany). Before use pyrrole was purified through Al_2O_3 column (0.4 mm diameter and 6 cm length) in order to remove all coloured components. Sodium dihydrogen phosphate monohydrate ($NaH_2PO_4 \cdot H_2O$) and poly-L-lysine solution (0.1% w/v in H_2O) were pursued from Fluka (Germany), enzyme Glucose oxidase (GOx(1)) from *Aspergillus niger* (304.8 U/mg) from AppliChem (Germany), sodium sulphate (Na_2SO_4) from Reachim (Russia) and potassium dihydrogen phosphate (KH_2PO_4) from Riedel-de-Haën (Germany). Budding yeast (Saccharomyces cerevisiae), also known as baker yeast, was kindly donated by H. Bussey (Canada). Yeast extract, peptone from casein and ultrapure, granulated agar-agar were purchased from Merck (Germany).

2.2. Sample preparation

2.2.1. Preparation of polypyrrole/gold nanoparticles composites

Chemical synthesis of polypyrrole

Polymerization of pyrrole was performed in a mixture of 0.05 M sodium phosphate and 0.05 M sodium acetate buffer pH 1.0 in 1 mL reaction solution, which consisted of 200 mM hydrogen peroxide and 200 mM pyrrole. In buffer solution firstly the monomer was added and stirred using an ultrasonic bath for 5 min then followed by the addition of hydrogen peroxide. The solution was stirred with a shaker for a minute and was kept at room temperature in darkness for 18 h. The polymerized pyrrole was used as a reference in the investigation of polypyrrole/(gold nanoparticle) composites.

Synthesis of gold seeds and gold nanoparticles (AuNP)

Gold seeds of 13 nm diameter were synthesized by reducing $HAuCl_4 \cdot 3H_2O$ using sodium citrate in the presence of tannic acid according to the earlier reported procedure [201]. An aqueous solution of tetrachloroauric acid (80 mL of 0.0125% (w/w)) was heated up to 60 °C. The second solution consisting of sodium citrate (4 mL of 1% (w/w)), tannic acid (0.025 mL of 1% (w/w)) and 15.975 mL deionized water was heated separately up to 60 °C as well. Both solutions were mixed, heated up to 95 °C and kept at this temperature for 10 min with continued mixing to yield colloidal gold nanoparticles. Before further use colloidal gold suspension was stored in darkness at 4 °C.

The experiment of AuNP synthesis using gold seeds enlargement strategy was carried out in water. Synthesis solution consisting 100 µL of gold seeds solution, 5 µL of 25 mM $HAuCl_4$ solution, and 895 µL of deionized water was mixed and kept at room temperature for 142 h.

Synthesis of polypyrrole/(gold nanoparticle) composites (AuNP/Ppy)

Pyrrole solution in distilled water was stirred in an ultrasonic bath for 5 min in order to dissolve pyrrole in water. Then 100 µL of prepared gold seeds solution and 5 µL of 25 mM $HAuCl_4$ solution were gently admixed. Prepared pyrrole solution and water were added at such amounts that the final volume of polymerization solution was 1 mL. Final concentrations of pyrrole in polymerization mixtures were 50, 100, 200 or 400 mM. The

processes that are assumed to occur in the synthesis solution are depicted in Figure 6. The synthesis procedure consists of two main steps. Firstly, the gold seeds were obtained using tetrachloroauric and citric acids in the presence of tannic acid. Then only tetrachloroauric acid or pyrrole monomers together with tetrachloroauric acid were added to the gold seeds solution. Tetrachloroauric acid acts as an oxidizing agent in the polymerization of pyrrole. Thus it is thought that after addition of tetrachloroauric acid the enlargement of gold seeds should be observed and polypyrrole composites with entrapped gold nanoparticles should be obtained when Py and tetrachloroauric acid is added.

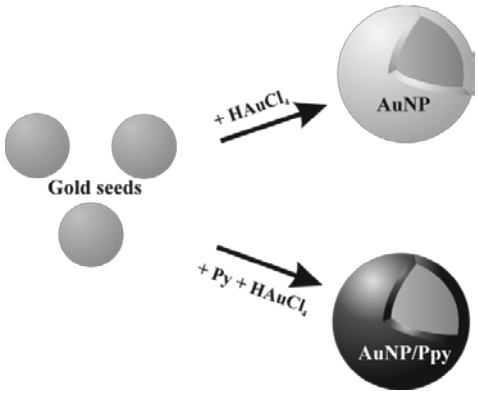

Figure 6 *Principle of gold nanoparticles (AuNP) enlargement using gold seeds and synthesis of polypyrrole/(gold nanoparticle) composites (AuNP/Ppy).*

2.2.2. Preparation of polypyrrole/(Glucose oxidase) biocomposites

Enzymatic polymerization of polypyrrole composites was performed according to the procedure presented before [38]. Briefly, the pyrrole monomer was added to 2 mL reaction solution containing 0.05 M phosphate buffer, pH 6.0. This was followed by the addition of enzyme (up to 1 mg/mL final concentration) and glucose solution (up to 50 mM final concentration) at the end. The concentration of pyrrole was varied from 50 to 400 mM to find out the influence of monomer concentration on the polymerization rate. In order to homogenize monomer solution in buffer, it was stirred in an ultrasonic bath for 3 min. After addition of each subsequent compound the solution was mixed with a shaker for a minute. Prepared solutions were kept at 30 °C temperature in darkness. No detergents or any other stabilizers were added**.**

Sample preparation for isotope ratio mass spectrometry

Polymerized samples were centrifuged at 12500 rpm for 15 min with IEC MicroCL 17 centrifuge, Thermo Electron Corporation (USA) and supernatant was separated from the

sediment. After centrifugation, sediment consisted of polypyrrole, Glucose oxidase, glucose and gluconic acid. Supernatant consisted of remaining pyrrole, glucose and gluconic acid. Supernatant was used for the isotope ratio mass spectrometric (IRMS) measurements as obtained. Sediment was also used for the IRMS analysis as obtained or additionally washed two times with distilled water and subsequently centrifuged each time to remove the residue of glucose and gluconic acid. After additional washing obtained sediment consisting of polypyrrole and Glucose oxidase was used for the stoichiometry determination using IRMS.

2.2.3. Synthesis of polypyrrole layer on gold electrode

Polypyrrole layer, electrochemically synthesized on golden SPR-chip, was used for the investigation of film formation, stability and repulsion. However, for the biocompatibility measurements the chemical synthesis was used.

Before the synthesis of Ppy layer a golden chip was rinsed with 1.0 M of NaOH for 20 min, then with distilled water and later it was followed by rinsing with 1.0 M of HCl for 10 min. For all Ppy layer stability experiments 50 mM of phosphate buffer (PBS), pH 7.0, with 0.1 M of KCl was used. 0.5 M pyrrole dissolved in PBS with KCl was used for electrochemical formation of Ppy layer. The electrochemical polymerisation was performed by application of sequence of 20 potential pulses of 1.0 V *vs* $Ag/AgCl/KCl_{sat}$ for 1.0 s and of 0.1 V *vs* $Ag/AgCl/KCl_{sat}$ for 10 s, all experiments were performed at controlled 20 °C temperature. The 10 s period of 0.1 V allowed equilibration of pyrrole monomer concentration close to the electrode surface. An applied potential pulse profile was defined by the oxidation potential of used monomer and the duration of this equilibration was determined by diffusion properties of the monomers [157].

Ppy layer preparation for electrochemical quartz crystal microbalance (EQCM) measurements

Before electrochemical polymerization, the EQCM cell was washed with PBS (50 mM $NaH_2PO_4 \cdot H_2O$, 50 mM $Na_2HPO_4 \cdot 12H_2O$ and 100 mM Na_2SO_4, pH was adjusted to 7.0. All solutions for polymerization mixture preparation and standard-solutions were prepared in PBS) and the electrode surface was electrochemically cleaned and activated in order to improve the adhesion of the formed polymer to the surface. Electrochemical

cleaning was performed in PBS according to the following procedure: the potential was cyclically swept between −0.2 and 1.5 V *vs* Ag/AgCl/KCl_{sat} at a 100 mV/s sweep rate. Electrochemical cleaning of the electrode was continued until steady cyclic voltammograms (CVs) were observed; steady CVs were observed after approximately 10 potential cycles. The electrochemical polymerization of pyrrole was performed in a polymerization mixture containing 50 mM pyrrole dissolved in PBS. Before the start of polymerization, the resonance frequency Δf and motional resistance R of the EQCM were monitored. Electrochemical polymerization was started only when Δf became stable: the variation of the signal within 10 min was less than ±1 Hz. The electrochemical formation of the Ppy layer was performed by a sequence of potential pulses of 1.1 V *vs* Ag/AgCl/KCl_{sat} for 10.0 s and of 0 V *vs* Ag/AgCl/KCl_{sat} for 1.0 s. In total, 300 potential pulses were applied.

Repulsion of the Ppy film

For the repulsion of Ppy film from the gold disc surface cyclic voltamperometry was applied. It was performed in the PBS with KCl. The effect of scan rate, number of pulses and potential range were investigated.

Layer preparation for biocompatibility experiments

Ppy was chemically synthesized onto 25 mm gold-plated glass slides (SPR-chip). Concentration of pyrrole in polymerization mixture was 0.1, 0.5, 2.5, and 5 mM. Polymerization was initiated with 0.6% H_2O_2, and took 7 days. The four different Ppy-modified gold surfaces were prepared. Total amount of polypyrrole (mg/cm^2) on gold surface was calculated according to Beer-Lambert law $A=cl\varepsilon$, at λ = 507 nm, where A - absorbance, c – concentration (mol/L), l – light path, ε - molar absorption coefficient. The molar absorption coefficient of polypyrrole is $\varepsilon \approx 10^5$ L mol^{-1} cm^{-1} [202].

2.2.4. Modification of electrodes by molecular imprints

2.2.4.1. DNA molecular imprints

Pencil graphite electrodes (PGEs) of 0.5 mm diameter were purchased from Tombo Ltd (Japan) and were used as disposable electrodes. PGEs of 3.0 cm length were prepared as previously described in literature [203]. The working area of the electrodes during

measurements was 20.6 mm^2. PGEs were pretreated applying constant potential (1.40 V) for 30 s in AcB, pH 4.8, while the solution in electrochemical cell was mixed.

Stock solutions of DNA (1000 ppm) were prepared with ultra pure water and kept frozen at –4 °C. More diluted solutions of DNA were prepared using 0.5 M acetate buffer (AcB), pH 4.8, containing 20 mM of NaCl. Pyrrole solutions were prepared in 50 mM PBS, pH 7.4, with 20 mM of NaCl. All experiments were conducted at room temperature (25 °C).

Electrochemical synthesis by means of potential pulse sequence (PPS) was carried out as previously described by Ramanaviciene et al. [157]. During this procedure the Ppy film was formed applying 25 potential pulses. The pulse potential profile was: 1.0 V *vs* $Ag/AgCl/KCl_{sat}$ for 1 s (synthesis of Ppy was performed at this stage) and 0 V *vs* $Ag/AgCl/KCl_{sat}$ for 10 s (the pyrrole monomer equilibration in the neighborhood of the electrode occurred at this stage). Both nonimprinted polypyrrole (NIPpy-PPS) and molecularly imprinted polypyrrole (MIPpy-PPS) were deposited on the electrode using the same potential pulse profile. NIPpy-PPS was deposited from 50 mM solution of pyrrole in PBS, while MIPpy-PPS was deposited from 50 mM of pyrrole and 5 ppm of template-DNA dissolved in PBS. After the deposition of NIPpy-PPS and MIPpy-PPS the electrodes were washed under stirring for 5 min in PBS in order to remove not polymerized compounds.

Electrochemical synthesis by means of cyclic voltammetry was carried out as described by L. Ozcan and Y. Sahin [159]. Thus electrochemical formation of polymer was performed by 10 potential cycles in the range from –0.6 V to +0.8 V *vs* $Ag/AgCl/KCl_{sat}$, at the sweep rate of 100 mV/s. Nonimprinted polypyrrole (NIPpy-CV) was deposited from 50 mM solution of pyrrole and molecularly imprinted polypyrrole (MIPpy-CV) was deposited from 50 mM of pyrrole solution containing 5 ppm of template-DNA in AcB, pH 4.8. Differently from synthesis conditions, which has been described by L. Ozcan and Y. Sahin [159], the upper vertex potential was reduced down to 0.8 mV because of possible guanine oxidation at 1.0 mV.

After the polymerization in order to remove the template-DNA from polymer, MIPpy-modified electrodes were washed by intensively stirred PBS for 30 min. To reduce pretreatment/washing effects on analytical signals, NIPpy-based electrode was pretreated/washed in the same manner as MIPpy-based one.

Evaluation of target-DNA interaction with NIPpy and MIPpy

In order to evaluate the specific interaction of target-DNA with MIPpy and nonspecific interaction with NIPpy, all these layer-based electrodes were divided in two groups containing 10 electrodes modified by MIPpy and 10 electrodes modified by NIPpy each. The first five electrodes modified by NIPpy after washing were left for further investigation without any additional incubation and it was estimated as a "blank" polymer, which is required in order to obtain baseline for differential pulse voltammetry. Second group of five electrodes modified by NIPpy was used for the investigation of target-DNA containing solution. The same was done using electrodes with MIPpy, for this reason five electrodes with MIPpy were not incubated in target-DNA containing sample and analyzed by DPV, the last five electrodes were analyzed by DPV after the incubation in the sample containing target-DNA.

In order to evaluate specific and nonspecific interaction of target-DNA with NIPpy or MIPpy, the electrodes modified by NIPpy and MIPpy were incubated for 30 min in the sample containing 5 ppm of target-DNA dissolved in AcB, pH 4.8. Specific and nonspecific interactions with target-DNA occurred after incubation in analyte containing aliquot. After the incubation the electrodes were washed by dipping for 3 times into the AcB, pH 4.8, for 30 s. $\Delta I/\Delta E$ for MIPpy (or NIPpy) represented in Figure 17 was calculated using the Equation 1:

$$\Delta I/\Delta E = \Delta I'/\Delta E' - \Delta I''/\Delta E'' \quad (1)$$

where:

ΔI – peak current evaluated by DPV of MIPpy (or NIPpy);

ΔE – peak voltage in DPV of MIPpy (or NIPpy);

$\Delta I'$ – peak current registered by DPV of MIPpy (or NIPpy) incubated in target-DNA;

$\Delta E'$ – peak voltage in DPV of MIPpy (or NIPpy) incubated in target-DNA containing sample;

$\Delta I''$ – peak current registered by DPV of MIPpy (or NIPpy) not incubated in target-DNA containing sample;

$\Delta E''$ – peak voltage in DPV of MIPpy (or NIPpy) not incubated in target-DNA containing sample.

Electrochemical measurements and assessment of the results for MIP and NIP samples.

The oxidation signal of guanine was registered by DPV in the blank AcB, pH 4.8, at 0.05 V modulation amplitude with an initial potential of 0 V and end potential of 1.4 V applying 0.008 V step [203].

2.2.4.2. Electrochemical formation of MIP with caffeine

Polymerization of MIPpy in the presence of caffeine ($MIPpy_{caff}$) as a template for molecular imprinting was performed applying potential pulse sequence as it was described in previous study [157]. This previously described electrochemical polymerization procedure was slightly modified in order to match the requirements of recent research work and the MIPpy was formed from polymerization mixture containing 50 mM of pyrrole and 5 mM of caffeine dissolved in PBS. Before the synthesis of Ppy layer the EQCM sensor disk was switched into electrochemical circuit as a working electrode and then it was cleaned by sequence of cleaning steps: (i) approximately 10 min EQCM cell was flushed at constant flow rate of 1 mL/min with PBS; (ii) then the PBS flow was stopped and the working electrode was electrochemically cleaned by application of potential cycling from −0.2 to +1.5 V *vs* $Ag/AgCl/KCl_{sat}$ at 0.1 V/s potential sweep rate. The oxygen adsorption and desorption peaks were observed during this cycling voltammetry based experiment and it was applied as indication of surface cleaning efficiency. Potential cycling was stopped when stationary CV curve was obtained (approximately after 10 cycles). Then the EQCM cell was filled with a polymerization mixture using 6-channel valve. The electrochemical formation of Ppy layer on EQCM sensor was performed by the application of potential pulse sequence. The pulse profile was based on rectangular potential profile of 1.0 V for 1.0 s and of 0.1 V for 10 s. The 10 s period at 0.1 V allowed equilibration of pyrrole monomer concentration close to the electrode surface. In total 300 potential pulses were applied. An applied potential pulse profile was defined by the oxidation potential of used monomer and the duration of this equilibration was determined by diffusion properties of the monomers [157].

Determination of caffeine and theophylline interaction with MIPpy

The interaction of $MIPpy_{caff}$ modified EQCM sensor with two homologous xanthine derivatives (caffeine and theophylline) was evaluated. The evaluated concentrations of both xanthine derivatives were in the range from 1 mM to 4 mM and these solutions were obtained by mixing stock solution of caffeine or theophylline with PBS. Solutions of caffeine and theophylline were evaluated in the following order: first, the cell was filled with PBS, then during constant flow of the PBS through the EQCM cell imprinted caffeine was washed away from the MIP-Ppy; simultaneously, during all these procedures the resonance frequency of the EQCM sensor was registered. Washing with PBS took approximately 30 min until the variation of Δf became less than 1 Hz/min. When required stability of the signal was obtained the solutions of caffeine or theophylline were pumped into the EQCM cell at the constant flowrate and simultaneously the resonance frequency of the EQCM sensor was registered. Administration of the liquids by the HPLC pump was programmed according the following order: (1) PBS (0 mM of caffeine); (2) 1 mM of caffeine; (3) PBS; (4) 2 mM of caffeine; (5)PBS; (6) 3 mM of caffeine; (7) PBS; (8) 4 mM of caffeine; (9) PBS. Each required concentration of target molecules was administered to the EQCM cell for 15 min and then it was washed out. During the evaluation the flow of liquids was kept constant as 1 mL/min. After the measurement the EQCM cell was washed with PBS for 30 min in order to obtain steady-state resonance frequency.

2.2.5. Sample preparation for the experiments with living cells

2.2.5.1. Bone marrow stem cells

Isolation and cultivation

Bone marrow was obtained from 6-8 week old BALB/c mice. All procedures were carried out in accordance with the guidelines of the European Union and approved by the Lithuanian Ethics Committee on the Use of Laboratory Animals under State Veterinary Service. The animals were sacrificed by cervical dislocation and bone marrow was flushed out of tibias and femurs. Cells were washed three times by centrifugation for 6 min at 400 g and the pellet was resuspended in culture medium consisting of DMEM with stable glutamine supplemented with 10% (v/v) FCS (Biological Industries, Kibbutz

Beit-Haemek, Israel), and 1% penicillin/streptomycin. Then cells were plated in 25 cm^2 flask. Non-adherent cells were removed by changing the medium. Medium was changed every 2-3 days until the monolayer reached 70% confluence. Then, mouse MSCs were harvested for reseeding or experimentation. The cells were maintained in an incubator at 37 °C and 5% CO_2 for the entire duration of culture.

Cell adhesion studies

The Ppy-modified gold-plated glass slides were sterilized by incubating them with 70% ethanol for 30 min followed by exposure to ultraviolet light for 20 min. Prior to cell seeding, all slides were soaked overnight in the culture medium at 37 °C. Passage 3 cells from 70% confluent culture flasks were used for all of the studies. Before seeding, cells were detached from the cell culture flask using trypsin-EDTA and viable cells were counted by trypan blue exclusion test. For cells visualization on lightproof Ppy surfaces, cells were stained with green fluorescent cell linker dye PKH67 (Sigma-Aldrich, St. Louis, MO, USA). The cells were seeded on each Ppy-modified or bare gold slides at the same density (10^5 cell/mL) and then allowed to adhere to the substrates undisturbed in a humidified incubator (at 37 °C, 5% CO_2) for 48 h. Standard tissue culture polystyrene plates (TCPs) for cell culture were used as such without any slide (control).

Cell proliferation studies

The Cell proliferation assay kit received from Millipore (Billerica, MA, USA) was used for quantification of cell viability and proliferation. Stem cells were seeded on all Ppy-modified and bare gold slides in the 6-well culture plates at the concentration of 10^5 cell/mL. After 48 h, the cell proliferation reagent WST-1 was added into culture medium. This mix was incubated in a humidified incubator (at 37 °C, 5% CO_2) for 4 hours. After that, a supernatant mixed with cell proliferation reagent WST-1 was transferred into a 96-well plate. The samples without stem cells were parallely incubated to serve as controls. The absorbance values were measured in triplicate at 440 nm using the spectrophotometer (microplate reader) TECAN sunrise (Mannedorf, Switzerland). The assay was repeated for three times.

Statistical Analysis

All results were expressed as the arithmetic mean ± SD. Differences between groups were evaluated by Student's t-test. $P < 0.05$ was considered significant.

2.2.5.2. Budding yeast cells

Growth and preparation of yeast cells

The *Saccharomyces cerevisiae* yeast cell strain Y00000 (BY4741 Matα *his*3Δ1 *leu*2Δ0 *met*15Δ0 *ura*3Δ0) was cultivated aerobically overnight (for 20 – 24 h) at 30 °C in a typical YPD media containing 1% of yeast extract, 2% of peptone and 2% of glucose. Cells were cultivated at constant shaking at 200 rpm. After cultivation, yeast cells were harvested by centrifugation. For this culture with growing media was centrifuged for ~2 min at 3000 rpm. Supernatant was disposed and cells were washed with 0.1 M PBS buffer. This washing procedure was repeated 2 – 3 times. The samples were centrifuged at 3000 rpm for 2 minutes. The supernatant was thoroughly disposed and the cells were weighed.

For the AFM measurements of intact cells the solution of 10 mL containing 0.2 g of glucose and 0.1 g of bakers yeast cells dissolved in distilled water was stirred and kept in room temperature for 30 min. additionally 0.9% sodium chloride solution in distilled water was used. The yeast cells solutions with presence or absence of additional chemicals (NaCl or glucose) were deposited on the atomically flat silicon substrate and left dry for 15 min.

Cell fixation precedure

Intact and Ppy modified yeast cells were immobilized on plastic Petri dishes or on the glass and later were used for optical analysis. For this water based 0.1% v/v poly–L–lysine (PLL) was added in the dish and left over night to adhere. After this modification the remaining PLL solution was removed and dishes were thoroughly washed with distilled (DI) water. Yeast cell suspension in DI water was then poured and left for 10 min. Subsequently, the suspensions were disposed and dishes were washed twice with PBS. Then the immobilized cells were additionally fixed with GA by 15 min incubation in GA vapor, in closed vessel over 25% of GA solution.

Cell modification with Ppy

Four 10 mL samples named *solution-1* consisting of 0.1 M PBS, 0.04 M of $[Fe(CN)_6]^{4-}$, and 0.2 M of glucose were prepared. Then 100 mg of centrifuged yeast cells were added into each sample of *solution-1*. Subsequently 0.1, 0.3 and 0.5 M of pyrrole was added to three out of four *solution-1* samples. These concentrations of Py were chosen because: 0.5 M is ~ half Py solubility in water; 0.1 M is still high enough to do impact on cells. Then all four samples were shaken at 200 rpm at 30 °C for 20 – 24 h. After this, the yeast cells were collected and washed with 0.1 M PBS buffer, pH 7.0. This described procedure will be named as "modification" and yeast cells with Ppy "modified" yeast cells.

For comparison Ppy synthesis induced by $[Fe(CN)_6]^{3-}$ with and without yeast cells were examined. Solutions were prepared in 0.1 M PBS buffer pH 7.0 containing 0.5 M of pyrrole and 0.04 M of $[Fe(CN)_6]^{3-}$ and part of them 100 mg of yeast cells.

Evaluation of viability of modified yeast cells

Four samples of cells were prepared as described before. After final washing procedure the yeast cell samples were re-suspended in 2 mL of 0.1 M PBS buffer, pH 7.0. Then the samples were diluted to reduce cell colony-forming unit (CFU) per volume unit. Serial dilutions were applied according to control sample cell concentration, which was measured with spectrophotometer. 0.1 mL of cells from diluted samples were transferred on agarose containing YPD media. The agar-covered petri dishes were incubated for 48 h in a thermostat at 30 $^{\circ}$C. Counting of grown colony was performed to determine modifications impact on cells viability.

Statistical evaluation of yeast cell viability

Statistical calculations of yeast cell viability were based on: (i) a Welch's T-Test in order to check if the counted mean form number of same type samples of the yeast with 0.3 M of Py, which is different from the mean of the yeast samples with 0.5 M at 99% confidence limit; The null hypothesis was based on the fact that there is no significant difference between the two means; (ii) Q-test to check for outliers at 99% confidence limit.

Yeast cell preparation for Raman measurements

For Raman and SERS measurements the cells were cultured in solid malt extract – agar plates (VWR, USA) in ambient atmosphere at 25 °C for three days. Once the culture was grown, it was stored at 4 °C. The cell culture was renewed every two weeks. The average size of single yeast cell is 3 – 5 μm. For the RS analysis only fresh cultures were used. Some living cells were grabbed with a sterile loop and stirred in distilled water. A drop of the suspension was placed on a substrate and left to dry for 30 min before the RS experiments. The samples were then analyzed with the Raman microscope. The measurements were performed within 4 h after the dispersion of the cells. The signal accumulation of each single Raman spectrum was 20 s repeated 20 times at 514.5 nm excitation. Spectra were acquired in the range from 700 to 1800 cm^{-1}. If not stated otherwise, in all measurements the laser spot was focused into the center of a single yeast cell, just above the substrate. The reproducibility of the spectral features was verified by comparing the Raman signal from several different cells.

Substrate preparation for Raman spectroscopy measurements of yeast cells

For Raman experiments the yeast cells were deposited on different substrates: objective glass slides (VWR, USA), silicon (111) with a native ~2 nm oxide layer, and 100 nm SiO_2 on Si (SilChem, Canada). Before the measurements, the substrates were sequentially washed in an ultrasonic bath in different solvents: deionized ultra-pure water (Milli-Q), acetone, ethanol, and once again in water, for 15 min each. The substrates were dried under a nitrogen flow. A highly oriented pyrolytic graphite (HOPG) substrate was obtained from NT-MDT (Moscow, Russia). Just before cell deposition, the HOPG substrate was cleaved with scotch tape producing a clean and flat surface. A gold substrate was obtained by evaporation of 60 nm Au layer on top of a freshly cleaved mica substrate. The preparation of the sample was adopted from a protocol previously reported [204]. An ultra-flat and clean gold substrate was obtained by gluing a glass plate on top of the evaporated gold film. The mica/gold/glass stack was then immersed in tetrahydrofuran for 20 min allowing the gold film to be stripped away from the mica substrate.

The structured silver substrate was produced by galvanic deposition in a solution of silver citrate on top of two surfaces, a gold substrate and a silicon substrate. The silicon substrate was mechanically patterned with parallel grooves in order to remove the native oxide layer before Ag particle deposition. The Au and Si substrates were biased at 2.0 and 4.0 V, respectively, with a gold wire used as a counter electrode. Silver single crystals attached onto the silicon substrate were obtained in this way. The silver particles on the substrates were cleaned in ultrasonic bath in several solvents: acetone, ethanol, water, and in a solution of HNO_3 1.5%. Energy-dispersive X-ray spectroscopy (EDX) and scanning electron microscopy verified the formation of silver crystallites.

2.3. Instrumentation

2.3.1. Surface analysis method

Atomic force microscopy

Surface structure and roughness of Ppy/GOx composites, electrodes with MIPpy and NIPpy, chemically and electrochemically synthesized Ppy on gold electrode as well as modified and intact yeast cells were evaluated using atomic force microscope Bioscope Catalyst (Bruker, USA) and 5420 from Agilent Technologies (Keysight, USA). The topography images were obtained using peak force tapping mode for Ppy/GOx composites, tapping mode for the yeast cells and contact mode for the rest of the samples. All the measurements were executed in air, at room temperature. For peak force tapping mode silicon tip (k = 0.4 N/m; f_{0nom} = 70 kHz) was employed while for contact mode the silicon nitride tip with k = 0.06 N/m; f_{0nom} = 16 kHz was used. In the intermittent contact mode with conventional silicon cantilevers were also employed. All images were processed using the program NanoScope 8.0 provided by Bruker.

Force curve measurements were performed in phosphate buffer, pH 7.0, using conventional silicon nitride tip with similar characteristics as for contact mode. The polycarbonate membrane (Millipore, Germany) with the entrapped yeast cells were attached with the double side tape on the glass substrate, immersed in water and were investigated by AFM without any additional preparation. During the measurement firstly the image of the entrapped cell was registered. Later at least 5 yeast cell stiffness

measurements in the middle of the single cell were performed by atomic force microscopy based registration of force-distance (indentation) curves.

Scanning electron microscopy

Size of the synthesized AuNP/Ppy and Ppy/GOx composites was evaluated with the high resolution field emission scanning electron microscope SU-70 (Hitachi, Japan). Accelerating voltage for the electron beam was set to 5 kV. Samples for the measurement were prepared by depositing a drop of 2 µL of the solution on the fragment of silicon wafer. The polypyrrole modified gold surfaces were evaluated with scanning electron microscope ZEISS (Oberkochen, Germany). Later they were used for the biocompatibility study. The SEM characterization of structurised silver sample was performed using a FEI NovaNanoSEM 200 (Oregon, USA) in secondary electron mode with beam energy of 5 kV.

2.3.2. Optical methods

UV-Vis spectrophotometry

UV-Vis absorption spectroscopy measurements were performed with a double-beam spectrophotometer Lambda 25, PerkinElmer (Shelton, USA). The samples for UV-Vis measurements were dispersed in aqueous solution and acquired spectrum interval was adjusted taking into account the most important regions. Absorption spectra were collected for AuNP/Ppy and Ppy/GOx composites.

Dynamic light scattering

Dynamic light scattering (DLS) measurements were performed with a Malvern Zetasizer Nano ZS (Malvern, Herrenberg, Germany) equipped with a 633 nm He-Ne laser and operating at an angle of 173°. The data were collected and analyzed by the Dispersion Technology Software version 6.01 from Malvern. All measurements were performed at a position of 4.65 mm from the cuvette wall with an automatic attenuator and at a controlled temperature of 25 °C. DLS measurements were performed for AuNP/Ppy and Ppy/GOx composites and Py dispersed in buffer.

Optical microscopy

Bone marrow stem cells adhesion was evaluated using bright field (phase contrast) and fluorescence microscopy using a microscope Nikon eclipse TE2000U (Tokyo, Japan). The bright field of the same microscope was used for the optical evaluation of polypyrrole modified gold surfaces that were later used for the biocompatibility measurements.

Raman microscopy

Raman spectroscopy experiments were performed with a micro-Raman spectrometer LabRam HR800 (HORIBA, France). Two excitation laser lines were used: 514.5 nm (Ar+ laser, Coherent, USA), 514.7 nm (solid state laser, Coherent, USA) The laser intensity measured at the sample was set to 2 mW and 1 mW for the 514.5 nm and 514.7 nm, respectively. Laser light filtered by a plasma filter was focused onto the sample with a 100x objective (numerical aperture, N.A. = 0.9). The scattered Raman signal was collected with the same objective in the backscattering geometry and detected by an EM CCD detector cooled down to –64 °C. For the cells immobilized on the structured silver substrate, the laser power was decreased to 100 μW. Since such substrate provided a high enough Raman intensity, a line map scan was performed along a single cell using a step size of 500 nm. Statistical averages were obtained from at least 10 spectra for an exposition time of 10s each.

Data processing

For a better comparison of the spectra, the substrate signal was subtracted and the baseline background was corrected using a linear function. Before subtraction, the spectra of the bare substrate and the substrate with yeast cells were normalized to the highest background peak for silicon, silicon oxide, glass, and HOPG. For the gold substrate the background was normalized in the range, where no signal from the cell was registered (at 1800 cm^{-1}). For the structured Ag substrate only a background subtraction process was performed.

2.3.3. Electrochemistry

Potentiostat - galvanostat

All electrochemical procedures were performed using potentiostat-galvanostat Autolab "PGSTAT 30" from Echochemie (Utrecht, The Netherlands). Electrochemical cell consisted from three-electrode system. The platinum electrode was used as an auxiliary electrode and $Ag/AgCl/KCl_{sat}$ was used as a reference electrode. Both of them were purchased from CH instruments (Austin, USA). The 30 mm diameter SPR-chip, which was initially coated by 50 nm gold layer and received from XanTec bioanalytics GmbH (Muenster, Germany), was used as working electrode for the evaluation of electrochemical stability of the Ppy film and as a platform for biocompatibility measurements. For detection of target-DNA the disposable pencil graphite electrode was chosen as working electrode. Electrical contact for graphite leads holder with the lead was obtained by soldering a metallic wire to the metallic part [205].

Electrochemical modification of pencil graphite electrodes with polypyrrole layer molecularly imprinted with template-DNA was performed by PPS and CV. Two types of nonimprinted Ppy based pencil graphite electrodes were similarly prepared. Detection of target-DNA was investigated using DPV.

Quartz crystal microbalance

The analytical system was based on binary HPLC pump HP 1100 (model G1312A) from Hewlett Packard (Germany), electrochemical quartz crystal microbalance (EQCM) from Maxtek (USA), potentiostat/galvanostat/ZRA Reference 600TM from Gamry (USA), 6 channel 2 position valve from Rheodyne (USA), homemade flow-through cell. For the evaluation of mass changes the EQCM data logging software from Maxtek (USA) was used; electrochemical polymerization was performed by potentiostat/galvanostat controlled by software 'Gamry framework', version 5.30 from Gamry (USA). 5 MHz gold coated quartz crystal, model SC-501-1 from Maxtek (USA) was used for EQCM measurements. The geometric area of the working electrode surface was equal to 1.37 cm^2, and the active oscillating region was 0.342 cm^2. EQCM cell was placed in a Faraday cage in order to reduce the influence of variations of electromagnetic fields and temperature. The temperature was maintained constant at 20 °C.

2.3.4. Isotope ratio mass spectrometry

Nitrogen and carbon isotope ratios in the Ppy/GOx composites were measured using an elemental analyzer (EA) (Flash EA1112) coupled to IRMS (Thermo delta plus advantage) *via* ConFlo III interface. A sample was placed in a tin capsule and combusted in the elemental analyzer with the oxygen excess. Cr_2O_3 granules in the oxidation column were used as an additional oxygen source, while copper wires in the reduction column were used for the reduction of nitrogen. Oxidation and reduction columns were operating at the 1020 and 650 °C temperature, respectively. Pure He 5.0 was used as a carrier gas, while magnesium perchlorate was used for the water removal. Gases evolved after combustion were separated by the packed column and transferred to the ConFlo III interface. This interface allowed the passing of calibration gases from the laboratory tank (N_2 and CO_2) and EA to the IRMS at different time intervals that allowed to measure nitrogen and carbon isotope ratios with high accuracy. A reference material with known nitrogen and carbon isotopic values (caffeine IAEA 600, $\delta^{13}C$ = -27.771‰$_{VPDB}$, $\delta^{15}N$ = 1‰$_{airN2}$) [206] was used for the laboratory N_2 and CO_2 tank calibration. The analytical precision and calibration of the used reference gas CO_2 to PDB ($\delta^{13}C$ = -31.1 ± 0.08‰) have been estimated by the repeated analysis of certified reference material IAEA 600, which gave an average value of $\delta^{13}C$ equal to -27.77‰ (certified value $\delta^{13}C$ = -27.77 ± 0.04‰) and standard deviation equal to 0.08‰. The same calibration procedure was applied for the calibration of laboratory N_2 tank ($\delta^{15}N$ = -2.4 ± 0.09‰) to air N_2. The analytical precision for the measured samples was 0.15‰ or better (both for the nitrogen and carbon).

2.3.4.1. Calculations for the isotope mixing model

When the isotopic composition of the initial substances – polypyrrole and Glucose oxidase (respectively: δ_{Ppy} and δ_{GOx}) and the isotopic composition of the composite material (δ_{sample}) are known, it can be expressed as:

$$\delta_{SAMPLE} = \delta_{Ppy} * f_1 + \delta_{GOx} * f_2 \quad (2)$$

$$f_1 + f_2 = 1 \quad (3)$$

where f_1 and f_2 are the fractions of the polypyrrole and Glucose oxidase in the sample respectively. Combining equations 2 and 3 the equation 8 is obtained:

$$\delta_{SAMPLE} = \delta_{Ppy} * f_1 + \delta_{GOx} * (1 - f_1) \quad (4)$$

$$\delta_{SAMPLE} = \delta_{Ppy} * f_1 + \delta_{GOx} - \delta_{GOx} * f_1 \quad (5)$$

$$\delta_{SAMPLE} - \delta_{GOx} = \delta_{Ppy} * f_1 - \delta_{GOx} * f_1 \quad (6)$$

$$\delta_{SAMPLE} - \delta_{GOx} = (\delta_{Ppy} - \delta_{GOx}) * f_1 \quad (7)$$

$$f_1 = (\delta_{SAPMLE} - \delta_{GOx})/(\delta_{Ppy} - \delta_{GOx}) \quad (8)$$

The number of carbon atoms in the fraction f_1 can be calculated according to the formula:

$$N_{Ppy} = f_1 * N_{GOx}/f_2 \quad (9)$$

where N_{GOx} is the number of the carbon atoms in the Glucose oxidase. From equation 9 the number of carbon atoms from polypyrrole that are stacking on the Glucose oxidase, can be calculated. The same arithmetic is valid for the calculation of the isotope ratio of nitrogen atoms.

2.4. Numerical simulations

Simulations of electromagnetic properties of an yeast cell on the different substrates were performed employing the commercial product ANSYS EMAG. This software is based on the finite element method (FEM) to model 3D electromagnetic fields based on a full-wave formulation of Maxwell's equations in terms of the time-harmonic electric field. The mesh was created with the HF119 high-frequency tetrahedral element and contains several million degrees of freedom. Measured complex refractive index data for substrates were taken from reference [207] and the dielectric constant of the cell was approximated to that of water (ε = 1.77) since water makes up around 70% of the total weight of a cell [208]. Moreover, the refractive index of cells has been reported in the range 1.35-1.40 that can be approximated to that of water 1.33 [209]. Laser beam propagation was approximated by a plane electromagnetic wave with an electric field component E = 1 V/m at the wavelength of 515 nm. The computational domain was truncated with a surface impedance absorbing boundary condition.

3. Results and discussion

3.1. Electrochemical synthesis and stability of polypyrrole

In this section the electrochemical synthesis of polypyrrole and its possible application as matrix for molecular imprints are presented. The improvement of sensor performance is possible by electrochemical and/or chemical modification of signal transducer [210]. For this aim, polymers have been used in sensor and biosensor design as matrixes for the formation of analyte-sensitive layer. One of the most important requirements for the sensor is that polymer layer has to be smooth and possess good adhesion to the transducer surface [211, 212]. This includes the adhesion of the polymer to the substrate-surface [213, 214] during all analytical processes under measurement conditions. Electrochemical synthesis of polypyrrole ensures a rather homogenious layer of polymer, which could easily be repulsed by applying higher voltage than a certain value, which must be known for the system. What is more, the initial formation of polymer is not a homogenious but rather possesses a spot like behavior until all the electrode surface is covered by the polymer. To evaluate if polypyrrole could be used as a matrix for molecular imprints the Ppy was formed electrochemically and the repulsion of such layer was evaluated. In the next section the formation of matrix with several molecules: DNA strand, caffeine and theophylline was executed.

This part of the study reports the electrochemical synthesis of polypyrrole film on the gold surface and the evaluation of this film repulsion conditions from the electrode surface. It is known that overall stability of the conducting polymer layer on the electrode is critical for many applications including biosensors. It can be affected by many factors, however, electrochemical treatment of electrode is mostly well-known among them. Here presented experiments were mainly based on the preparation of the polymeric layer and the investigation of its stability. Overoxidised polypyrrole film was synthesized on the gold electrode. A particular number of low and high potential pulses were applied for the preparation of proper thin layer of Ppy [215]. Application of high and low potential pulses of different duration provides additional options for regulation of polymerization process. Diffusion of pyrrole and/or other materials present in polymerization bulk solution is one of the limiting factors at the interface of electrode

surface and formed Ppy. This limitation of diffusion is especially important for the preparation of molecularly imprinted polypyrrole (MIPpy) [157, 215]. Later this layer was treated by potential cycling in wide potential intervals. The stability of Ppy layer deposited on electrode was evaluated.

Firstly, polypyrrole film was deposited on the quartz substrate covered by 50 nm thick gold layer, which served as working electrode in electrochemical cell consisting from three-electrode system. The anodic electrochemical formation of Ppy was performed without elimination of oxygen from the polymerization media. Potentiostatic and potentiodynamic electrochemical Ppy synthesis methods are described in previous studies [216]. Potential pulses based method for the deposition of Ppy was selected regarding the previous works of our group [157]. The selected method is the most promising for the future application in the preparation of biosensors. Later in order to better understand the polymer formation mechanism, EQCM was employed. This technique enables to measure even a very small change of mass on gold surface. For this reason it was suitable for registration of Ppy formation from the initial phase.

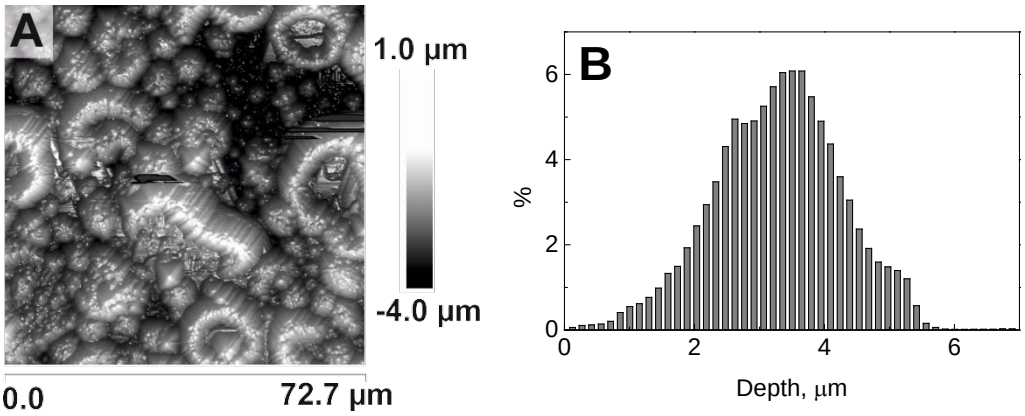

Figure 7 *A) The AFM image of the Ppy film on gold electrode. Polymerization conditions: 500 mM of pyrrole dissolved in 50 mM phosphate buffer, pH 7.0 with 0.1 M of KCl. The electrochemical formation of polymer coating was carried out by 20 potential pulse cycles as 1.0 V vs Ag/AgCl/KCl$_{sat.}$ for 1 s and 0.1 V vs Ag/AgCl/KCl$_{sat.}$ for 10 s; B) Distribution of formed Ppy film roughness measured by AFM.*

Two different concentrations of monomer 500 mM and 50 mM were used for the formation of Ppy layer. The obtained films were analysed using atomic force microscopy. Firstly, the analysis of morphology (Figure 7 A) and distribution of surface roughness (Figure 7 B) were evaluated for the sample with 500 mM of initial monomer concentration. Ppy was formed during high potential (1.0 V) pulse and therefore pyrrole monomer was considered to be exhausted close to electrode surface. For this reason

during long (10 s) period of low potential the pyrrole molecules diffused towards electrode and these molecules were polymerized during next high potential step. It was found that approximately 95% of formed Ppy roughness was in a range from 1 to 5 μm and in 45.5% of formed Ppy the roughness was 3.2 – 4.1 μm. The AFM investigation of the conducting polymers allows to identify Ppy film structure since problems of uniformity are as well important as Ppy film thickness. Some AFM studies performed by other authors have presented Ppy nucleation and growth elongation mechanisms during electrochemical polymerization of Ppy [217, 218]. The typical form of Ppy layer deposited on the electrode surface had a toroidal or doughnut-like structure. The toroidal structure was indeed formed by small Ppy nuclei [217]. Because of the nucleation based Ppy polymerization, the polymer film has been mentioned as uniform and dense [218]. The AFM image of this work confirms doughnut-like structure of the Ppy film (Figure 7 A). It was found that the average width of cross-section of doughnut-like structures of formed Ppy was approximately 14.4 μm. The thickness of the layer was evaluated measuring the end of polymerized film, where both – gold and Ppy – were scanned. The obtained thickness varied in the range from 1 to 3 μm (Figure 8) and calculated average roughness value (RMS) was 790 nm. Such high thickness distribution and large structures are not suitable for the formation of molecular imprints. For this reason a lower concentration of pyrrole monomer and slightly changed polymerization conditions were chosen and polymerized film was evaluated again.

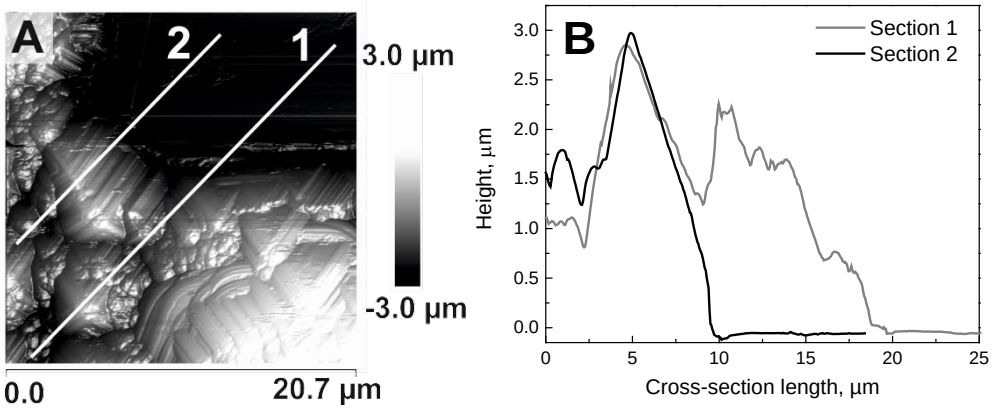

Figure 8 *A) AFM image of the border of synthesized Ppy layer on the gold electrode, lines indicate the cross-section places. B) Cross-section profiles of the Ppy layer.*

The AFM image of Au electrode coated with a Ppy layer (initial monomer concentration was 50 mM) after 300 high-potential pulses (1.1 V for 10 s) is depicted in Figure 9 A. The longer interval for high-potential pulse was chosen as to be sure that all

the adsorbed monomer was polymerized. The grain like structure of the Ppy layer was formed on the electrode surface. A statistical evaluation of the AFM image revealed that the dominant height of the Ppy layer roughness is 37 nm (Figure 9 C). The RMS of the Ppy-based layer, which was calculated from AFM investigation (Figure 9 A), was 2.61 nm, while the RMS of the clean gold electrode (Figure 9 B) was 0.744 nm. After the formation of the Ppy-based layer, the RMS has increased 3.5 fold. In comparison to previous polymer layer the RMS was changed drastically (RMS value in previous sample 790 nm and now 2.61 nm). Thus the concentration has a very high impact on the formation of Ppy film. The surface structures differ as well. In the first experiments a donugth like structures of the size 14.4 μm and thickness of 3 – 1 μm were obtained while here a small grain like structure is seen with the grains from 30 up to 100 nm size. The thickness of the latter layer was not evaluated, however, some pits were obsedved and the depth of 15 nm was measured.

The function of the EQCM sensor can be described by the Butterworth−van Dyke equivalent circuit [219]. In this model, the motional resistance (*R*) describes the dissipation of mechanical vibration energy [220]. During the electrochemical polymerization of pyrrole, both parameters Δf and *R* were registered. The registered shift of *R* in time is represented in Figure 10 as a solid line. It was found that the most significant shift of *R* during polymerization was obtained within the time period ranging from 0 until 150 s, which is the framework between the 1^{st} and 15^{th} potential pulse. The increase in *R* was found to be 8.5 Ω. During the following potential pulses, the shift in *R* was very low and it decreased by 0.2 Ω (Figure 10, the interval from t_d until the end of polymerization).

The mass of deposited Ppy was calculated using the Sauerbray equation. The density of the Ppy film (1.25 g cm^{-3}) was an average value calculated from the literature [221] and was used for the calculation of the increase in Ppy layer thickness during electrochemical polymerization (Figure 10, dashed line). As is obvious from Figure 10, the change in *R* became significantly less after 150 s. We assume that this effect was observed due to the termination of Ppy layer formation. As a consequence, the viscosity change at the sensor surface has also decreased. We think that the formation of the Ppy layer could be divided into several phases: at the beginning, Ppy does not form a complete layer and could be described as an ‘island’-based structure, which is deposited

on the surface (interval from t_b to t_c, Figure 10); during the next phase, the islands of Ppy merge and a monolayer consisting of Ppy particles is formed (interval from t_c to t_d, Figure 10); during the other phases of electrochemical formation of the Ppy coating, the multilayered structure, which consists of Ppy particles, is obtained (interval from t_d to the end, Figure 10).

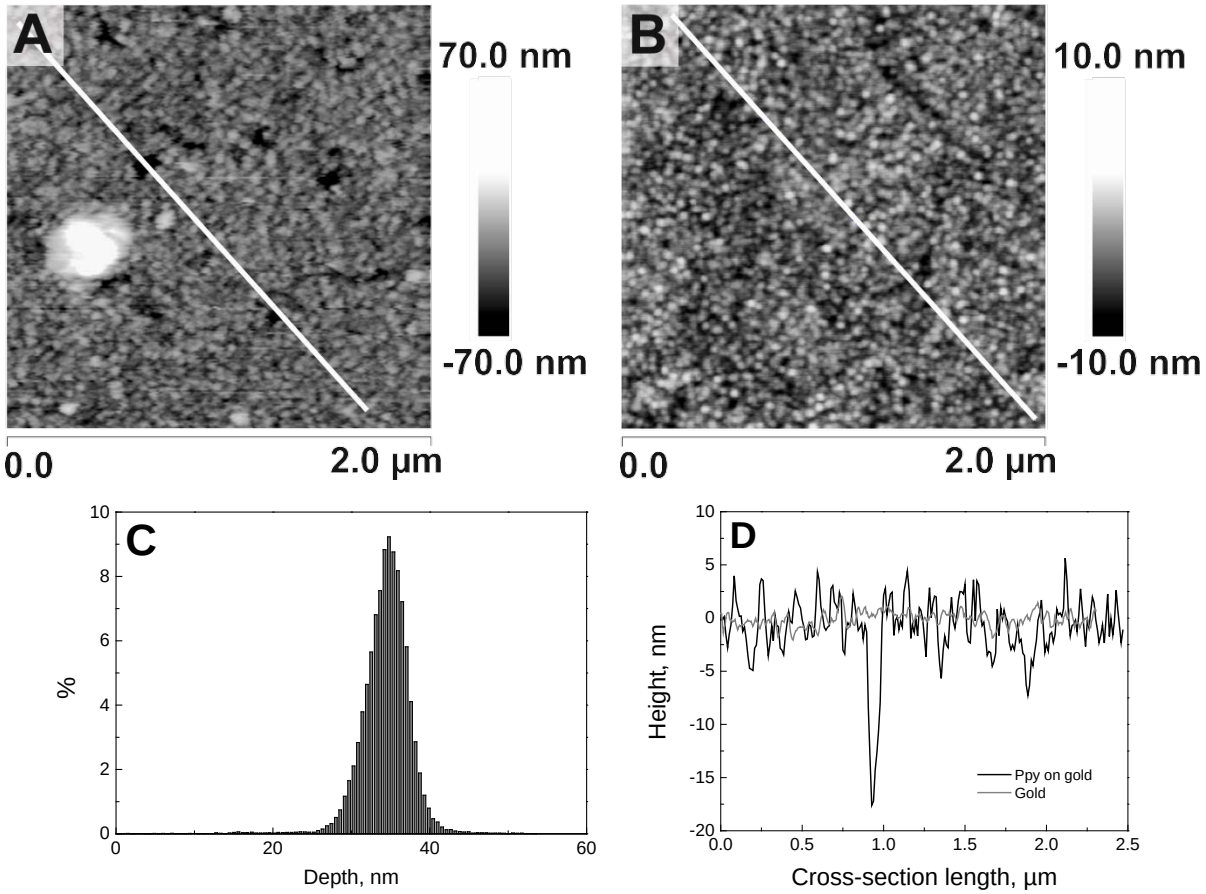

Figure 9 *AFM images of A) the formed Ppy layer (height scale 140 nm, polymerization conditions: 50 mM of pyrrole dissolved in PBS, pH 7.0 with 0.1 M of Na_2SO_4. The electrochemical formation of polymer coating was carried out by 300 potential pulse cycles as 1.1 V vs Ag/AgCl/KCl$_{sat.}$ for 10 s and 0 V vs Ag/AgCl/KCl$_{sat.}$ for 1 s) and B) gold surface before the polymerization (height scale 20 nm), with the dimensions of both images being 2 × 2 µm^2; C) statistical distribution of surface roughness and D) cross-sectional topography of Ppy layer (black line) and gold surface (gray line). A large pinhole that was crossed in part A is visible in part D as a deep pit.*

As it was determined the 'island'-based formation of Ppy layer, the size of the initial pyrrole micelles dispersed in buffer should also have a high impact to the obtained structure of polypyrrole. The average size of such pyrrole-based emulsion nanodrops was observed by DLS. It was determined that in the solution used for the electrochemical formation of the Ppy layer, pyrrole emulsion nanodrops of 80 nm average diameter dominated when the initial concentration was 50 mM and average nanodrops of 325 nm

was dispersed in buffer containing 500 mM of monomer concentration. These results support the previous statement that the initial monomer concentration is of high importance to the final polymer film. The polymerization of large monomer micelles results in the formation of rough, doughnut-like film and small micelles form uniform grainlike structures despite the fact, the number of pulses for the formation of 50 mM pyrole was 15 times larger than the number of pulses used for the formation of film from the higher concentration of Py. The previous studies have shown that both Ppy and gold were biocompatible [12, 222], hence, the presented result could be impetus for the further investigation of such kind of Ppy films suitable for some technological applications.

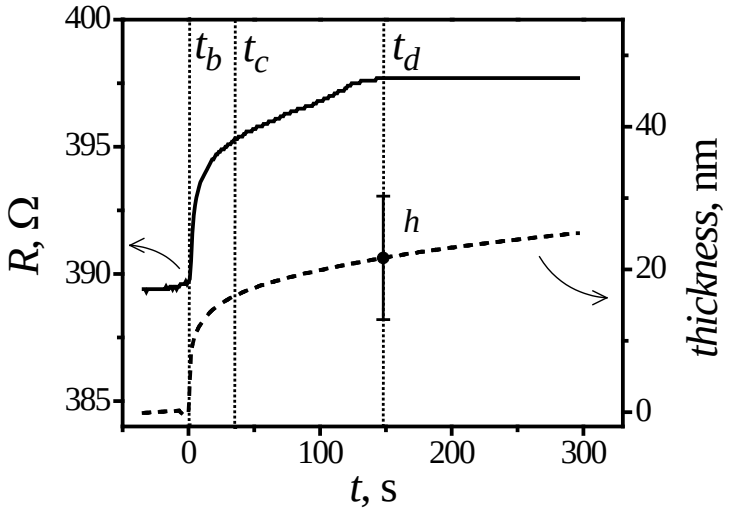

Figure 10 *Motional resistance R and thickness of the Ppy layer calculated using the Sauerbray equation and registered Δf, taking into account that the density of Ppy is 1.25 g cm^{-3}. Synthesis procedure was the same as in Figure 9.*

The repulsion experiments were executed with the thick polymer layer formed using 500 mM of initial polymer concentration. For this cyclic voltamperometry was applied. Method provides opportunity to follow the sequential changes of current, recognize current instability problems and observe possible outcome. As it is presented in Figure 11, the cyclic polarization of Ppy-modified electrode was performed at four different potential ranges (0-1.2; 0-1.1; 0-0.95; 0-0.9 V *vs* Ag/AgCl/KCl$_{sat.}$). If the upper potential range value reached 1.0 V, clear current instability was observed and the Ppy layer was repulsed out from the Au layer after 10 potential cycles. Simultaneously, the interface of Ppy and electrode surface could be affected because of the repulsion of Ppy. In previous studies it was shown that gold formed gold oxide film at the potential range

of 1.0-1.2 V *vs* Ag/AgCl/$KCl_{sat.}$, potential scan rate was 20 mV/s. The reduction of gold oxide started at potentials exceeding 0.4 V [223]. Hence, during cyclic polarization Au-based electrode oxidation of Au took place with formation of gold oxides [224-226]. The pH of the media was also very important for the oxidation of gold surface. It was demonstrated that oxidation of Au in aqueous solution, at pH 7.0, started when potential exceed 1.0 V *vs* Ag/AgCl/$KCl_{sat.}$ [225]. The results of these experiments are in agreement to the published data.

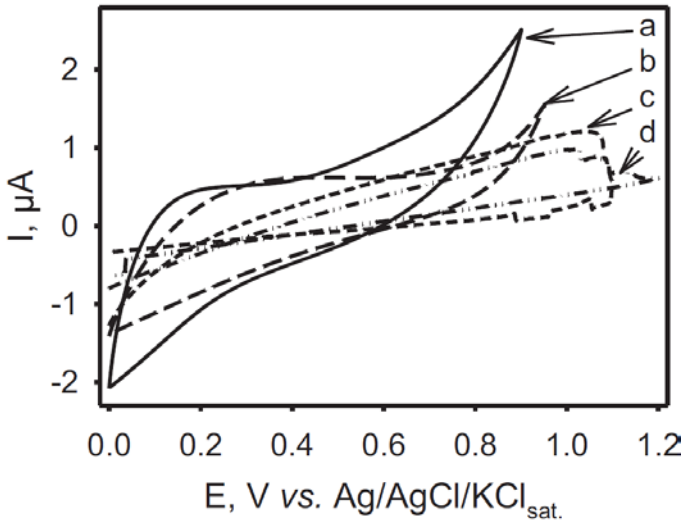

Figure 11 *Cyclic voltammograms of gold electrode and electrochemically deposited Ppy film in PBS; potential ranges: a) 0-0.9 V; b) 0-0.95 V; c) 0-1.1 V and d) 0-1.2 V vs Ag/AgCl/$KCl_{sat.}$; potential scan rate was 20 mV/s vs Ag/AgCl/$KCl_{sat.}$*

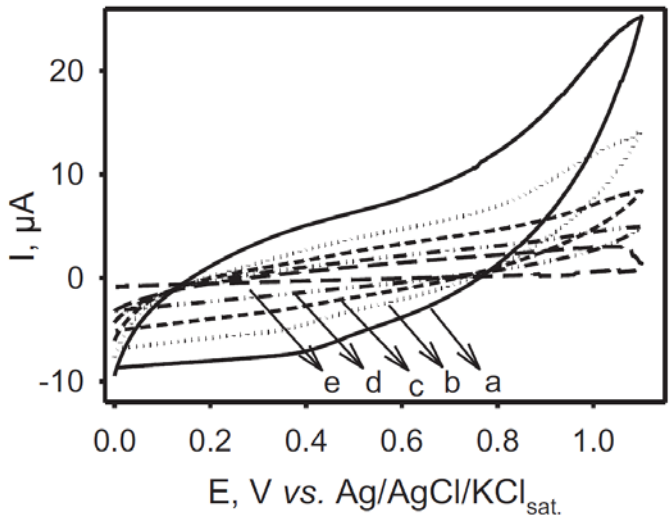

Figure 12 *Cyclic voltamograms of Ppy layer on gold electrode: (a) 3rd, (b) 5th, (c) 7th, (d) 9th, (e) 10th cycles at potential range 0–1.1V vs Ag/AgCl/$KCl_{sat.}$. Potential scan rate was 20 mV/s vs Ag/AgCl/$KCl_{sat.}$.*

The Ppy film from the gold layer deposited on the quartz slice was repulsed. After this procedure the Au-layer became significantly thinner and even some distinct cracks appeared on this film. For the preparation of biosensors it has been mentioned that usual thickness of Ppy film could be in the range from a few micrometers to several angstroms [157], but the Ppy layer on the not noble metal electrodes could be thicker by several times and it exceeded tens of micrometers [227-229]. The thicker Ppy film on the carbon or stainless steel or other metal surface was described as it provided an excellent adhesion [227, 230]. This ability of Ppy was explained by delocalized charge at the metal surface and it has shifted the corrosion potential towards positive side.

Cyclic voltammograms registered during the repulsion of Ppy film are presented in Figure 12. The first cycle of cyclic polarization of Ppy is complete and smooth. During the next cycle the current instability is clearly observable when the potential exceeds 1.1 V *vs* $Ag/AgCl/KCl_{sat.}$. It can be also noted that the first cycle is the broadest and the current (ΔI) is significantly reduced from cycle to cycle.

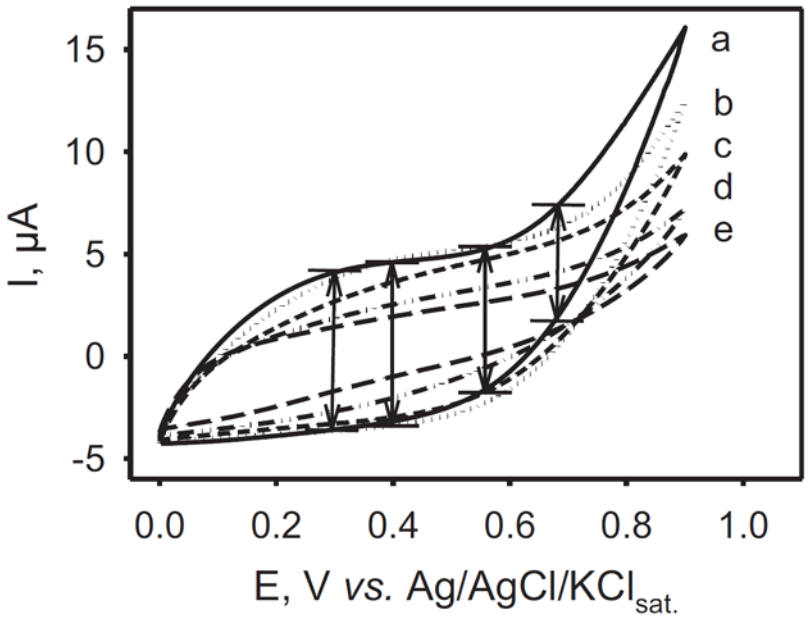

Figure 13 *Cyclic voltamograms of Ppy film: (a) 2nd, (b) 4th, (c) 6th, (d) 8th, (e) 10th cycles. Other conditions were the same as in Figure 11.*

It was found that during repulsion of the Ppy the ΔI decreased (Figure 13). Loop width shrinked by 60% from the first to the last 10th cycle regardless of the potential, at which the width was measured, whereas the repulsion of Ppy film at some extent is the opposite process to the polymerization, therefore reduction of the CV-loop is a measurable indication of repulsed Ppy film (Figure 14). The typical formation of

conducting polymers has been mentioned as the increased charge passed through working electrode as a function of the number of potential cycles [217]. During the typical formation of Ppy, the increase of current was observed which was related to the formation and elongation of Ppy oligomers, but during repulsion of the Ppy the reverse process occurs and the thickness of film is reduced (Figure 13).

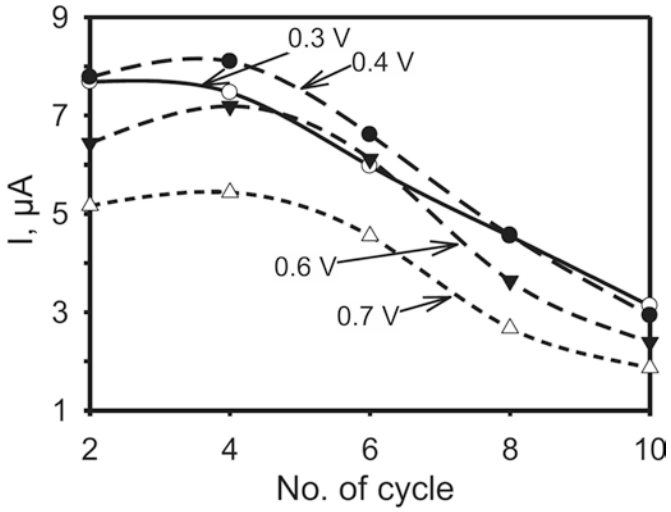

Figure 14 *The decrease of cycle loop width (ΔI) during cycling of potential in the range of 0-0.95 V vs Ag/AgCl/KCl$_{sat.}$. Width of cycle loop (ΔI) was measured at potentials of 0.3, 0.4, 0.6 or 0.7 V vs Ag/AgCl/KCl$_{sat.}$. Other conditions were the same as in Figure 11.*

An additional observation of Ppy film stability gave information about influence of aqueous solution [231]. According to the data of described study it is obvious that in aqueous solution oxidation of Ppy was mainly possible and swelling of film was leading to the film degradation. The impact of aqueous solution in reported study was concluded after Ppy was soaked in PBS for various periods of time and the impedance was measured before and after soaking. The results of the referred article were not indicating any instability of Ppy backbone. However, the electron transfer process was restricted due to the possibly partially isolate electronic communications between polymer molecules in the Ppy film [231]. Hence, the stability of Ppy film on the Au-based substrate was evaluated by potential cycling from 0 to 0.9 V *vs* Ag/AgCl/KCl$_{sat.}$. It was found that after 1000 cycles the Ppy film was still stable and it was not repelled from the Au surface.

Conclusions of 3.1. section

Polypyrrole films were electrochemically synthesized and repulsion possibility of the Ppy film by potential cycling was investigated. It was found that the initial monomer

concentration has a huge impact on the obtained Ppy layer on the electrode. Using 50 mM of initial monomer concentration smooth and small grain like structures are obtained. However, when the concentration is 10 times higher rough and donugth-like structures are obtained with the average size of 14 μm. From the EQCM data it was determined that polymerization of pyrrole is not a homogenious process, but is executed in different places depending on the adsorbed monolayer and a partial bloking of the electrode by already polymerized Ppy is observed.

It was found that the efficiency of repulsion of the Ppy layer depends on the applied potential value and it is the most efficient if it exceeds 1.0 V *vs* Ag/AgCl/$KCl_{sat.}$. The repulsion of Ppy film from the gold-based substrate was observed by decreased CV-loop during cyclic polarization of the gold electrode with Ppy layer. The results let us to suggest how a controlled repulsion of Ppy layer from gold-based substrate could be performed. It is asumed that Ppy layers obtained by controlled repulsion of Ppy film could be applied for various purposes including biomedical applications in scaffold design or environmental tasks related to the development of semi-permeable membranes suitable for water purification. It is important to note that even in the presence of dissolved oxygen a very stable Ppy layer is formed on the gold electrode surface what opens a new avenue for formation of molecularly imprinted Ppy based layers. Overoxidation forms carboxyl, carbonyl and hydroxyl groups in Ppy, therefore, such groups are capable for the electrostatic interaction with imprinted analyte what potentially increases selectivity and sensitivity of formed Ppy layer.

3.2. Formation of molecularly imprinted polypyrrole

Polypyrrole is a very popular conducting polymer, which could be used in a very wide range of applications. In this chapter two of possible applications are presented. Here it is demonstrated that electrochemically synthesized polypyrrole with DNA or caffeine imprints could be used as a sensor for the same molecules. Firstly, DNA molecular imprints were synthesized on the graphite electrode using potential pulse sequence and cyclic voltammetry methods and it was determined that PPS is more suitable for the detection of analyte. For this reason the second molecular imprints for two xanthine derivatives were accomplished with PPS method. However, as the EQCM method was

applied for the formation of imprints the electrode was changed from graphite to quartz disk with the thin layer of gold.

3.2.1. Molecularly imprinted polypyrrole for DNA determination

Electrochemical sensors for target-DNA detection are applied in various practical applications including environmental monitoring [232], evaluation of polymorphism [205], detection of specific pathogens [233] or toxic agents like herbicide – atrazine [234, 235]. Chronopotentiometric and voltammetric methods are applied in electrochemical DNA sensors [233, 236, 237]. Early works on electrochemical DNA sensors have been mainly based on the application of electrochemical labels suitable for the indication of immobilized single stranded DNA (ssDNA) interaction with target-DNA, which is present in the sample. Other applications of Ppy for DNA determination involved the direct electrochemical detection, which is carried out by monitoring of target-DNA hybridization induced conductivity changes of DNA/Ppy composite [215]. A label-free electrochemical detection of DNA hybridization based on electrostatic modulation of the electrochemically driven chloride ion-exchange of modified polypyrrole-bilayer films deposited at microelectrodes has been also reported [238].

The above described methods for the target-DNA analysis are based on the immobilization of biomolecules on the conducting polymer surface. However, such sensors have limited applicability due to poor chemical and physical stability of immobilized ssDNA even if it is efficiently immobilized. Therefore, molecularly imprinted polymers and artificial receptor based sensors gained the importance as a possible alternative to other affinity sensors (e.g. immunosensors, DNA sensors, etc.), which are based on immobilized biomolecules.

The aim of this section of doctoral dissertation was to perform electrochemical polymerization of molecularly imprinted polypyrrole (MIPpy) with template-DNA. The comparison of two electrochemical polymerization methods (electrochemical synthesis by sequence of potential pulses and by potential cycling) was performed. Nonimprinted polymer (NIP) or MIP modified pencil graphite electrodes were investigated using DPV. Differences of guanine oxidation peaks were evaluated as analytical signals.

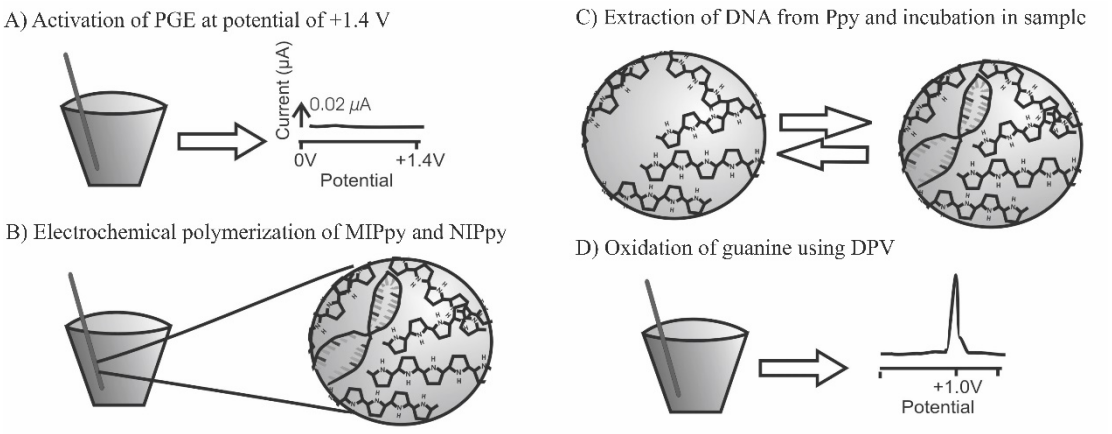

Figure 15 *Schematic presentation of procedures and manipulations applied for MIP formation and target-DNA detection. A) Activation of PGE, at potential of 1.4 V; B) Electrochemical polymerization of MIPpy and NIPpy; C) Extraction of DNA from Ppy and incubation in sample; D) Oxidation of guanine by using DPV.*

Electrochemical polymerization of Ppy was performed in order to modify electrodes by NIPpy and MIPpy. During the formation of the MIPpy layer the polymerization was carried out in 50 mM of pyrrole with 5 ppm template-DNA. Figure 15 represents the procedures applied in this study. The polymerization mixture was produced by thorough mixing of the monomer with the template-DNA at a certain ratio. During the electrochemical polymerization of Ppy the template-DNA molecules were captured in the matrix of Ppy. After electrochemical polymerization the washing procedure was performed in order to ensure the complete extraction of template-DNA from Ppy matrix while forming cavities complementary to target-DNA. It should be noted that the template-DNA used during the electrochemical polymerization process is identical to the target-DNA.

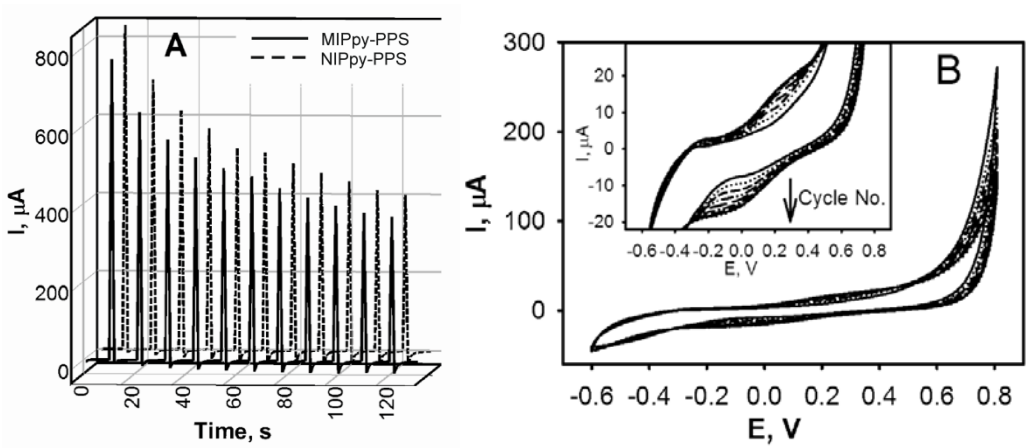

Figure 16 *Amperometric signals registered during: A) electrochemical formation of NIPpy-PPS and MIPpy-PPS by means of potential pulse sequence; B) electrochemical formation of NIPpy-CV by means of cyclic voltammetry.*

The electrochemical formation of the polymer on the working electrode is represented in Figure 16. During the electrochemical formation of NIPpy-PPS and MIPpy-PPS it was detected that the current registered during polymer formation has slowly decreased (Figure 16 A). One of the most plausible explanations of this effect is related to the conductivity difference of blank PGE and PGE modified by NIPpy-PPS and MIPpy-PPS. Electrochemical formation of MIPpy-CV- and NIPpy-CV-based layers was performed by potential cycling (Figure 16 B). During the electrochemical formation of MIPpy-CV and NIPpy-CV the obtained CVs were very similar (data not shown) in these CVs two specific oxidation and reduction peaks (at 0.2 V and -0.15 V, respectively) were observed. This effect of polymer formation is in agreement with cyclic voltammograms presented in other studies [159, 239].

DPV was selected as one of the most suitable methods for the detection of target-DNA. Guanine and adenine bases are the most important for DPV-based determination of target-DNA, because oxidation of guanine in AcB, pH 4.8, occurs at 1.0 V potential and adenine at 1.25 V *vs* Ag/AgCl/$KCl_{sat.}$ (Figure 15) [155]. Moreover, it was determined that oxidation of guanine can be affected by the pH of the selected buffer [240]. Therefore, the evaluation of guanine oxidation was performed only in AcB, pH 4.8. The oxidation of guanine is clearly detectable in voltammograms obtained by anodic stripping, thus, the evaluation of the concentration of target-DNA specifically bounded to MIPpy-CV and/or nonspecifically adsorbed on the electrode surface could be performed by estimation of these peaks. If MIPpy-CV electrode after the extraction of template-DNA was incubated in target-DNA containing solution and then evaluated by DPV, the typical DPV-peak, which is attributed to guanine oxidation, was observed. In this study during the determination of target-DNA only guanine oxidation peak current was estimated.

The results of the previous studies showed that the electrochemical synthesis method is important for the properties of the formed Ppy. In order to evaluate the influence of the Ppy formation method on the performance of MIPpy-based electrodes, different types of electrodes were designed. Potential pulse sequences were applied for the deposition the NIPpy-PPS and MIPpy-PPS layers on the electrode surface. The selection of the PPS method for MIP preparation was based on several of our previous studies [157, 160]. In one of these studies it has been shown that the PPS method is more

suitable for the design of molecularly imprinted Ppy because such MIPpy-PPS films possess better electrochemical activity, which is determined by their high specific surface area [156]. It should be noted that the comparison of potentiostatic and potentiodynamic electrochemical Ppy synthesis performed at the disposable graphite electrode have showed that depending on the preparation method the guanine oxidation potential can be shifted [241]. The diffusion of monomers in the polymerization solution is another important issue; the PPS in this respect is the most suitable polymerization method because it allows very easy adaptation of polymerization periods and duration of monomer equilibration by adjustment of the applied pulse profile [157]. Therefore, electrochemical polymerization by means of PPS polymerization method was performed by consecutive pulses of: (i) higher voltage (of 1.0 V), which is suitable for pyrrole polymerization, for 1 s and (ii) lower voltage (of 0 V) for 10 s, expecting that monomers and molecules of the template will equilibrate at the electrode surface during this frame of time. Hence, due to the applied PPS-based Ppy formation method the template-DNA molecules are equally distributed within the polymer matrix.

Four groups of disposable pencil graphite electrodes (based on NIPpy-PPS, MIPpy-PPS, NIPpy-CV and MIPpy-CV layers) were prepared. All of them after polymerization were pretreated using the same standardized washing procedure. In order to demonstrate that the removal of the target-DNA from the polymer by the applied MIPpy regeneration procedure is effective, two groups of NIPpy and MIPpy based electrodes were evaluated. One group of electrodes was incubated in target-DNA containing the sample and analyzed by DPV. The second group of electrodes was analyzed by DPV omitting the incubation step. In this way it was confirmed that template-DNA molecules were effectively washed out from the polymer surface during MIP preparation step. Figure 17 demonstrates the differences between DPV signals of incubated and not-incubated in target-DNA containing sample obtained by NIPpy and MIPy. In this way possible interfering effect of not removed template-DNA on DPV signal was eliminated. Figure 17 A illustrates that the target-DNA was not adsorbed on NIPpy-PPS-based electrode and in opposite – it was adsorbed on MIPpy-PPS-based electrode, because oxidation peak of guanine was registered. As follows from studies evaluating copolymers of polypyrrole, 3-pyrrolylacrylic acid [154] and poly[pyrrole-co-(N-pyrrolyl)-caproic acid] [155] some nonspecific adsorption of target-DNA can occur directly on the polymer

surface. Therefore, in our study method of subsequent comparison of not incubated and incubated NIPpy was applied and in the same way the comparison of not incubated and incubated MIPpy eliminates any possible distortion of results by nonspecifically adsorbed target-DNA.

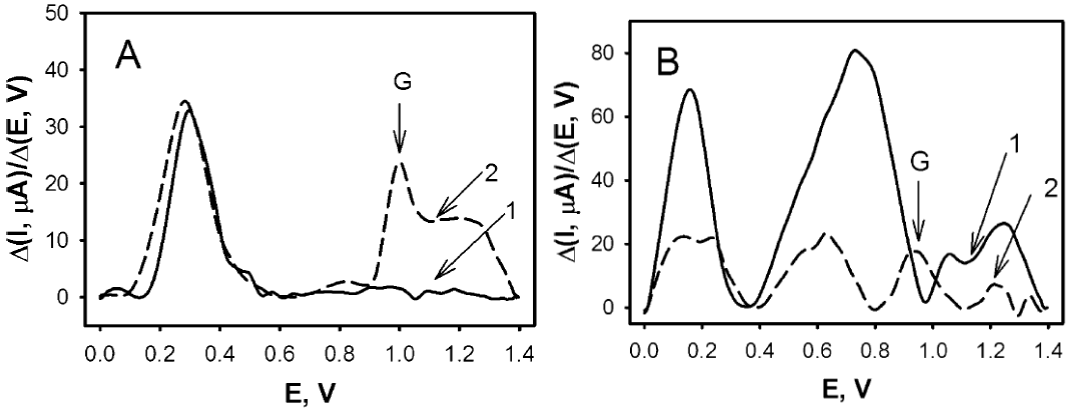

Figure 17 *Differences in differential pulse voltammograms of NIPpy and MIPpy modified electrodes (presented differences were calculated between analytical signals before and after incubation). A) NIPpy-PPS and MIPpy-PPS; B) NIPpy-CV and MIPpy-CV. 1) at NIPpy surface, 2) at MIPpy surface, G: guanine oxidation peak at 1.0 V potential. 5 ppm of target-DNA was dissolved in 50 mM phosphate buffer, pH 7.4, with 20 mM of NaCl. DPV was carried out in 500 mM acetate buffer solution, pH 4.8, with 20 mM of NaCl.*

The MIPpy formation and the principle of functioning are explained by three dimensional polymer matrix formation, which is complementary to the imprinted template molecule [159]. The complementary cavities are formed within the polymer during chain branching and cross-linking processes in the presence of the template-DNA molecule. As the >N–H group of the pyrrole unit can form the hydrogen bond with the >C=O groups of DNA nucleobases, the cavities formed are geometrically and functionally complementary to the structure of the target-DNA [157-160]. In contrast to some other studies, in pulsed amperometric polymerization we applied the upper potential equal to 1.0 mV, which is similar to the guanine oxidation potential [156]. It means that during the polymerization process guanine oxidation could occur. As shown in Figure 17 A the guanine oxidation peak registered by the MIPpy-PPS-based electrode was higher than that observed by the NIPpy-PPS-based electrode. Therefore, we conclude that guanine oxidation during the polymerization process had no negative effect on the three dimensional polymer matrix formation and cavities, which are complementary to the shape of the template-DNA molecule and to the location of functional groups, were formed in the Ppy film. For the formation of NIPpy-PPS

template-DNA was not used, therefore, no complementary cavities were formed. For this reason the target-DNA is adsorbing on NIPpy-PPS only nonspecifically and just at relatively low quantities. Therefore, no peak of guanine oxidation on the NIPpy-PPS was observed.

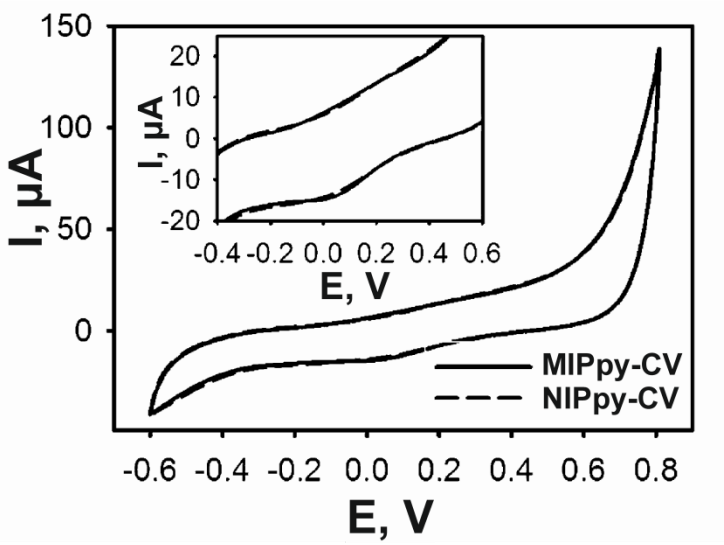

Figure 18 *Comparison of 10th cycles of CV's obtained during electrochemical formation of NIPpy-CV and MIPpy-CV.*

During the formation of NIPpy-CV- and MIPpy-CV-based layers the electrode potential was cycled in the range from –0.6 V to 0.8 V. The main reason for the selection of relatively low oxidation vertex potential (0.8 V) was based on the hypothesis that during the preparation of MIP the target-DNA can be oxidized if a higher potential would be applied. Comparison of 10th cycles of cyclic voltammograms obtained during electrochemical formation of NIPpy-CV and MIPpy-CV were similar (Figure 18). Therefore, the similarity of both cyclic voltammograms can be exploited as evidence illustrating that guanine was not oxidized during the electrochemical formation of MIPp-CV. Evaluation of NIPpy-CV- and MIPpy-CV-based electrodes demonstrated that no nonspecific target-DNA adsorption on NIPpy-CV-based electrode was detected and significant specific interaction with target-DNA was registered by the MIPPy-CV-based electrode (Figure 17 B).

Some researchers reported that potential cycling is a very efficient method for the formation of molecularly imprinted Ppy [158, 159, 242]. However results presented in our study (Figure 17 A, B) showed that pulsed amperometry is more efficient for the formation of MIPpy-PPS films. In the case of PPS-based synthesis, the polymerization

process consists of two major steps: (i) the polymerization of the monomer occurs during the higher potential phase (at 1.0 V) and (ii) during low potential phase (at 0 V) monomer and target molecule concentrations becomes equilibrated close to the surface of the electrode. In the case of electrochemical synthesis by means of cyclic voltammetry the potential is linearly changed versus time and at higher potentials the polymerization of the monomer is more intense. In this case due to the continuous polymerization process equilibration of template and monomer concentrations was not possible. Hence, during the preparation of MIPpy template-DNA molecules are entrapped within the three-dimensional polymeric matrix, but the linear decrease of the potential is influenced by some uncertainty of the slow diffusion of template-DNA molecules in polymerization bulk solution. Consequently, in the case of potential cycling, which was applied as an electrochemical polymerization method, some difficulties related to the formation of the polymer matrix can arise.

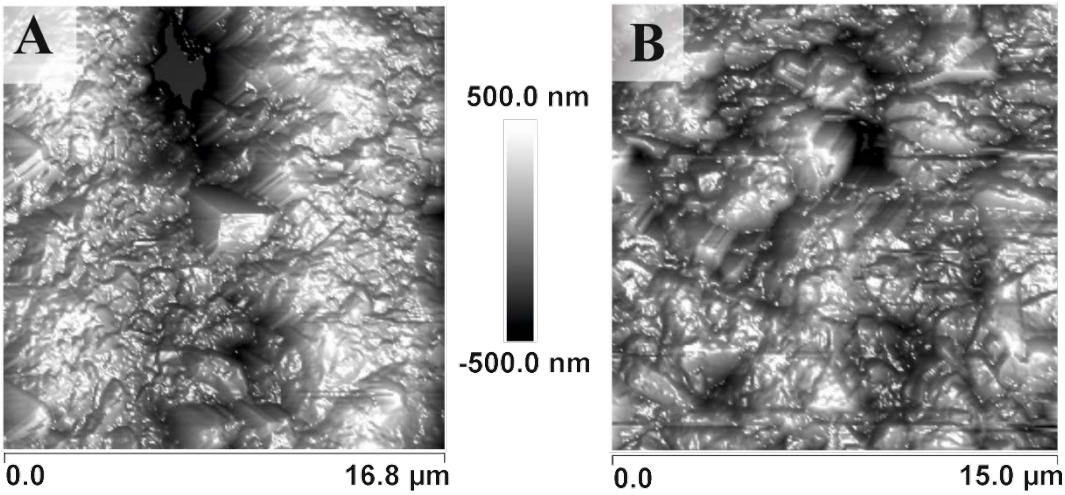

Figure 19 *The AFM images of: A) MIPpy-PPS and B) MIPpy-CV. MIPpy-PPS was formed applying potential pulse sequence and MIPpy-CV, using cyclic voltammetry.*

Next factor influencing the template molecule distribution in the final polymer structure is the ratio of monomer and template molecules. In this study the concentration of the monomer was 50 mM while the concentration of template-DNA was 5 ppm. Other studies have reported that the ratio of monomer and template molecule can vary from 2.5:1 to 25:1 [157-159]. Hence, the ratio of template and monomer used for the preparation of MIPpy layer was significantly higher. Taking into account the high molecular weights of template-DNA molecules and slow macromolecular diffusion rates, the electrochemical formation of MIPpy layer by means of potential pulse

sequence is more efficient in comparison to cyclic voltammetry; as during the low potential phase, which is 10 times longer than the high potential polymerization phase, the equilibration of template-DNA concentration close to electrode surface is more efficient. The presented results of this study confirm that if electrodes are modified using the PPS method (Figure 17) the specific interaction of target-DNA is stronger on MIPpy-PPS- than on MIPpy-CV-based films.

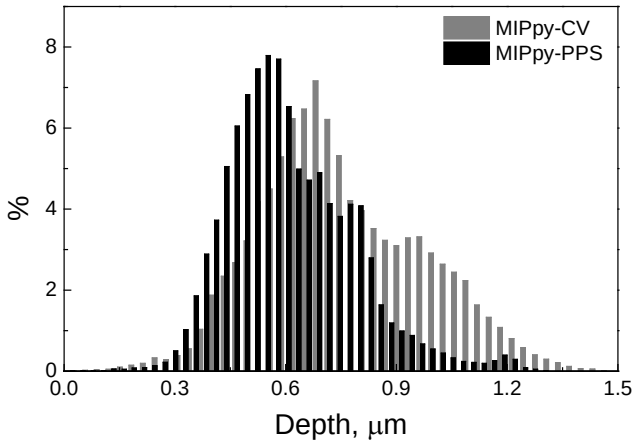

Figure 20 *MIPpy-PPS and MIPpy-CV surface roughness distribution measured by AFM.*

AFM was used to evaluate the surface structure of the obtained Ppy-modified electrodes (Figure 19). The AFM image illustrated the spheres-based structure of the Ppy. It was found that approximately 95% of the formed MIPpy-PPS structures were from 0.2 to 1.2 μm height and the most of dominant surface features were of 0.55 μm height (Figure 20). The evaluation of features in MIPpy-CV showed that height describing values were shifted and this shift was in the range from 0.3 to 1.4 μm. Also it was found that the most of surface structures were of 0.74 μm height. The surface RMS values were calculated as well. They were 90 nm and 113 nm for MIPpy-PPS and MIPpy-CV, respectively. In some studies nucleation mechanism and elongation of polymer during electrochemical polymerization was evaluated, which is in agreement with here presented AFM features [217, 218].

Conclusions of 3.2.1. section

In this study electrochemical synthesis of MIPpy with template-DNA was performed. Comparison of MIPpy, which was formed using two different electrochemical methods ((i) by potential pulse sequence and (ii) by potential cycling electrochemical synthesis), showed that MIPpy, formed by both methods, is suitable for target-DNA determination

in the sample. The obtained results illustrated that potential pulse sequence based electrochemical polymerization was more suitable for MIPpy formation in comparison to polymerization performed by the potential cycling based method. Adsorption of target-DNA on the NIPpy was lower or unnoticeable if compared to interaction with MIPpy. The presented results indicate that the oxidation of guanine during MIP formation is not a crucial factor and MIP is successfully formed even if the upper vertex potential of potential cycling is varying within a range of 0.8 – 0.1 V *vs* $Ag/AgCl/KCl_{sat.}$. It should be noted that the sequence specificity of the formed MIPpy was not evaluated and this issue needs some further investigations.

3.2.2. Molecularly imprinted polypyrrole for caffeine determination

In the development of affinity systems the xanthine derivatives are very interesting due to their molecular structure (Figure 21). The main differences among the described xanthine derivatives are the number and place of methyl groups in the molecule marked as R_1, R_2 and R_3. Methyl group number and position affect stereo structure and donor/acceptor properties of xanthine derivatives. The pH also significantly affects donor/acceptor properties of these molecules. In MIP based systems these donor/acceptor properties could be efficiently exploited for analytical purposes.

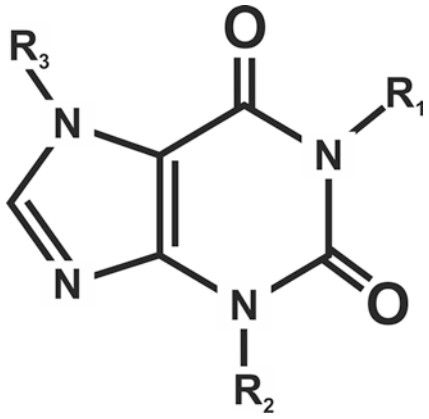

Figure 21 *Molecular structure of xanthine derivatives. The xanthine: R_1-R_2-R_3-H; theophylline: R_1-R_2-CH_3, R_3-H; caffeine: R_1-R_2-R_3-CH_3; and theobromine: R_1-H, R_2, R_3-CH_3.*

The EQCM is an attractive analytical signal detection tool, which has such advantages as low cost, simplicity, and low detection limits [243]. Other very important feature of EQCM is the ability to measure mass and energy dissipation properties of films together with shift of viscosity and density of the solution and therefore it is widely used in electrochemical applications [244]. In previous studies the EQCM in

combination with polypyrrole film was applied for enantioselective recognition of L-aspartic acid [245], bile acids like cholate, chenodeoxycholate, deoxycholateand taurocholate [246], for endocrine disrupter structural isomers of 1-naphthalenesulfonate [247] and others [248, 249].

The aim of this work was to develop an analytical system suitable for the detection of caffeine by EQCM. In order to achieve this aim caffeine molecularly imprinted polypyrrole ($MIPpy_{caff}$) was formed electrochemically on gold coated EQCM sensor. Formation of this $MIPpy_{caff}$ layer was performed by potential pulse sequence. From the previous measurements with DNA molecular imprints it was determined that PPS method is more suitable for the formation of molecular imprints. For this reason PPS was also selected for the formation of caffeine imprints. Association/dissociation kinetics and thermodynamical parameters of two xanthine derivatives (caffeine and theophylline) with the MIP-Ppy were analyzed.

Electrochemical polymerization of $MIPpy_{caff}$ was performed in order to modify gold-coated EQCM sensor. Polymerization was carried out using solution consisting of 5 mM of caffeine as template molecule, which was imprinted within formed polymer, and of 50 mM of pyrrole as monomer, which formed imprinted polymer, both were dissolved in PBS. Polymerization mixture was produced by thorough mixing of monomer with caffeine as a template molecule. In this study, the molar ratio of monomer and template molecule was also 10:1 as it is mostly recommended for the preparation of other MIPpy based sensors [157, 158].

During the electrochemical polymerization of Ppy the template molecules were captured in the matrix of polymer. A driving force of the process incorporating the template into the polymer is electrostatic interaction between charged parts of caffeine molecule and functional groups (-OH, -COH and -COOH), which appears in overoxidized polypyrrole. According to the most usual MIPpy formation strategy the template molecule used during electrochemical polymerization process is identical to the target analyte molecule. To ensure stable working conditions the same PBS was used to prepare polymerization mixture and standard solutions of theophylline and caffeine. During the sequence of potential pulses, which were applied for electrochemical polymerization of polypyrrole, the resonance frequency (Δf) has changed as the result of increased resonator mass due to Ppy adhered to the gold coated EQCM sensor.

After electrochemical polymerization the MIPpy-modified EQCM sensor was thoroughly washed with PBS until steady state of quartz crystal was reached what indicated the complete extraction of caffeine from MIPpy and the largest number of free cavities, which were complementary to caffeine, was obtained. To examine affinity and selectivity of the prepared MIPpy several solutions of theophylline and caffeine were prepared and analyzed by $MIPpy_{caff}$ EQCM sensor. Standard solutions were prepared in the 50 mM PBS, pH 7.0, as it was used for the preparation of polymerization bulk solutions in order to avoid distortion, which could be induced by changes of ionic forms of the molecules and, consecutively, their affinity related properties, such as capability to form donor/acceptor bonds. The first group of standard solutions contained 1 – 4 mM of caffeine and second group of standard solutions contained 1 – 4 mM of theophylline.

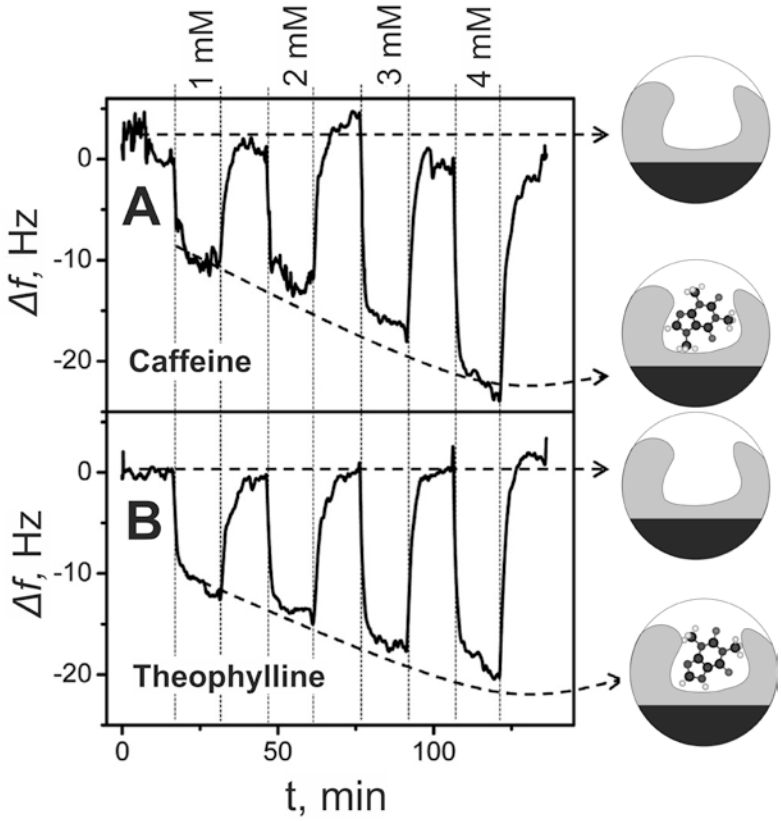

Figure 22 *Change in the resonance frequency (Δf, Hz) of the gold coated EQCM sensor modified with caffeine-imprinted MIPpy to the addition of different concentrations of A) caffeine B) and theophylline dissolved in 50 mM PBS, pH 7.0.*

Figure 22 demonstrates the change in the resonance frequency (*Δf*) of the EQCM sensor modified with $MIPpy_{caff}$ to the addition of solutions with different concentrations of caffeine and theophylline. Active sites of $MIPpy_{caff}$ (caffeine-imprinted cavities) after affinity interaction are filled with caffeine molecules and, therefore, formal mass of

MIPpy film is increasing. Moreover it was observed that the detection/regeneration cycles are reversible, thus after washing of caffeine or theophylline out from corresponding $MIPpy_{caff}$ layers the resonance frequency of EQCM sensor is recovering back to an initial level (Figure 22). The sensitivity of the $MIPpy_{caff}$ towards the analyte was calculated according to the *Δf* of the EQCM sensor *vs* concentration of the analyte. Here presented *Δf* is the difference of registered frequencies of the same EQCM sensor in the PBS without and with certain concentration of each analyzed analyte.

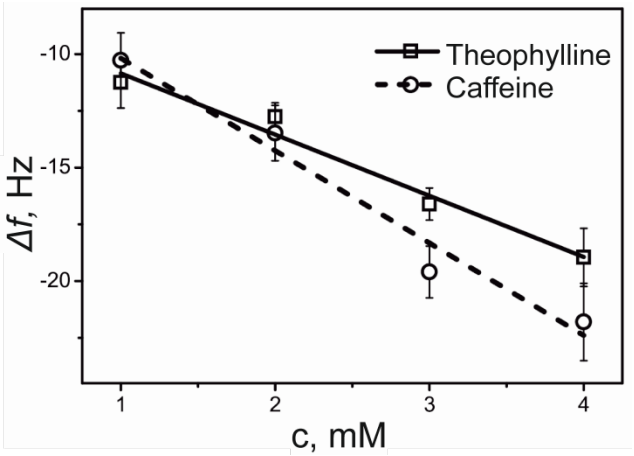

Figure 23 *Calibration curves of theophylline and caffeine obtained by EQCM sensor modified with MIPpy.*

Figure 23 represents the influence of caffeine and theophylline concentration on the *Δf*. The determined coefficients 'b' of the linear regression (y = a + b·x) for caffeine and theophylline are 4.1 ± 0.5 Hz/mM and 2.7 ± 0.3 Hz/mM, respectively. This data indicates that the EQCM sensor modified by $MIPpy_{caff}$ is more sensitive to caffeine than to the theophylline.

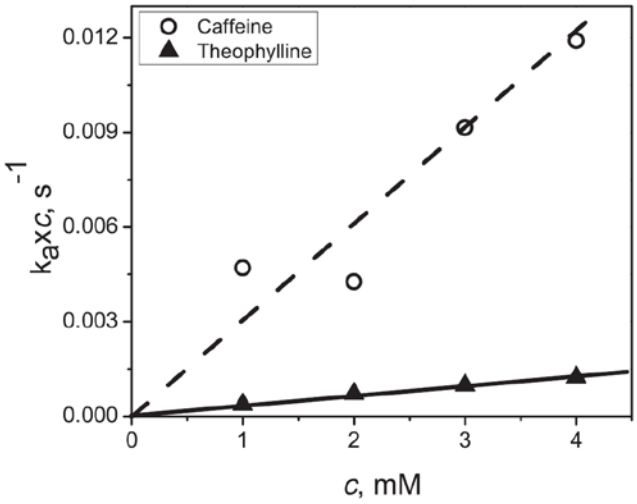

Figure 24 *Reverse characteristic of MIPpy association time $\tau^{-1} = k_a \times c$ with caffeine and theophylline vs concentration of caffeine (○) and theophylline (▲).*

Association and dissociation rate constants were estimated using data presented in Figure 22, which demonstrates the kinetics of theophylline and caffeine for different concentrations of analytes. These constants were determined according to the data corresponding to the initial stage of association and dissociation processes. Exponential growth and decay were replaced by linear function representing associated or dissociated amount of analyte in time. Figure 24 demonstrates the reverse characteristic association time $\tau^{-1} = k_a \times c$ (here k_a and c are association rate constant and concentration of analyte, respectively) as a function of concentration. The k_{a_theoph} and $k_{a\_caffeine}$ calculated from the slope of the straight lines (Figure 24) give the following values of association rate constants for both theophylline and caffeine with MIPpy: $k_{a\_theoph} = 3.18 \times 10^{-2}\ M^{-1}s^{-1}$ and $k_{a\_caffeine} = 30.6 \times 10^{-2}\ M^{-1}s^{-1}$. The dissociation rate constants (k_d) were calculated for different concentrations of theophylline and caffeine taking into account the averaged value. It was determined that k_{d_theoph} for MIPpy/theophylline complex was $2.1 \times 10^{-3}\ s^{-1}$ and $k_{d\_caffeine}$ for MIPpy/caffeine complex was $3.6 \times 10^{-3}\ s^{-1}$. The corresponding equilibrium dissociation constant (K_D) for MIPpy/theophylline and MIPpy/caffeine complex formation were $K_{D\_theoph} = 6.6 \times 10^{-2}$ M and $K_{D\_caffeine} = 1.17 \times 10^{-2}$ M. The values of equilibrium dissociation constants show that in the case of theophylline interaction with MIPpy it is 5.6 times lower than that in case of caffeine interaction with MIPpy. This means that caffeine has greater affinity towards $MIPpy_{caff}$ than the theophylline.

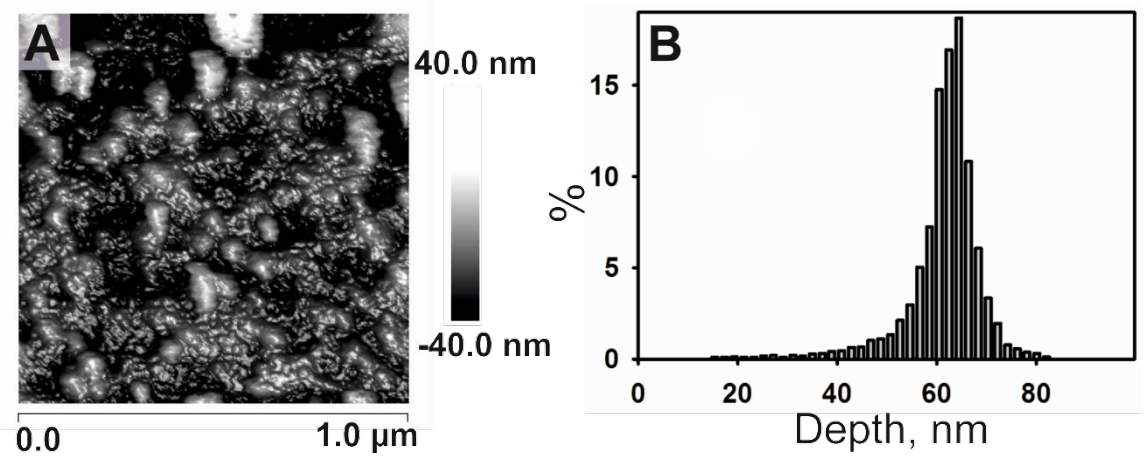

Figure 25 *The evaluation of dominant features of the MIPpy by AFM. A) The AFM image of the MIPpy film with caffeine imprints deposited on gold coated EQCM sensor. B) Height distribution diagram of the dominant surface features of caffeine-imprinted MIPpy film formed on the EQCM sensor surface.*

AFM was used to evaluate the dominant surface features of the obtained Ppy modified EQCM sensor (Figure 25 A). An AFM image of this study illustrate that spherical structures of Ppy are formed on the surface. It was found that formed MIPpy structures were very small in comparison to MIP of DNA and it was calculated that approximately 75 % of formed MIPpy structures were ranging from 58.5 to 68.3 nm in the height and the most of dominant height of observed surface features were 64.4 nm (Figure 25 B). The RMS was also calculated for this image. It was in the range of 4.6 nm, which is approximately 25 times lower in comparison to RMS calculated for DNA imprints. The major difference between these two imprints was the smoothness of the electrode, on which the structures were formed. For DNA imprints rough graphite rod electrode was used while for caffeine imprints a smooth gold electrode (RMS 0.74 nm, Figure 9 B) was choosen.

Conclusions of 3.2.2. section

Caffeine molecularly-imprinted polypyrrole was electrochemically synthesized on the EQCM sensor and it was applied for the determination of caffeine. Unique home-made flow-through cell was used for EQCM measurements. Using this system, standard solutions of theophylline and caffeine were actively administered through the cell, thus, the influence of diffusion was eliminated from the assessment of measured signal. Due to the selected liquid administration method continuous association/dissociation process was performed. Analysis of the obtained experimental data proved that the equilibrium of the interaction of $MIPpy_{caff}$ and dissolved caffeine at standard conditions is shifted towards the formation of MIPpy/caffeine complex while the equilibrium for the interaction of $MIPpy_{caff}$ and theophylline is shifted towards dissociation of MIPpy/theophylline complex. Therefore, the obtained caffeine-imprinted MIPpy demonstrated much higher selectivity towards caffeine in comparison with the selectivity towards its homologue – theophylline. It should be noted that the evaluations of EQCM signals are more sensitive if EQCM systems, which are able to oscillate at higher frequency, are applied. In addition, the registration of higher harmonics or dissipation signals could be applied [244].

3.3. Chemical synthesis of polypyrrole

The improved properties of the formed Ppy structures could be obtained by the addition of various nanoparticles, nanostructures, such as carbon nanotubes and others. In this section two different materials were inserted in the Ppy composite: gold nanoparticles and enzyme Glucose oxidase.

3.3.1. Polypyrrole composite with gold nanoparticles

Composites consisting of conducting polymers and metal nanoparticles (NP) have received considerable attention due to the potential possibilities to create suitable materials for electrocatalysis, chemical sensors, and microelectronic devices [250-252]. These composites were suggested as the possible layers for DNA sensing [253], for the protection and charge transfer in biosensors [201, 254-258], also for immobilization of antibodies [259] or cancer treatment [260]. Compared with composites constructed from insulating polymers, conducting polymers can serve as a novel electroactive relay among metal nanoparticles in the nanocomposites matrix [261, 262]. What is more important, such compounds could own interesting properties, including thermal energy transfer, which is not common for the bulk materials [263]. Therefore, the fabrication of novel composites based on metal NPs and conducting polymers would provide various interesting characteristics and new features in nanotechnological applications.

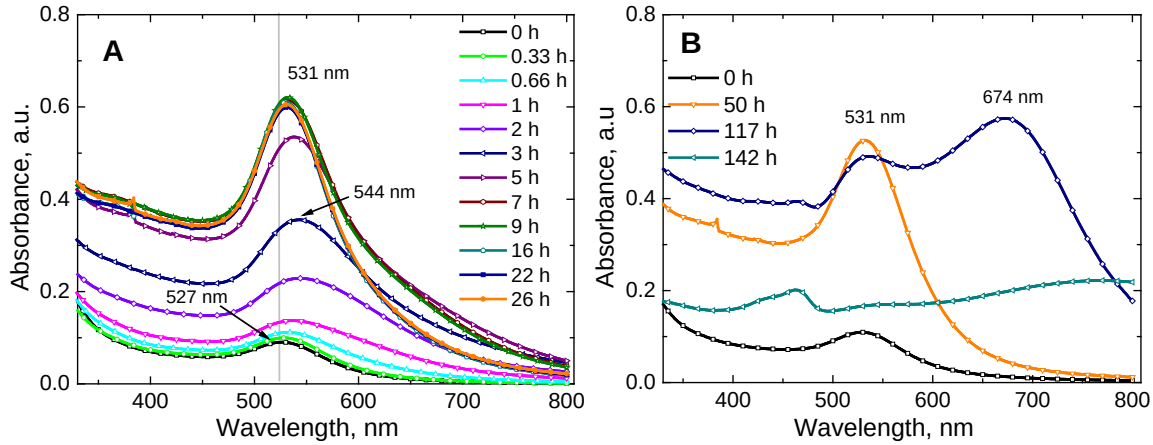

Figure 26 *Time dependent UV-Vis absorption spectra of colloidal gold nanoparticles in gold seeds solution after the addition of tetrachloroauric acid; A) the spectra registered from the initial mixture formation (0 h) until 26 h. Vertical grey line indicates the shift of the peak; B) the comparison of spectra registered after 0, 50, 117 and 142 h.*

The aim of this part of the work was to develop a single-step surfactant free synthesis of AuNPs/Ppy composite by using tetrachlorauric acid as gold source in the formation of AuNPs, and as an oxidant capable to initiate pyrrole polymerization reaction at room temperature.

Gold seeds of 13 nm were synthesized according to the protocol presented in experimental part (2.2.1 section) and were used for two main purposes: for the synthesis of larger gold nanoparticles and for the synthesis of gold nanoparticles and polypyrrole composites (Figure 6). After adding tetrachloroauric acid to the gold seeds solution some enlargement of gold seeds was observed possibly due to decomposition of $HAuCl_4$ and reduction of Au^{3+} to Au^0. This system was monitored by UV-Vis spectrophotometer (Figure 26). Initially, the increase of the absorbance intensity and a slight red shift was observed from 527 to 544 nm during the first 2 h. Later small blue shift was registered. After 7 h the peak reached 531 nm and become stable at this wavelength range as it is seen form the spectra monitored after 26 h (Figure 26 A). These shifts are related to the growth of gold seeds and formation of larger AuNPs. Moreover, some changes on the right slope of the spectra were observed. Firstly, it was growing together with the peak, but after 7 h small and after 16 h significant decrease was registered. This could be explained by the stabilization of colloidal solution and the increase of monodispersity of the nanoparticles. During growth process gold nanoparticles assumed different crystal forms and, therefore, the absorption peak becomes broader. In time the equilibrium of the growth was reached and the plasmonic peak of the particles became sharper. The stability of the AuNPs decreased after 117 h (Figure 26 B). The decrease of the intensity was observed without shifting the peak indicating the start of aggregation and precipitation processes. Aggregation process was also confirmed by the appearance of the second peak at about 674 nm wavelength. After 142 h the most of the particles were aggregated and dispersed at the bottom of the cuvette and acquired spectrum of the mixed solution is more influenced by scattering processes than by optical light absorption of the particles.

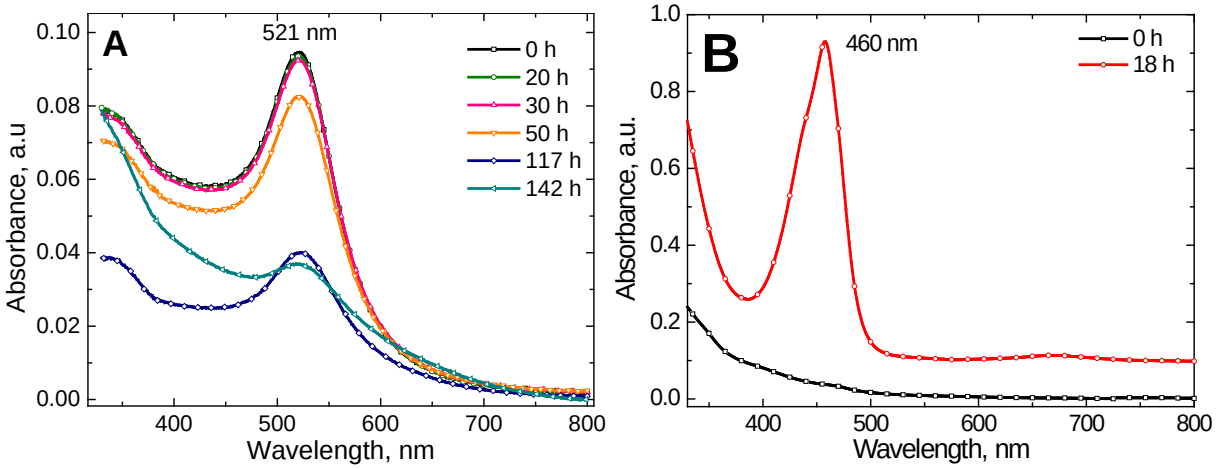

Figure 27 *Absorption spectra of A) gold seeds diluted in water and B) polypyrrole in buffer as a function of time.*

For the better understanding and comparison of the obtained results the control solution of gold seeds dissolved in distilled water up to the same concentration as it was in the previously presented experiment was prepared. The absorption curves are presented in Figure 27 A. The colloidal solution of gold seeds was stable until 30 h and later the absorption intensity started to decrease most likely due to the aggregation, precipitation, and sedimentation of gold seeds on the bottom of the cuvette. However, no shift of the absorption peak was observed.

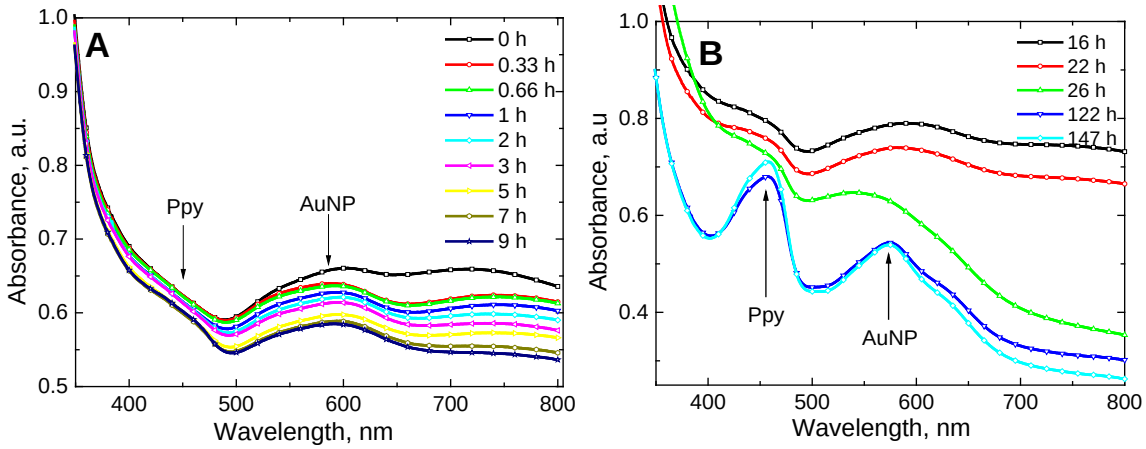

Figure 28 *UV-Vis absorption spectra of AuNP/Ppy composites in time A) from 0 to 9 h, and B) from 16 to 147 h during polymerization procedure. The concentration of pyrrole in the solution was 200 mM.*

Another direction of our research applying gold seeds was synthesis of gold nanoparticles and polypyrrole composites (AuNP/Ppy). The reaction mixture consisting of gold seeds, $HAuCl_4$ and pyrrole was prepared, and changes in UV-Vis spectra were recorded within 6 days (Figure 28). At the initial stage resonance modes of gold [264] at

750 nm were registered. In addition, the broad absorption band of gold seeds (where Au is in zero valent state) was observed at the interval 500 – 650 nm with the maximum intensity around 560 – 570 nm (Figure 28 A). This information suggests reduction of $AuCl_4^-$ ions. In comparison to the growth of AuNP when no monomer was added to the solution, here the peak is red shifted (final plasmonic peak of AuNP was at 531 nm and of AuNP/Ppy – 570 nm), which indicates that the growth of the AuNP is reinforced by the synthesis of Ppy. The peak, which is characteristic for polypyrrole formation (460 nm), was observed only after 7 h, but even up to 26 h it was still not well expressed. Also, relatively high scattering was noticed during all the measurements and only after 26 h it started to decrease. This might be explained by the light scattering from the pyrrole monomer micelles. Only after some time, when significant part of the pyrrole became polymerized, the light was more absorbed by Ppy and AuNP than scattered by micelles of unpolymerized pyrrole. Therefore, the background was reduced resulting in more expressed Ppy and Au plasmon peaks (after 122 h).

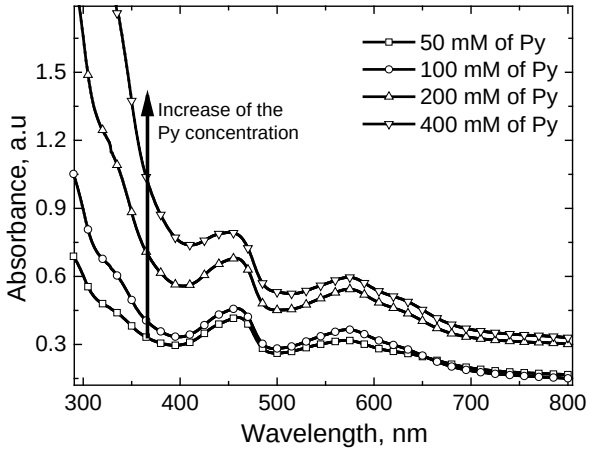

Figure 29 *UV-Vis absorption spectra of AuNP/Ppy composites formed at the 0.125 mM $HAuCl_4$ concentration and different pyrrole concentrations: 50, 100, 200 and 400 mM after 122 h of reaction.*

For verification of polypyrrole spectrum the chemical polymerization was initiated with the hydrogen peroxide at pH 1.0 and the absorption spectrum was registered in time. As could be seen in Figure 27 B UV-Vis spectrum of polypyrrole at the interval from 330 to 800 nm shows only the peak at 460 nm. Thus, during the AuNP/Ppy composite synthesis (Figure 28) other observed peak appears only due to the gold nanoparticles.

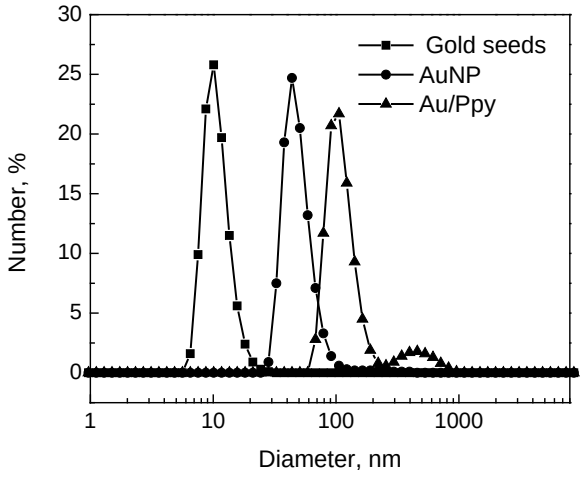

Figure 30 *The distribution of particle diameter measured by dynamic light scattering method: gold seeds (square), AuNPs after additional treatment by the $HAuCl_4$ solution (circle) and after the formation of AuNP/Ppy composites (triangle).*

Different concentrations of pyrrole (50, 100, 200 and 400 mM) were used to evaluate the influence of monomers concentration on the absorption properties of the AuNP/Ppy composites. The solutions were kept for 122 h and then spectra were registered. As could be seen from the Figure 29, only the intensity of the absorption of polypyrrole and gold plasmon band were changed but no shift of peaks was registered. This indicates that the tested concentrations of the monomer do not affect the size of the particles using 100 µL of prepared gold seed solution after 122 h of reaction. S.T. Selvan et al. also confirmed that mixing different concentrations of pyrrole with tetrachloroauric acid AuNP/Ppy composites of uniform 24 nm size are always obtained [265].

The size distribution of gold seeds, AuNPs and AuNP/Ppy composites formed in the presence of $HAuCl_4$ is presented in the DLS image (Figure 30). According to DLS data gold seeds diameter is in the range of 10 nm, after the treatment with $HAuCl_4$ solution and keeping for 147 h the size of AuNPs increased 5 times and was in the range of 51 nm. Bimodal distribution of the particle size was registered after gold seeds treatment with $HAuCl_4$ and pyrrole mixture after 147 h. For AuNP/Ppy composites one higher peak indicating 111 nm diameter of particles and another smaller one indicating 479 nm diameter of formed particles were observed.

The SEM measurements of gold seeds, AuNP and AuNP/Ppy composites were performed in order to evaluate the morphology of the particles and to compare the results obtained with the DLS method.

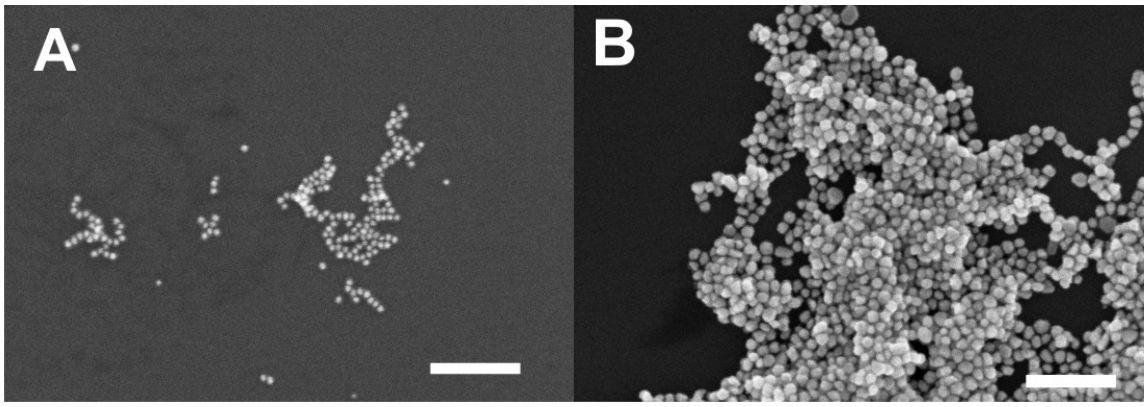

Figure 31 *SEM images of A) gold seeds and B) enlarged gold nanoparticles deposited on the silicon wafer. The bar corresponds to 200 nm.*

The obtained results correlated with the dynamic light scattering measurements. The gold seeds were about 10 nm in diameter (Figure 31 A). Enlarged gold nanoparticles were of 30 – 40 nm in diameter, although during the enlargement the round shape of the nanoparticles was lost and high heterogeneity was observed (Figure 31 B). The results of AuNP/Ppy composites obtained by DLS and SEM were more difficult to compare (Figure 32). Due to the absence of a detergent during the drying procedure the particles were agglomerated and it was not possible to distinguish the single particle and to evaluate the actual size. It is also possible that the aggregation started before drying in the solution of the polypyrrole. However, no separate gold nanoparticles on top of the polymer were distinguished that was recently done by B. Haghighi et al. [257].

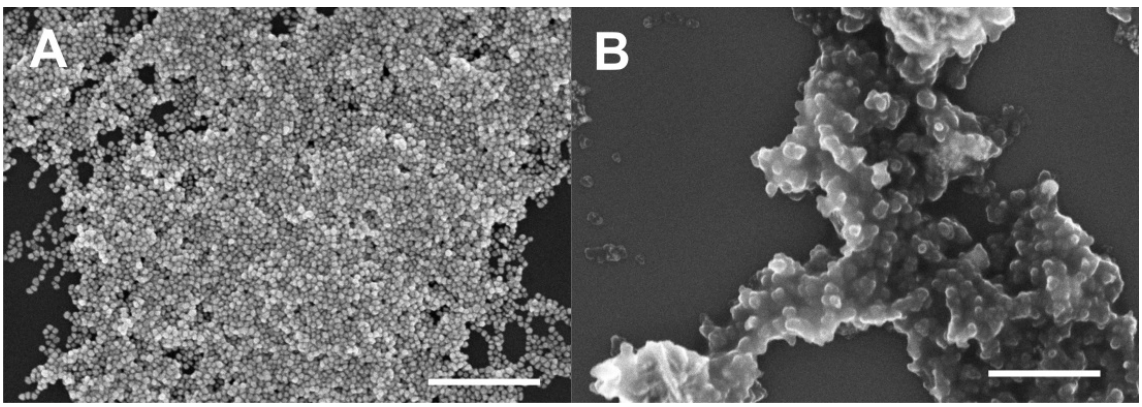

Figure 32 *SEM images of A) AuNPs and B) AuNP/Ppy composites deposited on the silicon wafer. The bar corresponds to 500 nm.*

Conclusions of 3.3.1. section

The obtained results indicated that gold nanoparticles were entrapped within the polymer layer during the polymerization procedure. Using this AuNP/Ppy composite synthesis protocol no separate core shell nanoparticles were observed by SEM, but the composites

of 100 – 200 nm were obtained. Also from the spectrophotometric results it was found out that gold nanoparticles were increased in size from 10 nm (gold seeds) to 40 nm (AuNP) or even larger when pyrrole is also present in the solution (AuNP/Ppy). The other scientists used some detergents for the separation of the particles, however, most of the detergents are not biocompatible, which is important if composites will be used for the experiments with living cells. Thus some new approaches of separation of the particles should be elaborated.

3.3.2. Development of enzyme/polypyrrole biocomposites

Biocomposites consisting of enzyme Glucose oxidase based core and polypyrrole shell have been developed [266]. Such nanoparticles can potentially be used for biomedical applications due to biocompatible polypyrrole shell [267]. Many nanostructures and nanoparticles based on Glucose oxidase core and conducting polymer polypyrrole [268, 269] or polyaniline shell [270] were developed. However, neither an internal structure, nor a stoichiometry of Glucose oxidase molecules and Ppy of these nanoparticles are still known. Therefore, the investigations of stoichiometry evaluation are of high interest.

In this part of doctoral dissertation the enzymatic polymerization of pyrrole induced by Glucose oxidase was investigated and the ratio of enzyme and monomer in the formed polypyrrole and Glucose oxidase biocomposite (Ppy/GOx) was quantitatively evaluated.

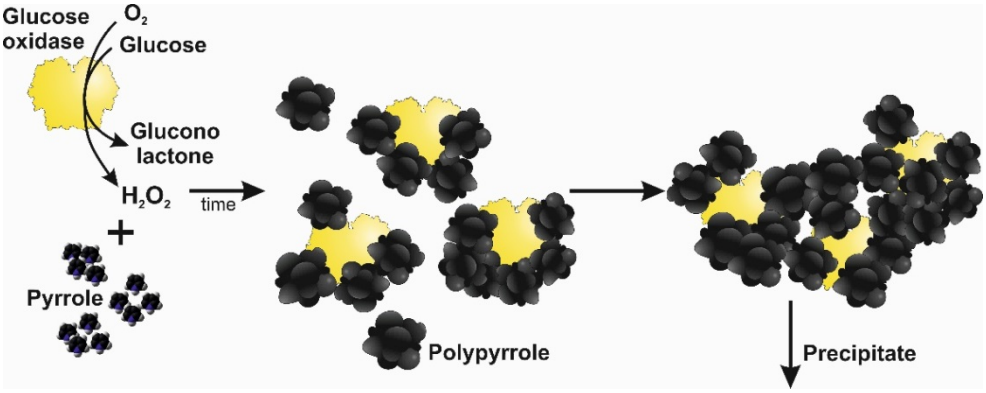

Figure 33 *Schematic representation of pyrrole polymerization induced by hydrogen peroxide generated in catalytic action of Glucose oxidase. GOx is surrounded by formed Ppy particles, later agglomeration and precipitation of such composites are observed.*

The enzymatic polymerization of pyrrole was evaluated using the DLS analyzer and UV-Vis spectroscopy. The predicted polymerization process and formation of the

Ppy/GOx biocomposites are presented in Figure 33. Enzyme, Glucose oxidase, in the presence of oxygen catalyzes the oxidation of glucose to gluconolactone and hydrogen peroxide. In close proximity of the enzyme the medium is more acidic due to the hydrolysis of gluconolactone to gluconic acid. Together with hydrogen peroxide, which is generated in the enzymatic reaction, gluconic acid creates a favorable environment for the oxidative-polymerization of pyrrole. For this reason the encapsulation of enzyme inside the polypyrrole is highly probable. During the polymerization procedure the Ppy/GOx biocomposite increases in size due to the formation of Ppy layer around the enzyme. Moreover, the aggregation of the Ppy/GOx biocomposite is also possible. Thus, precipitation of agglomerates was observed during the course of polymerization. As the monomer of pyrrole is poorly soluble in water even after the ultrasonic treatment the micelles of monomer are registered with DLS (Figure 34 A, the lowest curve at 0 h). In general, GOx is soluble in water, but some hydrophobic residues are also present. If the enzyme with its hydrophobic residues attaches to the micelle of the monomer, the polymerization of such micelle is also expected. Most likely both of the processes are possible and take place in the polymerization solution.

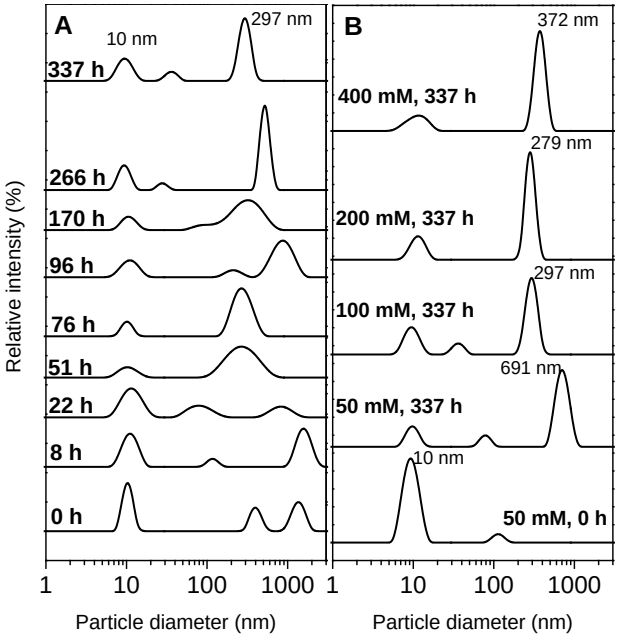

Figure 34 *DLS based evaluation of polymerization and biocomposite formation A) at 100 mM of pyrrole, in a time frame from 0 to 337 h and B) at different concentrations (50 mM, 100 mM, 200 mM and 400 mM) of pyrrole after 337 h of polymerization. For additional comparison a DLS spectrum of 50 mM pyrrole at 0 h is also presented in the B part.*

The size variation of Ppy/GOx biocomposite, which was formed from the solution containing 100 mM of pyrrole and 1 mg mL^{-1} of GOx, was followed using the DLS

analyzer in the polymerization time frame from 0 to 377 h (Figure 34 A). At the initial stage (0 h) three particle size peaks were observed. The first peak at 10 nm was registered in all samples and it is attributed to the dissolved Glucose oxidase. The other two DLS peaks could be attributed to the micelles of pyrrole, which are formed in water upon ultrasound treatment during the preparation step. The relative intensity of the GOx peak at 0 h is the highest in all evaluated samples at four different Py concentrations, which indicates that the quantity of light scattered from dissolved GOx is more significant than that from dispersed pyrrole micelles, which were formed in the initial solution before polymerization. During the polymerization process, the situation in the system has altered. First of all the composition and properties of materials inside the cuvette has changed. The monomer of pyrrole is more transparent in comparison with Ppy and in aqueous solution it is probably assembled in small micelles; however, the Ppy is of a very different nature. Dark color and randomly aggregated agglomerates are expected to form during the polymerization process. In addition, no clear simultaneous growth and/or aggregation of the composites in time are observed. During the course of the reaction new polymerization centers are continuously being formed and new Ppy/GOx biocomposites are generated. For this reason new and small peaks attributed to aggregated structures are observed at different time intervals. The DLS results illustrate that the intensity of the peak, which is representing the smaller sized Ppy/GOx biocomposites, is lower than that of the larger ones. This effect could be based on the fact that larger particles scatter more light. Due to all the mentioned aspects the relative intensity of GOx peak is decreased in comparison to the other peaks during the course of polymerization. However, after 76 h the small increase of the GOx peak could be observed in comparison with that attributed to the formed Ppy/GOx biocomposites. This change could be elucidated as the beginning of the precipitation of larger Ppy/GOx biocomposite aggregates to the bottom of cuvette as no colloid-stabilizing agents were used. For this reason the increase of the relatively high amount of free GOx was observed in the sample. Besides, a part of visible light is absorbed by the polymer and could influence the final amount of the light, which is reaching the DLS detector. Due to all the reasons mentioned above, the accuracy of quantitative comparison of DLS results is limited when the peak height is evaluated. Therefore, this method is better suited for qualitative than for quantitative measurements. The principle of the DLS measurement is

to register the dispersed light from the particles in the time frame and from the obtained results the size of idealized round shaped particles is calculated. In this respect all the scattered light in one measurement is attributed to 100% and it is distributed between the whole range of observed DLS peaks. The intensity from the single particle depends on several reasons – the deviation of the particle shape from the ideal sphere, the ability of the particle to scatter the light and the ability to absorb it. Moreover, in the presence of four different concentrations of monomer no principal difference in the polymerization process was noticed. After the same time interval (Figure 34 B) all DLS results showed a similar tendency: the peak attributed to GOx is reduced and the size of the Ppy/GOx biocomposite is in the range from 300 to 700 nm. The larger Ppy/GOx biocomposites could hardly be registered due to the relatively fast aggregation, which is followed by precipitation.

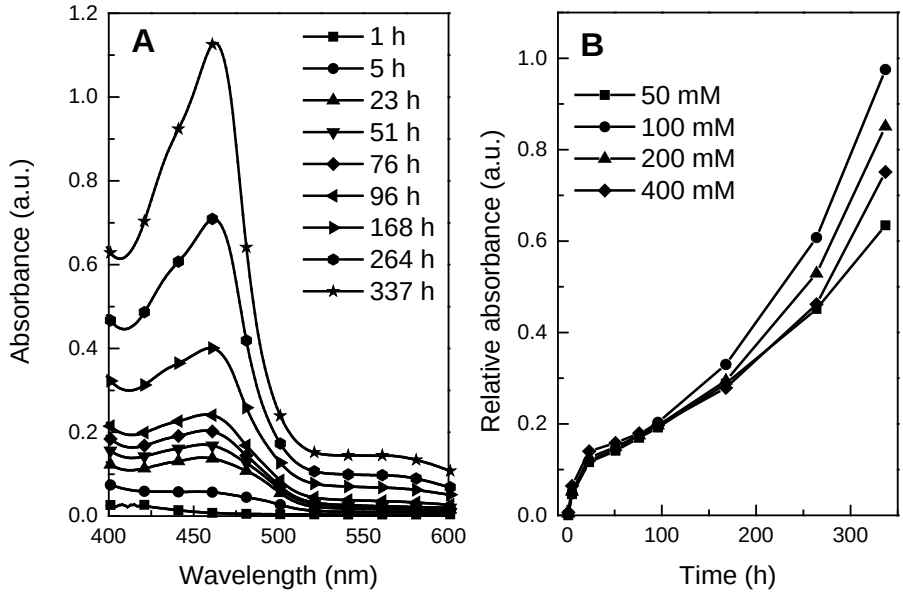

Figure 35 *Spectroscopic evaluation of polypyrrole formation during enzymatic polymerization A) in a time frame from the start until 337 h, at 100 mM pyrrole concentration and Ppy peak intensity at 460 nm B) using different concentrations (50, 100, 200 and 400 mM) of pyrrole monomer. Here ordinate represents the height of the absorption peak and abscissa corresponds to the duration of polymerization process.*

The characteristic absorption peak of Ppy at 460 nm [271] was registered in time during enzymatic polymer synthesis process (Figure 35 A). The absorption of polypyrrole in the solution is increasing during the time despite the fact that some of the composites are precipitated at the bottom of the cuvette. For a better comparison, several concentrations of monomer were evaluated (Figure 35 B). As could be seen from the results (Figure 35 B), at 100 mM concentration of pyrrole the highest changes in the

signal intensity were observed using UV-Vis spectroscopy. This might be due to the most optimal conditions of the polymerization reaction exploited here at 100 mM of pyrrole. Thus, for the next experiments of the Ppy/GOx biocomposite formation, a 100 mM concentration of pyrrole was chosen.

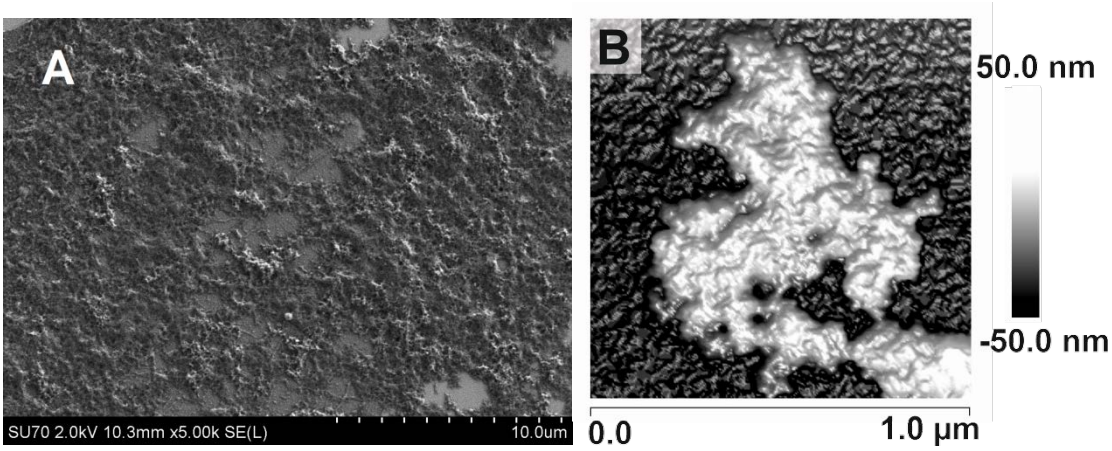

Figure 36 *Biocomposite structure evaluation. A) SEM and B) AFM images of Ppy/GOx biocomposite adsorbed on silicon substrate.*

The obtained reaction products were evaluated using SEM and AFM techniques (Figure 36). A complex and highly dense structure is presented in the SEM image. The structures seem to be aggregated, however, the small detail of the structure is hardly visible. The higher magnification image was impossible to obtain with SEM due to sample burning. For this reason the AFM technique was employed. As could be seen from the image Figure 36 B, the grain like structures were determined.

Evaluation of stoichiometry between compounds forming enzyme Ppy/GOx biocomposite

During the next stage of the experiments the isotopic composition of initial materials was measured and results are presented in Table 2. Two enzymes obtained from different suppliers were examined. The first enzyme GOx (1) was obtained from Applichem and the second one – GOx (2) from Sigma Aldrich. Both of them were produced by Aspergillus niger. However, only for GOx (1) the isotope ratio for nitrogen and carbon was remarkably different in comparison to pyrrole or glucose. Thus, for future calculations and interpretation of results GOx (1) was selected. Calculations of the carbon isotope ratio of the biocomposite should include three components: pyrrole, enzyme and glucose, as all three constituents contain carbon in their molecular structure.

Glucose and pyrrole have very similar carbon isotope ratio values and for this reason the separation of these two compartments is impossible. However, the glucose molecule does not contain any nitrogen, and hence the results calculated for nitrogen could be more precisely related to the stoichiometry of pyrrole and enzyme.

Table 2 *Isotopic characterization of initial materials used in enzymatic polymerization of Ppy: pyrrole, Glucose oxidase and glucose. C/N – ratio of carbon and nitrogen.*

	$\delta^{13}C$ (‰)	$\delta^{15}N$ (‰)	C (%) theoretical	N (%) theoretical	C/N	Molar mass (g/mol)	Reference
Pyrrole	-12	1.8	71.6	20.9	3.43	67	from supplier
GOx (1)	-24	-12.5	53.4	16.9	3.16	~ 186 000	[272] and from supplier
GOx (2)	-25.6	2.2	53.4	16.9	3.16		
D-(+)- glucose	-11.2	---	---	---	---	180	from supplier

As has been mentioned before, during the polymerization reaction of pyrrole, Glucose oxidase is expected to be surrounded by the formed polypyrrole chains. At present, there are no suitable analytical methods to quantify the ratio between formed Ppy and entrapped GOx, but a stable isotope ratio mass spectroscopy (IRMS) allows the quantification of the ratio of the initial materials, being involved in the Ppy/GOx biocomposite. The experimental results of the IRMS measurements of the Ppy/GOx biocomposite and supernatants are presented in Table 3.

The highest C/N ratio was measured in the Ppy/GOx biocomposite, which was not washed with water (Ppy/GOx biocomposite 4). In this Ppy/GOx biocomposite, an additional source of carbon is present, which is most probably from D-glucose used as the substrate for GOx and from glucono lactone, which is the product of the enzymatic reaction. During the cleanup step most of these soluble materials were successfully washed from the Ppy/GOx biocomposite using ultrapure water. The carbon isotope ratio in the formed composite changed after the washing procedure. This change is an indicator that substances (D-glucose or glucono lactone) with the different isotope ratios were removed from the composite. As it is evident from the C/N ratio (Table 3), the liquid phase – supernatant contained a relatively high amount of carbon, the origin of which is probably residual D-glucose, unpolymerised pyrrole monomer and glucono lactone.

Table 3 *$\delta^{13}C$ and $\delta^{15}N$ values for the biocomposites and supernatants. Biocomposite refers to the Ppy and GOx aggregations analysed after centrifugation (three separate measurements are presented; symbol 'w' indicates that the sample after centrifugation was 2 times washed with distilled water); supernatant refers to the solution which was removed after centrifugation. Other abbreviations: f1 – fraction of pyrrole; f2 – fraction of GOx; number of Py – estimated number of pyrrole molecules of formed Ppy, which is surrounding the GOx; n/d means that for the carbon approach is not possible to calculate the number of Py molecules in the composite because $\delta^{13}C$ value for the composite was lower comparing to the GOx.*

		$\delta^{13}C$ (‰)	$\delta^{15}N$ (‰)	C/N ratio	Carbon approach			Nitrogen approach		
					f1	f2	number of Py	f1	f2	number of Py
Biocomposite	1w	-21.9	-5.7	---	0.17	0.83	150	0.47	0.53	710
	2w	-24.6	-5.2	3.7	n/d	n/d	n/d	0.51	0.49	830
	3w	-24.4	-2.3	3.96	n/d	n/d	n/d	0.29	0.71	1970
	4	-19.3	-5.0	18.1	0.39	0.61	460	0.52	0.48	850
Supernatant	1	-14.0	2.1	9.7						
	2	-18.5	2.6	10.2						

The enzyme to pyrrole molecule ratio was estimated using the stable isotope mass-balance equation (2) – (9). Using the carbon approach 150 molecules (or 460 molecules when not washed) of pyrrole were obtained belonging to one molecule of Glucose oxidase. However, when nitrogen isotopes were evaluated in aggregates, 710 – 1970 of pyrrole molecules were assigned for each Glucose oxidase molecule. A higher number of the pyrrole molecules (more than 4 times) attached to the GOx was obtained. The carbon isotope ratio of glucose and pyrrole (about – 12‰) is similar and more positive compared to that of GOx (– 24‰). The difference between the carbon and the nitrogen approach might arise due to trapping of glucose or glucono lactone inside the Ppy/GOx biocomposite. Unfortunately, using only the carbon isotope ratio the discrimination of pyrrole, glucose, glucono lactone is impossible. On the other hand, nitrogen isotopes are absent in the glucose and later in the reaction product – glucono lactone. Moreover, as could be seen from the Table 2 the nitrogen isotope ratio is different between pyrrole (1.8‰) and Glucose oxidase (– 12.5‰). Glucose or glucono lactone, even entrapped within the aggregate, has no influence on the final result while calculating the ratio of the pyrrole in the Ppy/GOx biocomposite using the nitrogen stable isotope ratio. We suggest

that the nitrogen isotope approach based calculations of ratios in the Ppy/GOx biocomposite are more accurate in comparison with the carbon based isotope approach, because in the case of nitrogen the isotopic signal has no interference from carbon present in glucose or glucono lactone. It must be noted that in general precision of the elemental analyzer coupled to the IRMS is on the order of 0.15%. The uncertainty of estimation of carbon or nitrogen atoms in the biocomposite depends mostly on the polymerization reaction rate, because the isotope ratio measurement precision of 0.1‰ gives a variation of 10 pyrrole atoms in such a type of the Ppy/GOx biocomposite. The calculation uncertainty depends mostly on the carbon and nitrogen isotope ratio measurement precision. A higher accuracy of stoichiometry determination in the Ppy/GOx biocomposite can be obtained using initial materials that differ significantly in their isotope ratios.

Another reason for the inappropriate results for the carbon isotope approach can arise due to the fact that a relatively high amount of carbon (compared with nitrogen) is present in the Glucose oxidase. The enzyme molecule is composed of two subunits. Each of them is roughly composed from 2800 and 760 atoms of carbon and nitrogen, respectively, while pyrrole contains 4 carbon and one nitrogen atom. Thus $\delta^{13}C$ ratio is very close or even higher than the pure GOx ratio and the model calculations do not give any results.

While designing isotope mixing experiments the best results can be obtained when the stable isotope ratio variation between substances of the natural isotopic composition is at the highest level. For instance, glucose can assume $\delta^{13}C$ values from -12‰ to -30‰, because two photosynthetic pathways, commonly designated C_3 and C_4, fractionate carbon isotopes in plants to different degrees, resulting in differences of about 20% in glucose derived from these two sources. Usually C_4 plants (i.e. sugarcane) have $\delta^{13}C$ values of about -12‰, while $\delta^{13}C$ values for C_3 plants are in the range from -24 to -30‰ [31]. For this reason, first, the initial materials must be carefully analyzed and the best ones should be chosen, as it was shown in our experiments with the selection of the enzyme. Moreover, the glucose from C_4 plants could also be used in these experiments, although the interference in calculations would still be appreciable. In this case, the carbon isotope ratio values of the enzyme and glucose would be similar.

Conclusions of 3.3.2. section

The Ppy/GOx biocomposite obtained during enzymatic polymerization of pyrrole was investigated using UV-Vis spectroscopy, the dynamic light scattering method and isotope ratio mass spectrometry. The applicability of the stable carbon and nitrogen isotope ratio method for the evaluation of the complex Ppy/GOx biocomposite stoichiometry was appraised. Using nitrogen isotope ratio mass spectrometry measurements approximately 710 – 1970 pyrrole monomers were estimated to surround Glucose oxidase during enzymatic polymerization. However, at a relatively high concentration of GOx in the solution the carbon isotope approach was not suitable for the stoichiometry determination in the Ppy/GOx biocomposite because the stacking of GOx determines the $\delta^{13}C$ ratio to the final Ppy/GOx biocomposite. A higher accuracy of stoichiometry determination in the Ppy/GOx biocomposite can be obtained using initial materials, isotope ratios of which differ significantly.

3.4. Biocompatibility of polypyrrole evaluated with bone marrow-derived stem cells

In vitro studies have proved that polypyrrole supports the adhesion and growth of various kinds of cells, such as neuronal cells [110, 111], endothelial cells [112], keratinocytes [113], skeletal muscle cells [114], rat pheochromocytoma cells [115]. Nevertheless, the impact of Ppy on stem cells was not widely investigated, except for neural stem cells. It was found that the Ppy-coated nanowire surfaces facilitates *in vitro* C17.2 neural stem cell line adhesion, proliferation and differentiation [116]. V. Lundin et al. have shown that Ppy can be tailored to promote cell survival and maintenance of rat fetal neural stem cells and the biocompatibility of polypyrrole with neural stem cells depend on the counter ion incorporated in the polymer [117]. It was shown, that Ppy due to its electrical conductivity is very suitable for the construction of scaffolds for nerve tissue engineering [115, 118]. Conducting polymer polypyrrole is used in many biomedical applications and our aim of the following work was related to the Ppy application for the living yeast cells. However, for the biocompatibility study we have chosen primary cell cultures because they are more sensitive and more representative of cells *in vivo* [273] in comparison to the yeast cells. Therefore, the aim of this section was

to evaluate the influence of polypyrrole on attachment and proliferation of bone marrow-derived stem cells.

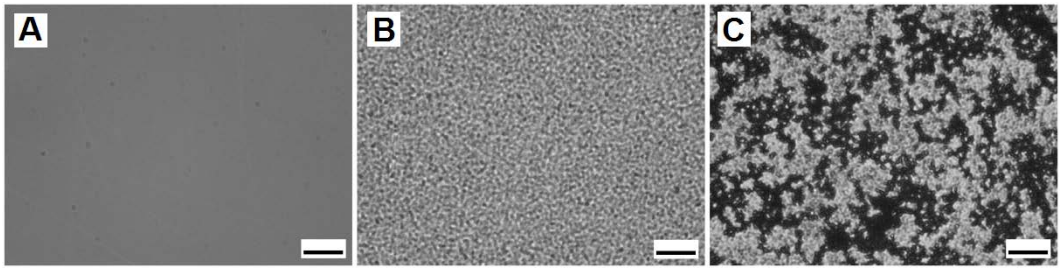

Figure 37 *Brightfield microscopy images of the polypyrrole-modified surfaces: A) 1.24 mg cm^{-2} Ppy; B) 2.48 mg cm^{-2} Ppy; C) 4.41 mg cm^{-2} Ppy. The scale bar corresponds to 20 μm.*

Mesenchymal stem cells due to their ability to self-renew and differentiate into specialized cells are attractive for the regenerative medicine. MSCs comprise of about 0.01 – 0.001% of the total nucleated bone marrow cells. Nevertheless, these rare, heterogeneous cells can be isolated from bone marrow and used in various tissue-engineering strategies. A number of techniques have been developed that permits the isolation of MSCs from mouse bone marrow (BM). However, these methods have inconvenient effects on the biological properties of mesenchymal cells such as decline in proliferation and differentiation potential of mouse MSCs [274]. Moreover, the every stage of cells purification is related to their loss. Consequently, we isolated MSC from mouse BM by method based on plastic adherence of MSCs.

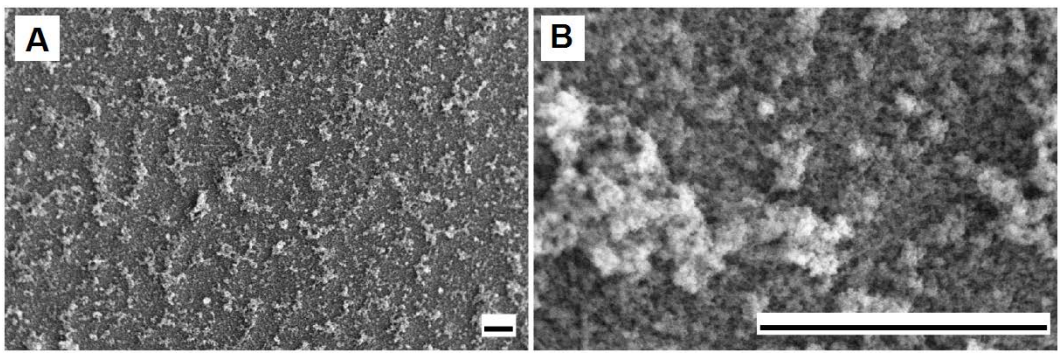

Figure 38 *SEM images of the polypyrrole-modified gold surface (7.17 mg cm^{-2} Ppy). The scale bar corresponds to 10 μm.*

We performed chemical synthesis of polypyrrole on gold-plated glass slides. The optical images of Ppy-modified surfaces are shown in Figure 37. The deposition of Ppy particles was scarce in Figure 37 A, and, therefore, is almost invisible. The coating of Ppy particles was clearly displayed in Figure 37 B and C.

Figure 38 gives the SEM images of the highly non-uniform Ppy layer on the gold substrate. It shows that the deposited Ppy particles completely covered the gold surface.

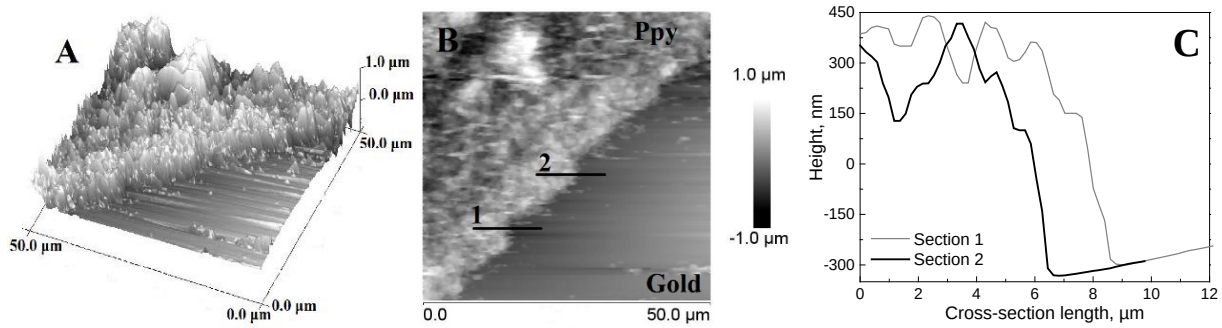

Figure 39 *AFM images of polypyrrole-modified gold surface: A) the 3D AFM image of the Ppy layer (7.17 mg cm^{-2}) coated on the gold surface, the size of the image is 50 µm; B) 2D AFM image of the boundary between the gold surface and Ppy layer, the height scale is 2 µm. Black lines in the image refer to the cross-sections; C) the graph of the cross-sections marked in the part B.*

The AFM images of polypyrrole-coated gold surface are presented in Figure 39. As could be seen from the 3D and 2D pictures, the layer is not homogenous, the conglomerated Ppy peaks could be observed up to 2 µm in height. The boundary between the gold substrate and the polypyrrole was obtained by gently scratching the surface with plastic stick for the removal of the Ppy layer, but not the deposited gold. As seen from the graphs of the two cross-sections, the average thickness of the Ppy layer was approximately 600 nm.

The capacity of these polypyrrole-modified gold surfaces to maintain cell adhesion and proliferation was tested. We plated cells in the tissue culture polystyrene plates without or with gold-plated slides, coated with polypyrrole, in a culture medium. Then, the stem cells were let to adhere on the substrate and the morphology of these cells was observed using a bright field and fluorescence microscope. Figure 40 clearly demonstrates, that the polypyrrole did not induce any significant effect on the cell morphology. The mouse bone marrow-derived stem cells appeared spindle shaped on TCP, bare gold and Ppy-modified surfaces. The cell shape on all surfaces tested was normal fibroblastic-like morphology.

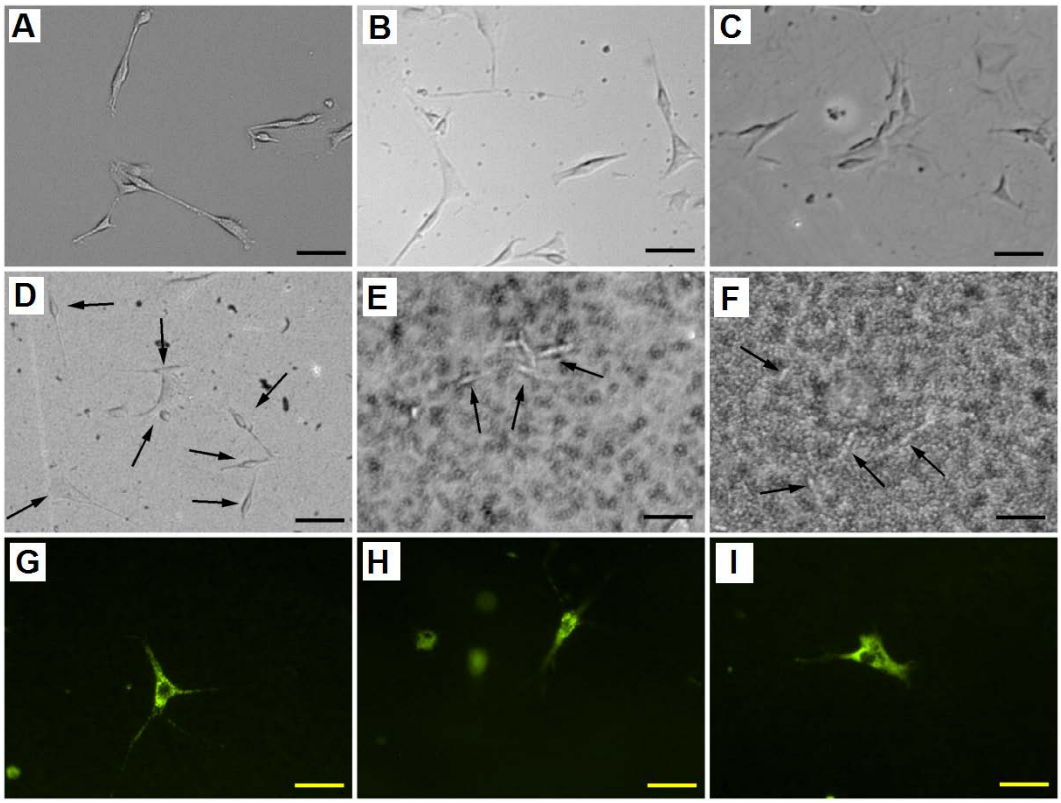

Figure 40 *Bright field and fluorescence microscopy images of mouse bone marrow-derived stem cells cultured on Ppy-modified gold surfaces. Bright field microscopy images of cells cultured on A) tissue culture plate (control without slide), B) bare gold, and Ppy-modified gold surfaces: C) 1.24 mg cm^{-2} Ppy, D) 2.48 mg cm^{-2} Ppy, E) 4.41 mg cm^{-2} Ppy, F) – 7.17 mg cm^{-2} Ppy for 48 hours. Fluorescence microscopy images (G, H, I) of PKH67 stained mouse bone marrow-derived stem cells cultured on Ppy-modified (7.17 mg cm^{-2} Ppy) surface for 48 h. The scale bar corresponds to 50 μm.*

The proliferation rate was evaluated for each polypyrrole coating in order to quantify and compare the ability of the mesenchymal stem cells to adhere and proliferate on Ppy-modified surfaces (Figure 41). The cell proliferation rate after 48 h incubation on Ppy-modified slides was similar to that in the control set up (which was considered as 100%) on standard TCPs without Ppy-modified slides and varied within the range of 86 – 110%. As is seen from Figure 41, all Ppy-modified gold surfaces supported cell proliferation. The lowest concentration of polypyrrole (1.24 mg cm^{-2} Ppy) increased cell proliferation by 10%, while highest concentration (7.17 mg cm^{-2} Ppy) of this polymer decreased cell proliferation by 14%, as compared to the control (TCP) cell proliferation rate. However, no statistically significant differences between the cell proliferation rates were determined. B. Lakard et al. have evaluated the adhesion and growth of osteoblastic cells on Ppy films. They demonstrated that the development of the cells was quite normal on this polymer and consequently concluded that these Ppy films were non-toxic

for osteoblastic cells and could be used as cell culture substrate [275]. Most of the studies of Ppy interaction with biological tissue were described in the review [276]. The conclusion of our study is not different since Ppy seems to support adhesion and proliferation of mouse bone marrow-derived stem cells.

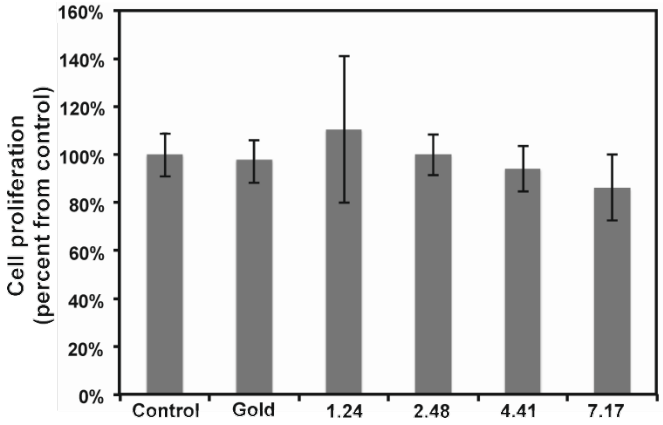

Figure 41 *Proliferation of mouse bone marrow-derived stem cells cultivated on tissue culture plate (Control), bare gold (Au), and 1.24, 2.48, 4.41 and 7.17 mg cm^{-2} Ppy-modified gold surfaces for 48 h. Proliferation rate was evaluated using WST reagent, and absorbance was measured at 440 nm. Error bars indicate standard deviation.*

It is difficult to compare precisely our work with those of other groups since no previous study was dedicated to the effect of polypyrrole on the culture of mouse bone marrow-derived stem cells. Nevertheless, H. Castano et al. carried out similar studies [161]. They prepared Ppy thin films by admicellar polymerization, and evaluated the ability of rat pre-differentiated mesenchymal stem cells to attach, proliferate, and differentiate on these films. They found that Ppy films, generated by different monomer concentrations, induced completely different cellular events. The strongest cell attachment was on the films, prepared by using 20 mM pyrrole. 35 mM monomer concentration considerably decreased cell attachment, and when the pyrrole concentration reached 50 mM practically no cell adherence was observed. Thus, they concluded that 20 mM Ppy thin films were most suitable for induction of the MSC osteogenicity. Moreover, recently it was reported that Ppy coated materials supported the adherence and proliferation of adult human mesenchymal stem cells and human fibroblasts [277]. The results of our studies showed that polypyrrole (1.24, 2.48, 4.41 and 7.17 mg cm^{-2}) have no statistically significant impact on mouse mesenchymal stem cells adhesion and proliferation. Therefore, we have concluded that polypyrrole-modified surfaces could be used for biomedical purposes.

Conclusions of 3.4. section

The results of our studies showed that conducting polymer polypyrrole was not toxic to mouse bone marrow-derived stem cells. Polypyrrole deposited on the gold-plated glass slide did not strongly impair cell attachment and proliferation. These cells adhered well on polypyrrole-modified surfaces and exposed normal fibroblastic like morphology. Therefore, our prepared polypyrrole-modified gold surfaces are suitable substrates for maintaining stem cell attachment and proliferation, and can be used for different purposes where adhesion and proliferation of these cells is required.

3.5. Investigation of the substrate for an intact and Ppy modified yeast cell

In this chapter of doctoral thesis the substrate for AFM measurements of modified and intact yeast cells as well as for Raman spectroscopy was evaluated. For Raman measurements several different substrates, including silicon, silicon oxide, HOPG, gold, glass and structurised silver were evaluated and the most suitable ones to obtain an intense Raman signal was emphasized. For AFM measurements a conventional silicon substrate was employed due to its low roughness for the measurements of NaCl, glucose or polypyrrole modified yeast cells and polycarbonate membrane for the force-distence measurements of polypyrrole modified yeast cells. Viability of such cells has also been evaluated.

3.5.1. The substrate influence to Raman spectra intensity of yeast cells

Raman spectroscopy is a powerful analytical method that allows deposited and/or immobilized cells to be evaluated without complex sample preparation or labeling. However, a main limitation of RS in cell analysis is the extremely weak Raman intensity that results in low signal to noise ratios. Therefore, it is important to seize any opportunity that increases the intensity of the Raman signal and to understand whether and how the signal enhancement changes with respect to the substrate used. The experimental results presented here show clear differences in the spectroscopic response from cells on different surfaces. Several non-conventional substrates, such as silicon, silicon oxide, gold, graphite, and a structured silver substrate were systematically studied for yeast cell deposition. This result is partly due to the difference in spatial distribution of electric field at the substrate/cell interface as shown by numerical simulations. It was

found that the substrate also changes the spatial location of maximum field enhancement around the cells. Moreover, beyond conventional flat surfaces, an efficient structured silver substrate that largely enhances the Raman signal intensity from a single yeast cell was introduced.

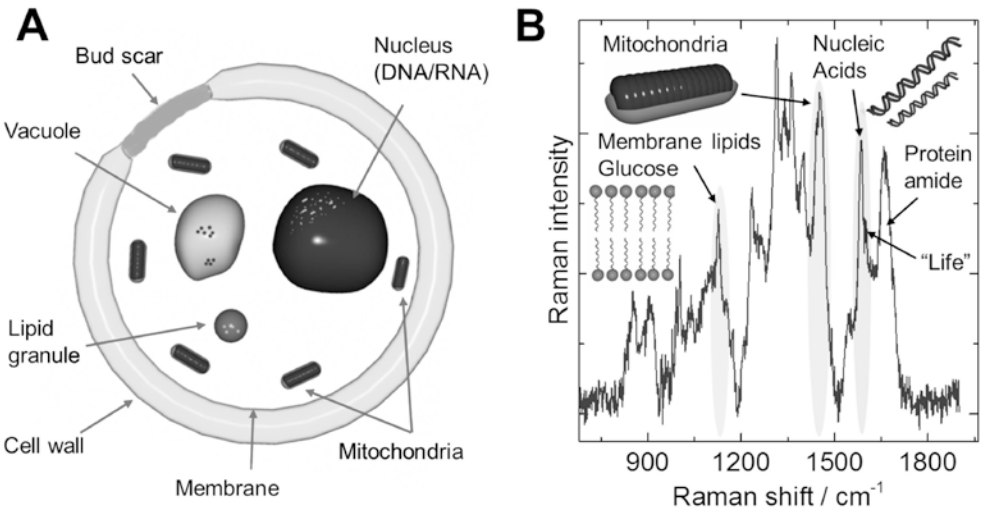

Figure 42 *A) Sketch of a yeast cell and B) different components of the cell identified by RS under 514.5 nm laser excitation.*

The different cell components are sketched in Figure 42 A. The Raman spectrum of yeast cells is shown in Figure 42 B. It was acquired under green laser excitation and the bands arising from the molecular vibrations of different cell components are marked. Yeast cells are one of the best-known systems in cell biology used in the fermentation process of alcohols for thousands of years. For cell research obtaining the chemical fingerprints of yeast cell components is a key that Raman spectroscopy can provide. The indexation of the most prominent Raman bands is shown in the Table 4. In the Raman spectrum, Figure 42 B, the mitochondria band around 1451 cm^{-1} as well as the shoulder at 1602 cm^{-1}, which was associated with the cell viability and programmed death [190, 192] could be observed. The appearance of the latter band, in addition to the band at 1125 cm^{-1} from glucose, and membrane lipids can provide an indication of the state of the cell [278]. This information, and how mitochondria reacts to external changes and stress, is essential with respect to the understanding of the cellular function and survival mechanisms that ultimately could provide insights in aging of humans [278-280]. However, as shown below, the substrate, on which the cells are deposited, can significantly affect the intensity of some of these bands.

Table 4 *Raman bands assigned for different molecular vibrations of the yeast cells. Abbreviations: ν, stretching; δ, deformation; P, protein; L, lipid; Man, D-mannose; Phe, phenylalanine; Trp, tryptophan; Tyr, tyrosine; Psch, polysaccharides; A, adenine; G, guanine; C, cytosine; U, uracil. Substrates: Au, Si, SiO_2, glass, and HOPG.*

Ram. shift, cm^{-1}	**Assignment**	**Observed under 514.5 nm excitation**					**Ref.**
		Au	**Si**	**SiO_2**	**Glass**	**HOPG**	
753	ν(O—P—O) symetric (**L**), Trp (**P**)	-	-	-	-	-	[281, 282]
845	Tyr, (breathing mode)	+	+	+	+	+	[283]
896	Trp (**P**), ν(C-O-C)	+	+	+	+	+	[284]
998	ν(C-C) aromatic ring breth (**Psch**), Phe (**P**)	+	+	+	+	+	[284, 285]
1034	ν(C-C), Phe (**P**), C-H in plane, ν(C-O-P) (**L**)	-	-	+	+	-	[285]
1081	ν(CO-C-O) symmetric (**L**), ν(C-O-C) asymmetric in aliphatic esters, ν(C-C) (**L**)	+	-	-	+	-	[284, 285]
1104	(O=P=O) (**DNA/RNA**), ν(C-C) (**L**), Man	-	+	-	+	-	[285]
1130	ν(C-O-C) symmetric glycosidic ring, ν(C-N) (**P**), ν(C-C) (**L**), Man	+	+	+	+	+	[284-286]
1153	ν(C-C), ν(C-N) (**P**)	+	+	+	-	+	[285]
1234	Amide III (**P**), U, C (**DNA/RNA**)	+	+	+	+	+	[285]
1265	Amide III (**P**), δ(=CH) (**L**)	+	+	+	-	-	[284]
1310	δ(-CH_2), in plane δ(-OH), δ(C-H)	+	+	+	+	+	[283, 284, 286]
1342	δ(C-H) (**P**), A, G (**DNA/RNA**)	+	+	+	+	+	[285]
1358	δ(-CH_2), δ(-OH), Trp (**P**)	+	+	+	+	+	[285, 286]
1401	ν(pyr quarter-ring)	+	+	+	+	+	[287]
1450	δ(-CH_2) (**L, P**), (-CH_2) scissoring	+	+	+	+	+	[284, 286]
1547	Amide II (**P**)	+	+	+	+	-	[288]
1583	G+A ring stretch (**DNA/RNA**)	+	+	+	+	-	[281, 282, 284]
1603	ν(C=C) aromatic, Phe, Tyr (**P**), Trp, **life band**	-	-	+	-	+	[191, 284]
1616	Tyr, ν(C=C) (**L**), Amide I (**P**)	+	+	-	-	-	[284]
1659	ν(C=O), Amide I (**P**), ν(C=C) cis of fatty acids (**L**), ν(C=N)	+	+	+	+	+	[283, 284, 286]

For the sake of clarity, the Raman spectra of the bare substrates are shown in Figure 43 A. The silicon and silicon oxide/silicon substrates present their characteristic second order peaks between 900 and 1100 cm^{-1} that partly overlap with the Raman signals from the cells. The graphite surface displays a strong peak around 1580 cm^{-1}. The clean microscope glass substrate shows a small but broad background around 1100 cm^{-1}. Only the gold substrate shows no characteristic peaks in the spectral range investigated here, except for a small periodic background due to the optical detection system.

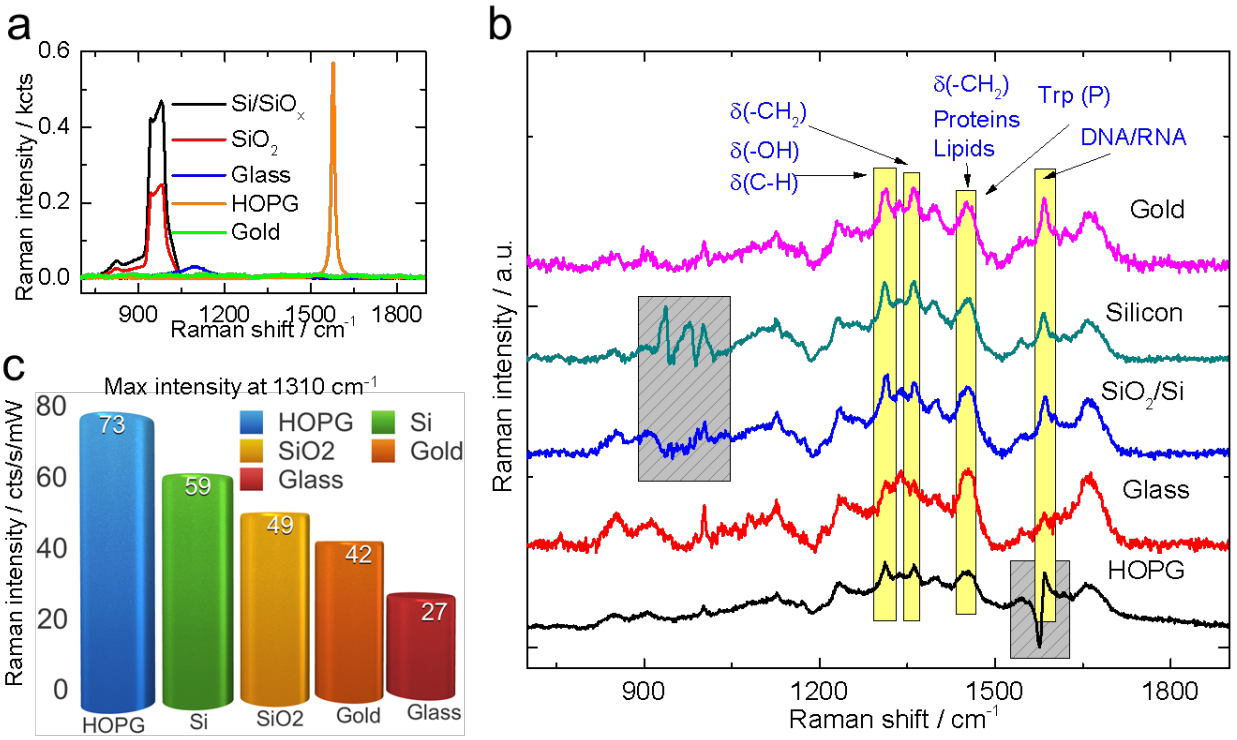

Figure 43 *A) Raman spectra of the five substrates used for the Raman spectroscopy analysis of yeast cells: silicon with native 2 – 3 nm layer of SiO_x; 100 nm SiO_2 on Si; objective glass slide; highly oriented pyrolytic graphite (HOPG), and gold. A 514.5 nm laser was used at 2 mW power, acquisition time 10 min. B) Raman spectroscopy results of the yeast deposited on the different substrates. The gray boxes show the spectral regions overlapping with the (subtracted) substrate signal. Trp refers to tryptophan Raman band. C) Maximum intensity of the band at 1310 cm^{-1} for the different substrates.*

In Figure 43 B the Raman spectra of cells from the same culture deposited on different substrates are shown. In order to compare the signal intensity for yeast cells on different substrates, the maximum intensity of the Raman band at 1310 cm^{-1} is displayed in a chart in Figure 43 C. There are two differences in the spectral signature of yeast cells on the substrates shown in Figure 43 B. The first one concerns intensity changes. We can see that for silicon, SiO_2, and HOPG substrates the Raman intensity is higher than for cells on glass. A first attempt to explain this result lead us to consider the

difference in sample transparency since all other substrates except glass reflect back photons that were not scattered by the cell. In order to further expand on this hypothesis, reflectivity experiments for all five bare substrates were performed (Figure 44). We found that the reflectivity decreases in the following order: Au>HOPG>Si>SiO_2>glass. The elastic Rayleigh scattering was recorded at 25 different locations for each substrate using the same laser excitation employed in Raman experiments ($\lambda = 514.7$ nm). Therefore, it is reasonable to assume that the substrate reflectivity plays a role in the Raman intensity differences observed.

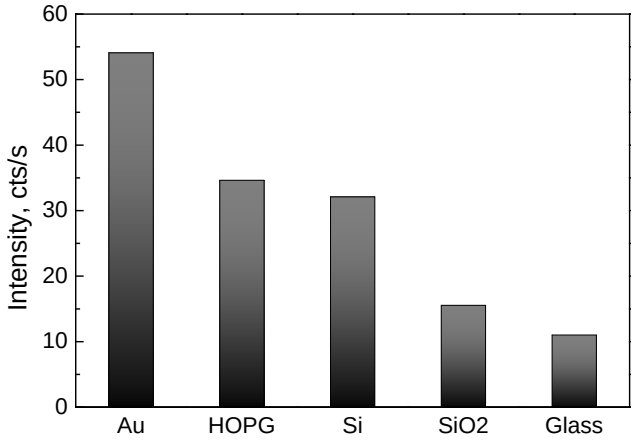

Figure 44 *Rayleigh scattering results of the different substrates obtained from the average of 25 spectra over different locations for each bare sample. Excitation wavelength used was 514.7 nm. In the back scattering geometry the Rayleigh scattering is a direct indication of reflectivity. The experiments were done using the same Raman spectroscopy setup. The maximum value of each spectrum was choosen.*

However, the reflectivity results do not follow the order of the Raman intensity amplification observed in Figure 43 C HOPG>Si> SiO2>Au>glass; consequently, other factors besides reflectivity must be contributing to the substrate-dependent Raman intensity changes. The second difference, in addition to the overall intensity variations, regards the intensity ratios between different Raman bands. For example, let us consider the band around 1584 cm^{-1} representative of nucleic acids (DNA/RNA) and its intensity with respect to that of the lipids band around 1450 cm^{-1} (Figure 43 B). The DNA/RNA band is barely visible for cells on glass, while for the other substrates this band is much more pronounced. For the case of cells on HOPG the strong signal from the substrate limits the evaluation of nucleic acids band, or any other band in that region. Cells on Au show the most intense DNA/RNA bands, this result can be linked to the highest reflectivity of gold directing photons back to the cell if they were not absorbed by the

nucleus in the first pass. Indeed, the reflectivity results (Figure 44) rank the five substrates in a similar order as the sharpness of the DNA/RNA band appears in the Raman spectra. However, the question remains open why the nucleus band is enhanced more than others. One possible explanation is that multiple reflections from gold (interference) and charge mirror dipole contribute to increasing the signal from the cell nucleus. The numerical simulation results discussed below shed more light on this question.

The intensity of light I is proportional to the electric field squared $I \propto |E|^2$. This nonlinear dependence on E can produce large changes in the Raman intensity when the cells are deposited on different substrates. The simulation results allow the spatial distribution of electric field inside a cell and its surroundings to be visualized (Figure 45). Such information would be extremely challenging to obtain experimentally, and to our knowledge such endeavor has never been attempted. In our case the simulations are particularly beneficial since they could help explaining the selective Raman intensity changes of different cell components depending on the substrate used and for the illumination wavelengths commonly used in Raman investigations.

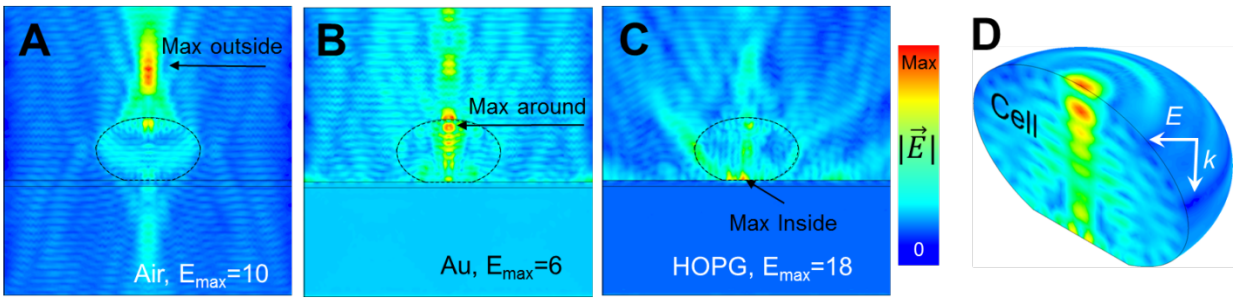

Figure 45 *Numerical simulations using finite element method of electric field distribution in a yeast cell and its surroundings deposited on different substrates: A) air, B) gold, and C) HOPG substrate D) 3D image of electric field distribution in the yeast cell on gold. The simulations were performed under 515 nm excitation.*

The simulation results shown in Figure 45 under 515 nm illumination confirm the impact of the substrate on the electric field enhancement in the cell and in the surroundings of the cell. For the case of the cell in free space (air) the electric field distribution with the highest intensity is located outside of the cell (Figure 45 A). This is a consequence of the cell acting as a focusing medium. Notice that the illumination was introduced in the simulations as a plane wave so no objective focusing is considered. Unfortunately, for Si, SiO_2, and glass substrates the calculations were not reliable and,

therefore, they are omitted in this section. An interesting result of the simulations arises for a cell on the Au substrate, where the two electric field maxima are located at the inner and outer sides of the cell membrane (Figure 45 B, and the 3D representation in Figure 45 D). In the case of a cell on graphite (HOPG) the cell regions closest to the substrate (cell wall and membrane) are the ones that will dominate the Raman spectra due to the highly localized electric field. This represents a significant difference in terms of Raman spectroscopy due to the non-linear relation between Raman intensity and electric field. The simulation results help to explain why the Raman band from the DNA/RNA in the nucleus is high for cells deposited on gold. If we consider that the cell nucleus is not located immediately close to the cell membrane but somewhere deeper into the cell, then the substrate (Au) that induces the maximum field located in the inner cell would result in the enhancement of cell components such as the nucleus. Similarly, if we consider cells simulated in air to be close to the case of cells on glass, then the electric field amplification that occurs outside of the cell accounts for the lower Raman intensity when using the glass substrate as shown in Figure 43 C. Contrary to cells on Au, for the cell in air the location with highest electric field inside the cell is close to the wall and cell membrane. These conclusions derived from the calculations are in agreement with the spectral differences experimentally observed in Figure 43 B where the Au substrate amplifies the Raman signal from the nucleus while the glass substrate shows that of the lipids membrane.

As mentioned above, different substrates can provide different degrees of enhancement of different cell components. In order to go a step beyond in terms of enhancement, cells deposited on a structured silver substrate were studied. The reason why the silver substrate is of particular interest here is that it offers the possibility to increase the Raman intensity by several orders of magnitude producing what is known as surface-enhanced Raman spectroscopy (SERS) [289]. The enhancement is due to the excitation of localized surface plasmons that greatly amplify the electric field around plasmonic structures, and in particular in regions between closely-spaced particles known as hotspots [290].

The structured silver substrate presented particular challenges for SERS since the as-prepared surface had strong Raman bands due to hydrocarbons and ambient contaminants [291]. The bands due to the contaminants unfortunately cover the spectral

region of the yeast bands as shown in the Raman spectra represented in Figure 46 A. The conventional cleaning procedure with ultrasound in different solvents was not sufficient to remove the contamination signal. A breakthrough occurred when the silver substrate was additionally cleaned in an ultrasonic bath containing a diluted solution of nitric acid (HNO_3): the carbon contaminant signal was drastically reduced as can be seen from the spectra change in Figure 46 A. Although the cleaning with HNO_3 decreased the contamination signal, it also has induced the surface roughness of some crystal facets of Ag particles (data not shown).

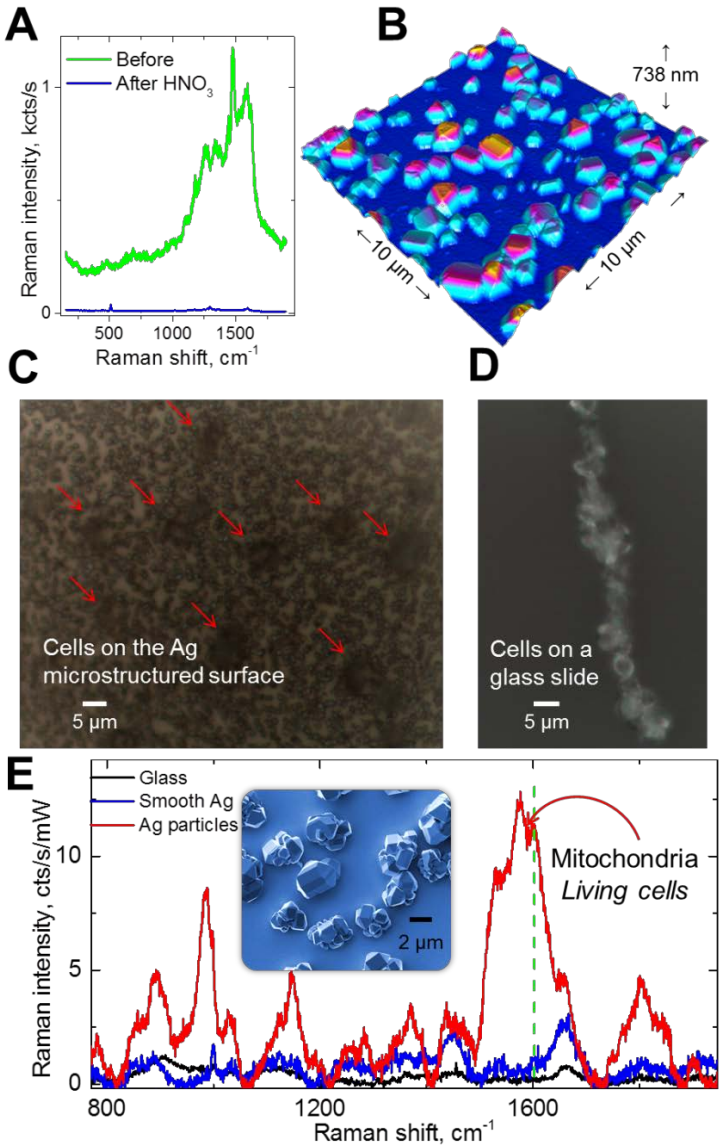

Figure 46 *A) Raman spectra of a silver SERS substrate before and after cleaning in a diluted HNO_3 solution; B) the AFM visualization of the structured silver substrate; C) Selective single-cell attachment on the structured Ag substrate is observed as compared to D) the multiple cell aggregate formation on the glass substrate. E) Raman spectra comparison of yeast cells deposited on a smooth Ag surface, glass, and on Ag particles. The inset shows a SEM image of some Ag nanocrystals.*

After such cleaning procedure yeast cells were deposited on the substrate such as the one in the AFM image in Figure 46 B and Figure 47 A. The high Raman signal intensity allowed both the excitation laser power to be decreased by half and the acquisition time by an order of magnitude. Such an increase in signal intensity also made the acquisition of a Raman line scan map along a single yeast cell possible. Full spectral information was acquired at each point, as illustrated in Figure 47 B by the intensity line map of the $\delta(\text{-CH}_2)$ mode at 1446 cm^{-1} related to lipid vibrations. One representative spectrum of the single yeast cell on the Ag substrate is shown in Figure 47 C. To put this in perspective, acquiring a Raman spectrum under the same power and acquisition time for the yeast on a flat glass substrate such as in Figure 46 D shows an almost featureless background.

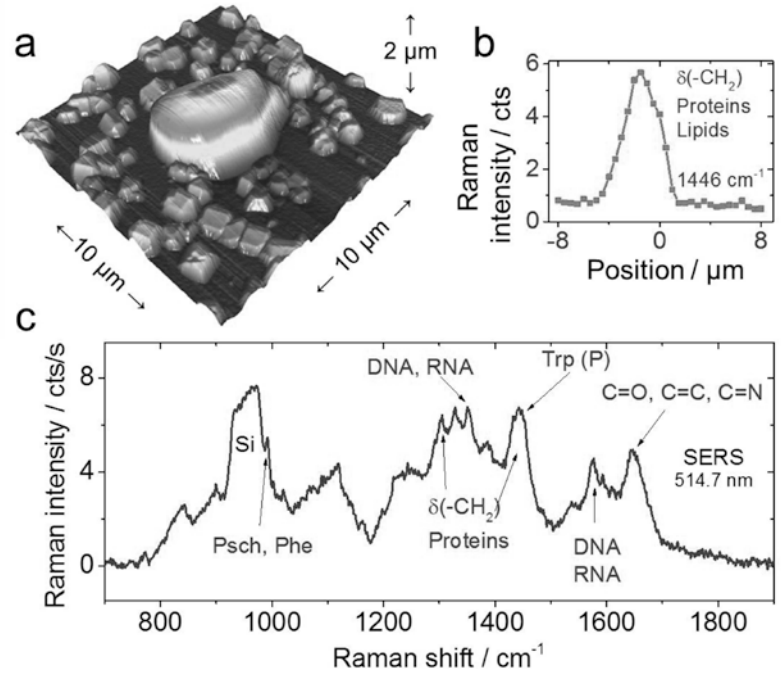

Figure 47 *A) Atomic force microscopy image of a single cell on the silver nanoparticle substrate. B) Raman line scan showing the spatial distribution of the -CH_2 vibration at 1446 cm^{-1} related to proteins and lipids. C) Raman spectrum of a single cell using SERS, the high enhancement even makes the bands visible at the same level as the silicon substrate allowing the observation of the phenyl band that was previously masked. No substrate background subtraction was necessary in this case.*

An unintended consequence of using the silver crystals was the apparent improvement in cell attachment. For the cells deposited on a glass slide (with no poly-L-lysine treatment) only few cell aggregates were visible under the optical microscope (Figure 46 D), while on the silver substrate the cells appear isolated (Figure 46 C). The cell aggregation can be inhibited by decreased cell mobility either due to high roughness

of the silver surface, or due to toxic effect of silver on yeast cells [292]. However, the observation in Figure 46 E of the Raman band at 1602 cm^{-1}, the so-called “life band” associated with cell metabolism is clearly visible; this suggests that the cells remain alive on the SERS substrate during the experiment and the toxic effect was not the predominant one.

In order to verify the plasmonic origin of the enhancement and also help to elucidate the SERS performance, cells were deposited on a smooth Ag substrate that also contained a region covered with Ag particles. The spectra comparison is shown in Figure *46* E, and evidences the largest signal enhancement produced by the silver particles in comparison to cells on glass and on the smooth Ag film. With respect to glass, the smooth Ag film shows larger enhancement similar to the case of cells on a Au film (due to high reflectivity). We attribute the large electric field enhancement in SERS to the high density of hotspots formed by gaps between Ag particles.

In the AFM image in Figure 47 A an yeast cell is shown on top of the silver substrate. The silver structures appear with high symmetry forming octahedral and dodecahedral particles; shapes typical for Ag single crystals as also shown in Figure 46 B. It is possible that during the drying process morphological changes occur in the cell, this was the case for the cell imaged with AFM that shows a morphology deviating from an ideal spheroid. We cannot rule out any modification of the cells due to the presence of the silver nanocrystals. Although from the optical microscope image in Figure 46 D, it appears that the cells on glass have also lost their spheroidal conformation. Therefore, it is likely that the drying process is the reason for the cell shape modification. The asymmetrical shape of the cell is also evidenced in the Raman line scan showing differences between the right and left sides of the intensity profile in Figure 47 B. In the case of yeast cells, cytochrome c absorbs light in the green range of the spectrum (at 520 nm) [293] making it possible to selectively enhance the signal from mitochondria that is responsible for the cell breathing and thus can be correlated with its state. For large particles such as Ag-coated spheres 450 nm size, simulation results show that the electric field enhancement extends over 100 nm. Such large spatial extension of the enhancement should be enough to amplify the Raman signal from inner components of the cell beyond the membrane. This possibility is experimentally verified by SERS displaying features corresponding to mitochondria and cell nucleus (Figure 46 E).

Moreover, if RS would be used for time dependent investigations of the cell state, such as in aging studies, the use of the SERS substrate presented here with its decreased acquisition time and laser power would be tremendously beneficial.

Conclusions of 3.5.1. section

In this section the suitability and the effect of different substrates were investigated for RS analysis of yeast cells in order to find out whether or not the Raman signal could be improved and why. Experimentally, silicon, silicon oxide, and HOPG were found to give intense and clear Raman features from yeast cells, although these substrates also present intrinsic Raman signals that partially overlap with the spectral features from the cells. The numerical simulation results for green excitation showed that in the case of yeast in air the cell acts as a focusing medium, while yeast cells on the Au and on the HOPG substrates have higher fields at the inside and at the cell membrane, respectively. Even though different laser excitations can be in resonance with some parts of a cell, the substrate can change the spatial location of the maximum electric field providing selective amplification of different cell components. The two main differences we observed, the Raman intensity and the intensity ratios, are both a consequence of the substrate reflectivity and signal amplification due to the optical properties of the substrate. Therefore, the absence of certain Raman bands and appearance of the others observed in cell research might not be only attributed to a given molecular process or influence of the external perturbations, but it could also be a consequence of the substrate employed. Finally, whenever Raman signal amplification is desired, we demonstrated a versatile and inexpensive SERS substrate based on Ag single particles that could be in principle reproduced in any lab with a minimum production cost. The considerable signal increase for the yeast on the SERS substrate was illustrated in a line map along a single cell. This work provides a significant advance for future Raman investigations of cells, in particular, by demonstrating the role of the substrate for cell studies and how it affects the Raman spectra.

3.5.2. Modification of yeast cells by polypyrrole

Yeast cells are often used in biosensor and biofuel design. In order to obtain the desired properties, cells could be modified genetically or chemically. One of the problems that

scientists are facing is the signal transfer from the inner cell medium to the signal transducer, due to relatively low permeability of yeast cell membrane and cell wall [294]. Therefore, some improvements are needed in order to increase charge permeability trough the cell wall and/or the cell membrane. Introduction of particular conducting structures, which will electrically connect cell cytoplasm and extracellular matrix, could solve this problem. For this particular application conducting polymers could be applied due to a number of suitable properties, mentioned before: conductivity; biocompatibility; elasticity; and stability at environmental conditions [51].

The AFM is very often used for the monitoring of a surface of living cells. Changes of the surface roughness and altered tip-cell surface interaction could provide scientists very important information about the viability and structural changes of the cell. However, for the AFM measurements the sample should be firmly immobilized and AFM tip should not be able to dragg the sample to the sides. For this reason several immobilization strategies are suggested by scientists, such as adsorption, chemical or biochemical fixation, physical entrapment into membranes or polymer layers. For Ppy modified yeast cells two strategies were applied: adsorption on the Si substrate for the measurements in air and entrapment in polycarbonate membrane for the measurements in liquid.

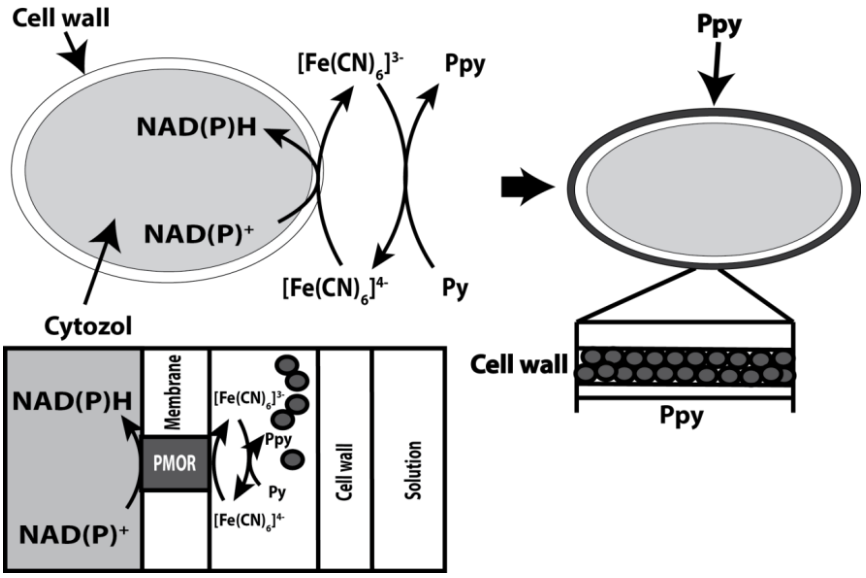

Figure 48 *Ppy formation scheme; yeast cell performed oxidation of $[Fe(CN)_6]^{4-}$ to $[Fe(CN)_6]^{3-}$, which is followed by $[Fe(CN)_6]^{3-}$ induced oxidative polymerization of pyrrole (Py) and returning of $[Fe(CN)_6]^{3-}$ to reduced form; PMOR – plasma membrane oxido-reductase.*

The aim of this research was to modify yeast cells by Ppy, which was formed by oxidative polymerization, initiated by $[Fe(CN)_6]^{3-}$. During here proposed polymerization process formed $[Fe(CN)_6]^{4-}$ was continuously regenerated by redox processes running in the cytoplasm and in the membrane of yeast cells. We assume that such modification of the cell wall will considerably improve its properties for formation of biosensors and/or biofuel cells.

The formation of the polymer layer in yeast cell periplasm and/or cell wall is thought to follow the scheme presented in Figure 48. Initially, the concentration of $[Fe(CN)_6]^{3-}$ is negligible, but it is formed in the reaction mixture due to oxidation of $[Fe(CN)_6]^{4-}$ to $[Fe(CN)_6]^{3-}$ by oxido-reductases, which are present in the membrane of the yeast cells [295]. Formed $[Fe(CN)_6]^{3-}$ initiates the polymerization of pyrrole molecules, which are in the close proximity of the cell wall. Thus it can be assumed that if some pyrrole monomers are trapped in periplasm or are adsorbed on the cell wall the polymerization of them occurs in the first place. Formed oligomers later can act as a basal body for chain elongation by further oxidation of pyrrole.

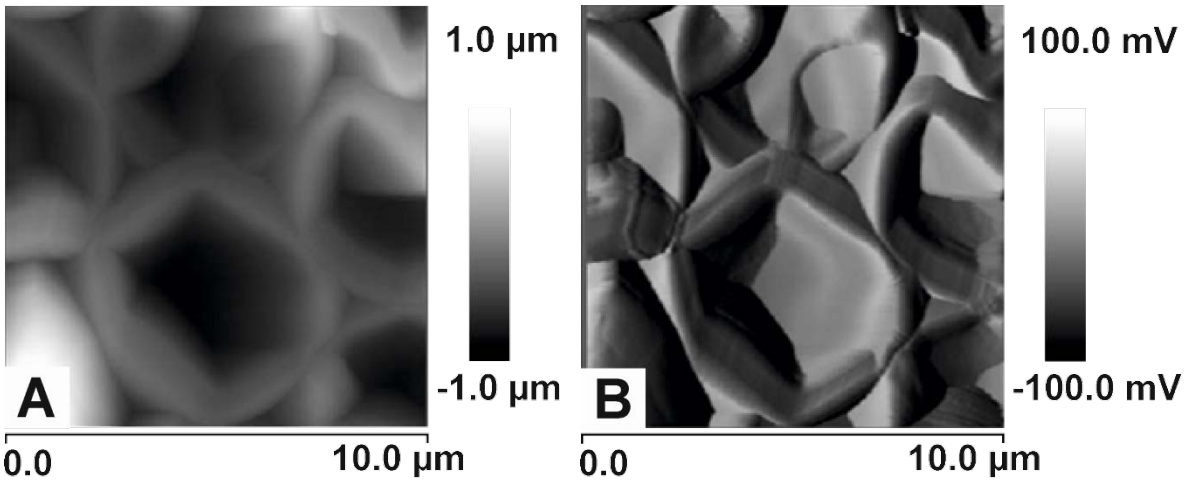

Figure 49 *Baker's yeast cells overheated by hot air: A) the AFM topography image and B) the corresponding amplitude error image.*

For a visualization of polymerized and intact cells the AFM technique has been employed. In order to scan the surface of the cell, the substarte should be stiff and sufficiently smooth. For this purpose flat Si substrate could be used which is extremely flat with the roughness below 1 nm. The baker's yeast cells on the Si substrate were measured in ambient environment. Prepared solution after the deposition on the substrate was dried by hot air. If cells were overheated their walls lose the rigidity and bend/arch/incurvate as shown in Figure 49. Two AFM images are presented, which

correspond to topography (Figure 49 A) and amplitude error (Figure 49 B). The former allows precise measuring of geometrical size of the investigated features in all three dimensions. The latter is a derivative of the topography image, which emphasizes any features on the surface including an estimated geometrical shape of features on the plane.

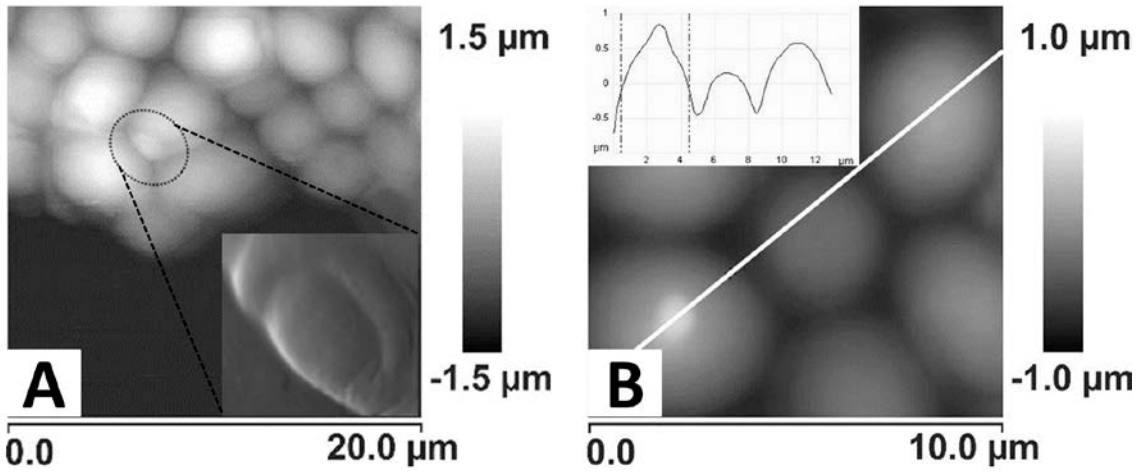

Figure 50 *Baker's yeast cells with visible scar structure shown by an outline. A) Topography; a zoomed image of the bud scar is presented in the inset; the smooth surface at the bottom part corresponds to the Si substrate. B) Calculation of geometrical sizes of measured features from the AFM topography image; white line indicates the cross-section place shown in the inset.*

Figure 50 presents baker's yeast cell topography. A bud scar is detected, which is emphasized by outline. The close up image in inset of Figure 50 A reveals a structure of the scar. Figure 50 B shows the topography image with the extracted cross section in the inset corresponding to the white line. The profile allows determination of geometrical sizes of measured features on the sample surface. As it is seen with the width of the three cells it is confined in 1 – 2 µm range. The bud on the top of the cell is 0.25 µm height and 0.5 µm width.

Figure 51 A presents amplitude error image, which shows the yeast cells measured in 'soft tapping' mode and in inset the outlined place is depicted obtained during the measurements with 'hard tapping' mode. A yeast cell wall is relatively rigid but can be damaged by the probe. In the first case (Figure 51 A) the dissipation of the mechanical energy to the surface is low and the probability of an induced damage to the surface is quite low. In the second case the contact force of the tip/sample is so high that the membrane of the cell is broken as shown by an outline in Figure 51 a inset. A bud scar can be distinguished on both images.

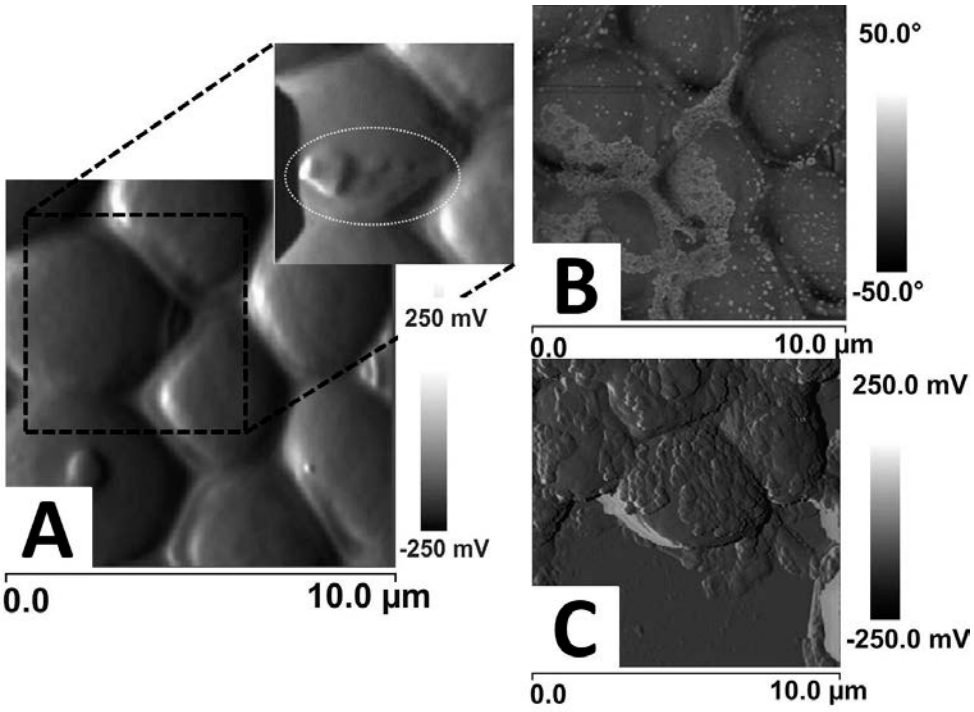

Figure 51 *The AFM amplitude error images measured in soft tapping mode A) and in hard taping mode (inset). The outline shows induced mechanical damages to the cell membrane by probe. The traces of B) glucose and C) sodium chloride crystals on yeast cell membranes formed after drying the yeast cells, which were kept in glucose and sodium chloride solutions correspondingly.*

The modification of yeast cell wall by various chemicals could also be investigated using AFM. In this study two kinds of modifications were made. Firstly, yeast cells were modified with glucose and sodium chloride solutions which resulted in the adsorption of the NaCl crystals or glucose molecules on the cell wall. Figure 51 shows cells, which have been kept in glucose (Figure 51 B) or sodium chloride solutions (Figure 51 C). After drying a visible amount of glucose and sodium chloride from the solutions is left on the surface of yeast cell walls that is apparently seen in both images. The glucose crystals are well revealed by the phase view while sodium chloride crystals on cells are clearly observed in the amplitude error image. The second modification was chemical and resulted in the polymer layer around the cell.

Table 5 *Evaluation of Ppy formation in different composition solutions. The concentration of* $[Fe(CN)_6]^{3-}$ *and* $[Fe(CN)_6]^{4-}$ *was 40 mM while that of the pyrrole was 500 mM.*

Sample No.	**Compositions**				**Ppy formation**
	$[Fe(CN)_6]^{3-}$	$[Fe(CN)_6]^{4-}$	Pyrrole	Yeast cells	
1	X		X		Instant
2	X		X	X	Figure 52D
3		X	X	X	Figure 52E

The synthesis of pyrrole induced by $[Fe(CN)_6]^{3-}$ was evaluated firstly without the addition of yeast cells (Table 5 Sample no. 1). The formation of Ppy clusters was observed using optical microscopy (Figure 52 C) as well as was registered spectroscopically. Then formation of Ppy in the presence of yeast cells was evaluated using $[Fe(CN)_6]^{3-}$ or alternatively its reduced form $[Fe(CN)_6]^{4-}$. In both experiments glucose was also present in order to keep the cell metabolism processes.

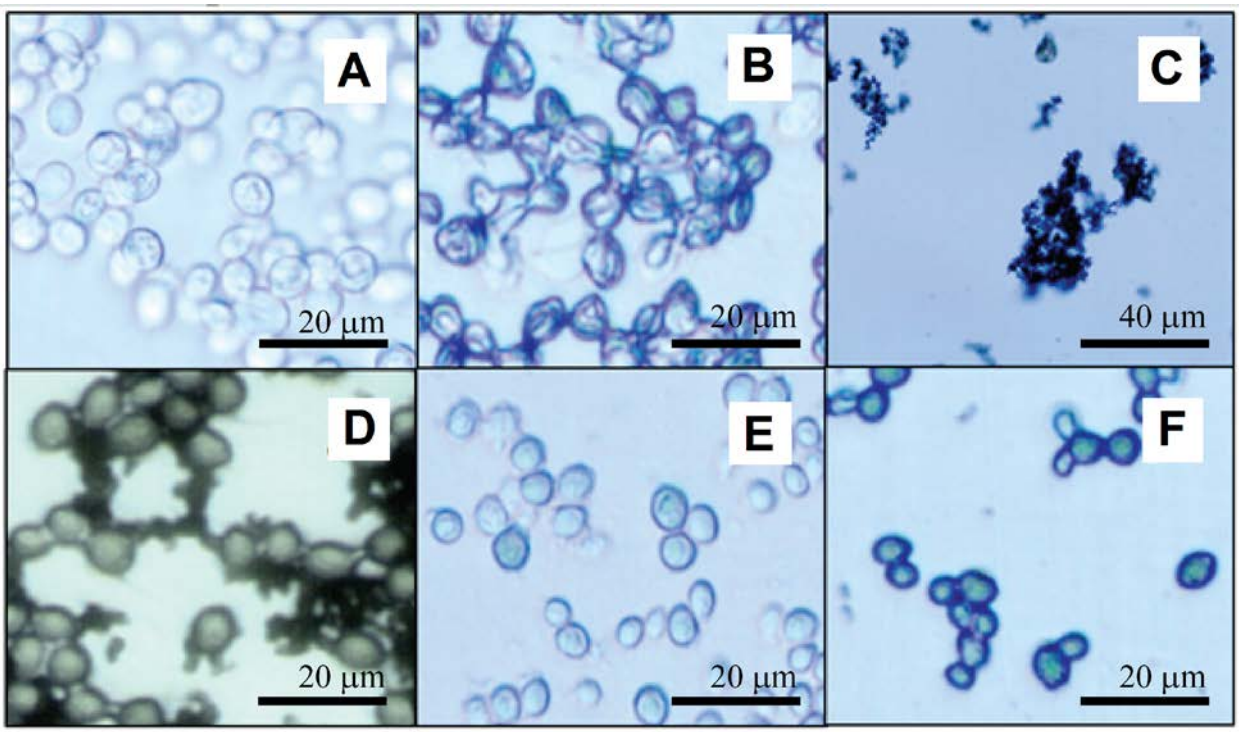

Figure 52 *Optical images of A) control, yeast cells in PBS buffer, which were incubated with no $[Fe(CN)_6]^{3-}$, $[Fe(CN)_6]^{4-}$ or pyrrole; B) PLL and GA immobilized and dried intact yeast cells after incubation in PBS; C) Ppy agglomerates formed from 500 mM of pyrrole and 40 mM of $[Fe(CN)_6]^{3-}$ with no yeasts; D) immobilized yeast cells after incubation in cell growth media with 500 mM of pyrrole and 40 mM of $[Fe(CN)_6]^{3-}$; E) immobilized yeast cells after incubation in cell growth media in the presence of 500 mM of pyrrole and 40 mM of $[Fe(CN)_6]^{4-}$; F) dried immobilized yeast cells after the incubation in cell growth media with 500 mM of pyrole and 40 mM of $[Fe(CN)_6]^{4-}$.*

In Figure 52 images from A to C represent control/reference samples: intact yeast cells incubated in PBS buffer; the same cells immobilized and dried afterwards on the objective glass slide using PLL and GA and solution of polypyrrole agglomerates formed from 500 mM of pyrrole and 40 mM of $[Fe(CN)_6]^{3-}$. As could be seen from image B, after drying the cells were shrank and wrinkled. The other two images (Figure 52 A and C) showed no abnormalities. From the Figure 52 D it can be observed that the yeast cells, which were incubated in the reaction mixture containing $[Fe(CN)_6]^{3-}$, glucose

and pyrrole, were surrounded and linked by structures composed of smaller dark spherical structural units of Ppy arranged between cells and within the cell wall.

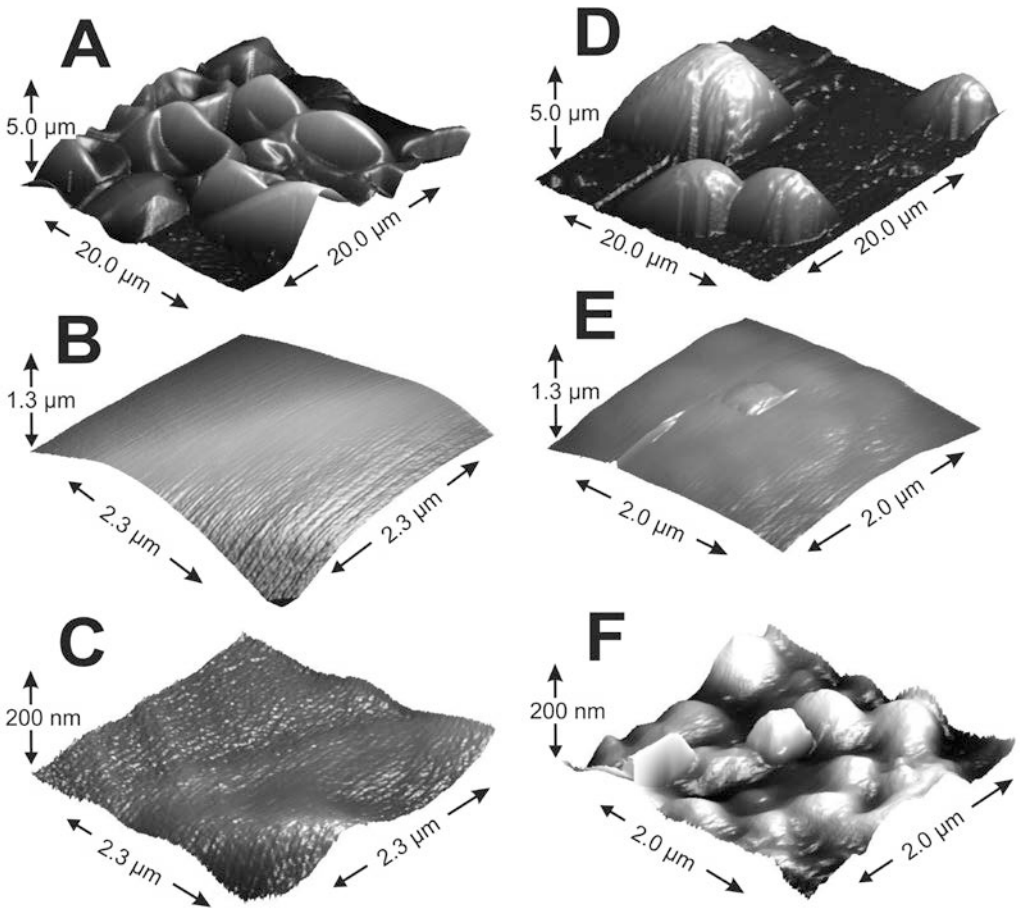

Figure 53 *Atomic force microscope images obtained in contact mode of unmodified (A, B, C) and modified yeast cells (D, E, F). For modification 500 mM of pyrrole and 40 mM of* $[Fe(CN)_6]^{4-}$ *were used. Figures A) and D) represent the whole cell images dried on the Si surface, image size 20 x 20* μm^2*; B) and E) represent the apex of the intact and modified cells, image size 2 x 2* μm^2*; in C) and F) images the second order flattening procedure is performed for the images of B) and E), image size is kept the same: 2 x 2* μm^2*.*

It was observed that Ppy-based structures had the same pattern as in control measurements from Figure 52 C. This was because $[Fe(CN)_6]^{3-}$ ions acted as an oxidator and induced fast formation of Ppy particles, which varied in size and shape although the composing units had the same spherical form. In contrast, when the yeast cells were incubated in solution containing $[Fe(CN)_6]^{4-}$, pyrrole and glucose (Figure 52 E and F) no separate particles or structures were observed around the cells. Only the dark envelope, formed from Ppy within the cell wall or periplasm was distinguished. The envelope became even more visible after the cells were immobilized and dried. For this reason it was assumed that the synthesis of Ppy was mostly localized in periplasm and/or cell wall. The oxidation of $[Fe(CN)_6]^{4-}$ to $[Fe(CN)_6]^{3-}$ is catalyzed by enzymes

(oxidoreductases), which are localized in yeast cell membrane, therefore, the most favorable environment of polymerization should be in the close proximity of the enzymes. Here proposed Ppy synthesis attracts a lot of interest, as conducting polymer based structures are formed in the space, which usually exhibit the highest electrical resistance or dieletric properties [296].

Atomic force microscopy was used for the comparison of Ppy modified and intact yeast cells. The surface structure and elasticity was evaluated. For these experiments yeast cells were grown and modified with usual 500 mM of pyrrole in presence of 40 mM of $[Fe(CN)_6]^{4-}$ and dried on the conventional Si substrate for imaging or immobilized in polycarbonate membrane for the stiffness measurements. The obtained imaging results are presented in Figure 53. During the overnight drying the intact cells have lost their shape and collapsed (Figure 53 A as well seen in optical image Figure 52 B) in contrast to the modified ones, that have preserved their spherical form (Figure 53 D). One considerable fact is that polymeric structure can increase thickness of the cell wall, as a result greatly suppressing cell drying process. For detailed surface examination high resolution images of the cell's surface was carried out (Figure 53 B and E). It was observed that modified cell surface possessed some surface structures while unmodified cell's surface was almost smooth. Figure 53 C and F were obtained from scans represented in B and E pictures by applying second order surface flattening algorithm. These computed images showed that modification with Ppy also alters cell surface roughness. The observed spherical hills suggested that polypyrrole is synthesized in small islands, possibly around PMOR systems.

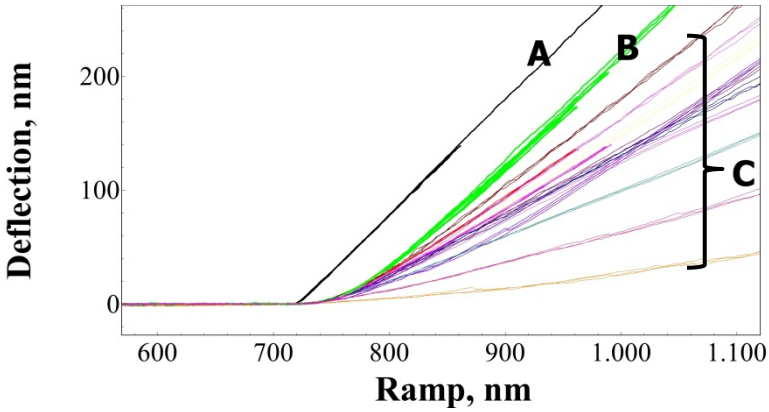

Figure 54 *Indentation curves of the AFM tip obtained for A) a stiff sample, B) unmodified yeast cells and C) for Ppy modified yeast cells.*

The AFM force measurements in liquid were performed for the evaluation of elasticity of modified and intact yeast cells. Yeast cells were immobilized into pores of polycarbonate membrane (pore diameter - 5μm) by filtering cell suspension (100 mM PBS, pH 7.0) through the membrane. The measurements were carried out in same PBS solution. The obtained results are displayed in Figure 54. Curve A represents a deflection of AFM tip on the solid surface of glass, multiple curves B represent surface elasticity of unmodified cells and C group of curves represents 500 mM pyrrole modified yeast cells. In order to compare different measurements, a rigid polycarbonate membrane surface was considered as solid surface. All the control samples of intact cells from different measurements were found to have the same elasticity profile (multiple overlapping curves Figure 54 B). Pyrrole modified cells even from the same batch not always possessed the same elasticity profile (curve group C, Figure 54). Although it was clear that in liquid all modified cells were softer than comparing to unmodified ones. We presume that no repeatability was observed due to several reasons. Firstly, the magnitude of modification was not possible to evaluate for a single cell. As modificatoion was noticed for all cells in general, the single cell could be modified with the different amount of pyrrole. Secondly, the viability of the cells after the modification was slightly reduced. During the AFM measurements it was impossible to determine if the cell was alive. Thirdly, as it was seen from AFM imaging (Figure 53) the surface of the cell became more rough and structured. AFM tip is extremely sensitive for the any shift or torsion which could appear due to the tip positioning on different place of the structure.

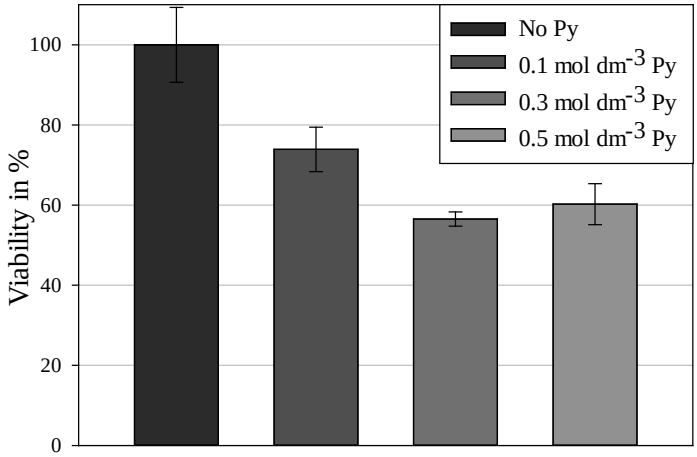

Figure 55 *Yeast cell viability after yeast cell modification with different Py concentrations.*

The viability of modified yeast cells was also evaluated. The yeast cell's sample with 40 mM $[Fe(CN)_6]^{4-}$, but without any Ppy was considered having 100% viability. When 100 mM of pyrrole was added into the cell suspension mentioned before, the viability of yeast cells has decreased by 26% (Figure 55). When the concentration of pyrrole has increased up to 300 mM, the viability has decreased by additional ~16%, this decrease was almost proportional to the concentration of pyrrole in cell suspension. However, when the concentration of pyrrole reached 500 mM, it was shown that there was no statistical difference between the viability of the two latest samples at 99% confidence limit when using the Welch's T-Test. This shows that pyrrole concentration in cell modification solution affects the viability of the yeast cells until 300 mM of pyrrole is reached. Further increase of pyrrole concentration does not affect the growth of yeast cells. These results confirm that the cytotoxicity of pyrrole depends only until a certain concentration. The Ppy can be integrated within the cell membrane what at high doses might lead to thermodynamic instability of cell membrane. This effect at some extent decreases the viability of the cells. Also, the Ppy is formed in cell wall or in periplasm, therefore, formed Ppy may slow down the diffusion of nutrients and/or metabolites in and out of the cells as well as watter. Therefore, high amount of Ppy formed within the cell wall may lead to insufficient diffusion of nutrients and/or metabolites what causes a decrease in the viability.

Conclusions of 3.5.2. section

In this part of doctoral dissertation a new way to synthesize Ppy by yeast cell induced redox-cycling of $[Fe(CN)_6]^{3-}/[Fe(CN)_6]^{4-}$ was reported. Ppy was formed by oxidative polymerization initiated by $[Fe(CN)_6]^{3-}$, during which the $[Fe(CN)_6]^{3-}$ was reduced to $[Fe(CN)_6]^{4-}$. Then the $[Fe(CN)_6]^{4-}$ was reoxidized back to $[Fe(CN)_6]^{4-}$ by redox processes running in the cytoplasm of yeast cells. In this way formed Ppy is mainly located within the cell wall and priplasm of the yeast cell. The applicability of atomic force microscopy for the evaluation of intact and modified yeast cell walls was shown. The atomic force microscopy could be used for the visualization of the yeast cell wall surface at high resolution, allowing to detect such small structures as a bud scar or the formed polymer. The local destruction of the cell wall could also be achieved using AFM with relatively high forces applied to the cantilever tip.

General conclusions

1. The concentration of the monomer strongly affects properties of formed Ppy layer: using 50 mM of initial monomer smooth and small grain-like structures are obtained; using 10 times higher concentration rough and donugth-like average ~14 μm structures are formed. Formation of Ppy layer on electrode proceeds in 'islands' dependently on the adsorbed monolayer.
2. Molecularly imprinted polypyrrole could be formed by two methods: potential pulse and potential cycle sequences, however potential pulse sequence based electrochemical polymerization was more suitable due to the recovery of monomer concentration near the electrode.
3. Continuous association/dissociation process of caffeine as well as theophylline showed that the equilibrium of the interaction of $MIPpy_{caff}$ and dissolved caffeine at standard conditions is shifted towards the formation of MIPpy/caffeine complex while the equilibrium for the interaction of $MIPpy_{caff}$ and theophylline is shifted towards dissociation of MIPpy/theophylline complex. Therefore the obtained caffeine-imprinted MIPpy demonstrated much higher selectivity towards caffeine in comparison with the selectivity towards its homologue – theophylline.
4. Gold nanoparticles (AuNPs) were entrapped within Ppy layer during chemical polymerization of pyrrole. During this entrapment the size of AuNPs increased from 10 nm (initial 'gold seeds') to 40 nm.
5. The stable carbon and nitrogen isotope ratio mass spectrometry was successfully applied for the evaluation of the complex Ppy/GOx biocomposite stoichiometry. Using 'nitrogen-approach' approximately 710-1970 pyrrole monomers were estimated to surround Glucose oxidase during enzymatic polymerization, while 'carbon-approach' was not reliable for this purpose.
6. The conducting polymer polypyrrole is not toxic to mouse bone marrow-derived stem cells. Polypyrrole deposited on the gold-plated glass slide did not impair cell attachment and proliferation. These cells adhered well on polypyrrole-modified surfaces and exposed normal fibroblast-like morphology.
7. Experimentally, silicon, silicon oxide, and HOPG were found to give intense and clear Raman features from yeast cells, although these substrates also present intrinsic

Raman signals that partially overlap with the spectral features from the cells. The gold and structured silver (suitable for SERS) substrates showed no intrinsic signals. The Raman intensity and the intensity ratios, both are a consequence of the substrate reflectivity and light distribution due to the optical properties of the substrate.

8. Polypyrrole synthesis induced by redox-cycling of $[Fe(CN)_6]^{3-}/[Fe(CN)_6]^{4-}$ within the yeast cell wall and/or periplasm could be performed without a significant loss of the cell viability. The atomic force microscopy is suitable for the visualization of the yeast cell wall surface at high resolution, allowing to detect such small structures, as bud scars or polymer structures formed within a cell wall.

Validation of the results

List of author's publications summarized in the dissertation:

1. **L. Mikoliunaite**, A. Makaraviciute, A. Suchodolskis, A. Ramanaviciene, Y. Oztekin, A. Stirke, G. Jurkaite, M. Ukanis, G. Carac, P. Cojocaru, A. Ramanavicius, Atomic Force Microscopy Study of Living Baker's Yeast Cells, Adv. Sci. Lett (2011) 4, 2, 368-376.
2. V. Ratautaite, A. Ramanaviciene, Y. Oztekin, J. Voronovic, Z. Balevicius, **L. Mikoliunaite**, A. Ramanavicius, Electrochemical Stability and Repulsion of Polypyrrole Film, Colloids and Surfaces A: Physicochemical and Engineering Aspects (2013) 16-21.
3. V. Ratautaite, S. N. Topkaya, **L. Mikoliunaite**, M. Ozsoz, Y. Oztekin, A. Ramanaviciene, A. Ramanavicius, Molecularly Imprinted Polypyrrole for DNA Determination, Electroanalysis (2013) 25(5), 1169-1177.
4. A. Vaitkuviene, V. Ratautaite, **L. Mikoliunaite**, V. Kaseta, G. Ramanauskaite, G. Biziuleviciene, A. Ramanaviciene, A. Ramanavicius, Some Biocompatibility Aspects of Conducting Polymer Polypyrrole Evaluated with Bone Marrow-Derived Stem Cells, Colloids and Surfaces A (2014) 442, 152 – 156.
5. **L. Mikoliunaite**, R. Kubiliute, A. Popov, J. Voronovic, S. Sakirzanovas, A. Ramanavičienė, A. Ramanavičius, Development of gold nanoparticle-polypyrrole nanocomposites, Chemija (2014) 25(2), 63-69.
6. A. Garbaras, **L. Mikoliunaite**, A. Popov, A. Ramanaviciene, V. Remeikis, A. Ramanavicius, The isotope method for the determination of stoichiometry between compounds forming the polypyrrole and glucose oxidase composite, Physical Chemistry Chemical Physics (2015) 17(3), 2252-2258.
7. D. Plausinaitis, V. Ratautaite, **L. Mikoliunaite**, L. Sinkevicius, A. Ramanaviciene, A. Ramanavicius, Quartz Crystal Microbalance-Based Evaluation of the Electrochemical Formation of an Aggregated Polypyrrole Particle-Based Layer, Langmuir (2015), 31, 3186-3193.
8. V. Ratautaite, D. Plausinaitis, I. Baleviciute, **L. Mikoliunaite**, A. Ramanaviciene, A. Ramanavicius, Characterization of caffeine-imprinted polypyrrole by a quartz

crystal microbalance and electrochemical impedance spectroscopy, Sensors and Actuators B (2015) 212 63–71.

9. **L. Mikoliunaite**, R. D. Rodriguez, E. Sheremet, V. Kolchuzhin, J. Mehner, A. Ramanavicius, D. R.T. Zahn, The substrate matters in the Raman spectroscopy analysis of cells, Scientific Reports (resubmitted after reviewers comments).

Application for patent

E. Andriukonis, A. Stirkė, **L. Mikoliūnaitė**, Z. Balevičius, A. Ramanavičienė ir A. Ramanavičius, Bio-polyperisation of pyrrole using redox mediator (2015) The State Patent Bureau of the Republic of Lithuania.

List of Conferences, where the results of the dissertation were presented:

Author:

1. **L. Mikoliunaite**, E. Sheremet, R. D. Rodriguez, A. Ramanavičius, D. R. T. Zahn, Importance of the surface and laser energy to the Raman spectroscopy of living yeast cells (Saccharomyces cerevisiae), Nanochemistry and nanomaterials: International conference of young chemists, Palanga, Lithuania, 2012 12 7 – 9.
2. **L. Mikoliunaite**, A. Popov, J. Voronovic, A. Ramanaviciene, A. Ramanavicius, Chemical and Enzymatic Synthesis of Polypyrrole and Polianiline Nanoparticles, Advanced Materials and Technologies, Palanga, Lithuania, 2013 08 27 – 31;
3. **L. Mikoliunaite**, R. Kubiliute, J. Svirelis, J. Voronovic, A. Popov, U. Samukaite-Bubniene, B. Bugelyte, A. Ramanaviciene, A. Ramanavicius, Synthesis of Gold – Polypyrrole Nanocomposites, Ecobalt 2013, Vilnius, Lithuania, 2013 10 25 – 27;

Coauthor:

4. V. Ratautaitė, J. Voronovič, **L. Mikoliūnaitė**, A. Ramanavičienė, A. Ramanavičius, Molecularly imprinted polypyrrole for analysis of bioactive

compounds, Advanced materials and technologies, Palanga, Lithuania, 2011 08 27 – 31.

5. A. Vaitkuvienė, A. Stirkė, **L. Mikoliūnaitė**, A. Suchodolskis, A. Ramanavičienė, A. Ramanavičius, Investigation of Transformed Cells by Atomic Force Microscopy, Pittcon 2012, Orlando, USA, 2012 05 12.
6. V. Ratautaitė, A. Alubeckas, **L. Mikoliunaitė**, A. Ramanavičienė, A. Ramanavičius, Electrochemical Polymerization of Conducting Polymer Polypyrrole, The Vital Nature Sign 2012, Kaunas, Lithuania, 2012 06 1 – 4.
7. R. Kubiliūtė, J. Svirelis, **L. Mikoliūnaitė**, J. Voronovič, A. Popov, A. Ramanavičienė, A. Ramanavičius, Self-Growth of Gold-Polypyrrole Nanocomposites, The Vital Nature Sign, Kaunas, Lithuania, 2013 05 16 – 19.
8. A. Ramanavicius, I. Baleviciute, **L. Mikoliunaite**, J. Voronovic, A. Ramanaviciene, Conducting Polymers in Nanotechnological Devices, Advanced Materials and Technologies, Palanga, Lithuania, 2013 08 27 – 31;
9. A. Popov, **L. Mikoliunaite**, J. Voronovic, A. Ramanaviciene, A. Ramanavicius, Comparison of Chemical and Enzymatic Sythesized Polypyrrole Nanoparticles, EcoBalt 2013, Vilnius, Lithuania, 2013 10 25 – 27.
10. A. Garbaras, A. Ramanavicius, **L. Mikoliunaite**, A. Popov, Application of isotope method for the determination of stoichiometry of complex nanocomposites, Isotopes in Biological & Chemical Sciences, Galveston, TX, USA, 2014 02 2-7.
11. A. Ramanavičius, A. Ramanavičienė, A. Popov, A. Kaušaitė-Minkštimienė, **L. Mikoliūnaitė**, V. Mažeiko, Y. Oztekin, Investigation of enzymatically synthesized conducting polymer nanoparticles. PITTCON conference and EXPO 2014, Chicago, USA, 2014 03 2-6.
12. A. Garbaras, **L. Mikoliunaite**, A. Popov, A. Ramanaviciene, V. Remeikis, A. Ramanavicius, Application of stable isotope method for the nanocomposites investigation, IMSC 2014, Geneva, Switzerland, 2014 08 24-29.
13. A. Ramanavicius, I. Baleviciute, D. Plausinaitis, V. Ratautaite, Z. Balevicius, L. Sinkevicius, **L. Mikoliunaite**, A. Ramanaviciene, Evaluation of molecularly imprinted polypyrrole. Bio-sensing technology, Lisbon, Portugal 2015 05 10-13.

Curriculum Vitae

Name, Surname Lina Mikoliūnaitė

E-mail lina.mikoliunaite@chf.vu.lt

Date of birth 1985 08 14

EDUCATION

2010 – 2015 Vilnius University, Faculty of Chemistry, post graduate studies, study program Chemistry.

2008 – 2010 Vilnius University, Faculty of Physics, MSc degree in Physics, study programme Biophysics.

2004 – 2008 Vilnius University, Faculty of Physics, Bachelor of Physics, study programme Management of Modern Technology.

CURRENT RESEARCH AND ACADEMIC POSITIONS

2015 02 01 – present Vilnius University, Faculty of Chemistry, leader of the department of project preparation and administration;

2012 10 15 – present Institution State Scientific Research Institute Center for Physical Sciences and Technology, Department of Semiconductor Physics, NanoBioTechnology Laboratory, junior researcher;

2012 10 01 – present Vilnius University, Faculty of Physics, Department of General Physics and Spectroscopy, junior researcher.

PROFESSIONAL TRAINING

1. Intensive summer school „EUCHEME 2013”, 2013 07 30 – 08 12, Camerino University (Italy);

2. Erasmus Student Placement, 2012 07 02 – 09 30, Chemnitz University of Technology (Germany);

3. Erasmus Studies Programme, 2007 02 – 07, Ghent University (Belgium);

4. Students’ Scientific Practice implemented by the Research Council of Lithuania, 2006 07 01 – 08 31, Institute of Immunology (Lithuania).

References

1. Turner, A.P.F., I. Karube, and G.S. Wilson, *Biosensors Fundamentals and Applications*. 1987, Oxford, UK: Oxford University Press.
2. Blum, L.J. and P.R. Coulet, *Biosensor Principles and Applications*. 1991, New York: Marcel Dekker.
3. Ivnitski, D., et al., *Biosensors for detection of pathogenic bacteria*. Biosensors & Bioelectronics, 1999. **14**(7): p. 599-624.
4. Rafael Vargas-Bernal, Esmeralda Rodríguez-Miranda, and G. Herrera-Pérez, *Evolution and Expectations of Enzymatic Biosensors for Pesticides*, in *Pesticides - Advances in Chemical and Botanical Pesticides*, R.P. Soundararajan, Editor. 2012, InTech.
5. D'Souza, S.F., *Microbial biosensors.* Biosensors and Bioelectronics, 2001. **16**(6): p. 337-353.
6. Toshima, N. and O. Ihata, *Catalytic synthesis of conductive polypyrrole using iron(III) catalyst and molecular oxygen.* Synthetic Metals, 1996. **79**(2): p. 165-172.
7. Korol, E.N., *Dependence of the Electroconductivity of N-Doped Polymers on Conjugation Length.* Synthetic Metals, 1994. **63**(3): p. 245-246.
8. Zhao, Y.X., et al., *Thin electroconductive hydrogel films by in situ electropolymerization of pyrrole within polyelectrolyte multilayers.* Rsc Advances, 2014. **4**(47): p. 24511-24517.
9. Lee, S., et al., *New Strategy and Easy Fabrication of Solid-State Supercapacitor Based on Polypyrrole and Nitrile Rubber.* Journal of Nanoscience and Nanotechnology, 2008. **8**(9): p. 4722-4725.
10. Chen, X.B., et al., *The Stability of Polypyrrole Electrical-Conductivity.* European Polymer Journal, 1994. **30**(7): p. 809-811.
11. Thieblemont, J.C., et al., *Stability of Chemically Synthesized Polypyrrole Films.* Synthetic Metals, 1993. **59**(1): p. 81-96.
12. Ramanaviciene, A., et al., *Biocompatibility of polypyrrole particles: an in-vivo study in mice.* Journal of Pharmacy and Pharmacology, 2007. **59**(2): p. 311-315.
13. Vaitkuviene, A., et al., *Evaluation of cytotoxicity of polypyrrole nanoparticles synthesized by oxidative polymerization.* Journal of Hazardous Materials, 2013. **250**: p. 167-174.
14. Chen, W., et al., *Ordered conducting polypyrrole doped with sulfopropyl ether of beta-cyclodextrin.* Macromolecules, 2003. **36**(2): p. 276-278.
15. Sigmund, W.M., et al., *Polymerization of monolayers of 3-substituted pyrroles.* Langmuir, 1999. **15**(19): p. 6423-6427.
16. Yamaura, M., K. Sato, and T. Hagiwara, *Effect of counter-anion exchange on electrical conductivity of polypyrrole films.* Synthetic Metals, 1991. **41**(1–2): p. 439-442.
17. Thombare, J.V., et al., *Optical properties of electrochemically synthesized polypyrrole thin films: the electrolyte effect.* Journal of Semiconductors, 2014. **35**(6): p. 063001.
18. Beck, F., U. Barsch, and R. Michaelis, *Corrosion of Conducting Polymers in Aqueous-Media.* Journal of Electroanalytical Chemistry, 1993. **351**(1-2): p. 169-184.
19. Billingham, N.C., et al., *Stability and Degradation of Some Electrically Conducting Polymers.* Polymer Degradation and Stability, 1987. **19**: p. 323-341.
20. McNeill, R., et al., *Electronic Conduction in Polymers. I. The Chemical Structure of Polypyrrole.* Australian Journal of Chemistry, 1963. **16**(6): p. 1056-1075.
21. Street, G.B., et al., *Modification of the electronic properties of (SN)x by halogens; properties of (SNBr0·4)x.* Chemical Communications 1977. **12**: p. 407.
22. Shirakawa, H., et al., *Synthesis of electrically conducting organic polymers: halogen derivatives of polyacetylene, (CH)x.* Chemical Communications, 1977. **16**: p. 578-580.
23. MacDiarmid, A.G. and A.J. Heeger, *Organic metals and semiconductors: The chemistry of polyacetylene, (CH)x, and its derivatives.* Synthetic Metals, 1980. **1**(2): p. 101-118.
24. Diaz, A.F., K.K. Kanazawa, and G.P. Gardini, *Electrochemical polymerization of pyrrole.* Journal of the Chemical Society, Chemical Communications, 1979(14): p. 635-636.
25. Wei, J., et al., *Photodissociation dynamics of pyrrole: Evidence for mode specific dynamics from conical intersections.* Faraday Discussions, 2004. **127**: p. 267-282.

26. Beljonne, D., et al., *Optical signature of delocalized polarons in conjugated polymers.* Advanced Functional Materials, 2001. **11**(3): p. 229-234.
27. Bredas, J.L. and G.B. Street, *Polarons, bipolarons, and solitons in conducting polymers.* Accounts of Chemical Research, 1985. **18**(10): p. 309-315.
28. Yakushi, K., et al., *Optical study of poly-β, β'-dimethylpyrrole perchlorate: Evidence for bipolarons.* The Journal of Chemical Physics, 1984. **81**(9): p. 4133-4137.
29. Brédas, J.L., et al., *Polarons and bipolarons in polypyrrole: Evolution of the band structure and optical spectrum upon doing.* Physical Review B, 1984. **30**(2): p. 1023-1025.
30. Shimidzu, T., et al., *A novel type of polymer battery using a polypyrrole-polyanion composite anode.* Journal of the Chemical Society, Chemical Communications, 1987(5): p. 327-328.
31. Ren, X., *Charge Transport in Polypyrrole-Based Conducting Polymers*, in *Dep. of Chemistry*1993, Memorial University of Newfoundland: Newfoundland.
32. Chen, X.B., et al., *The stability of polypyrrole and its composites.* Journal of Materials Science, 1997. **32**(6): p. 1515-1518.
33. Ayad, M.M., *Quartz-Crystal Microbalance Study for Chemical Synthesis of Polypyrrole.* Journal of Applied Polymer Science, 1994. **53**(10): p. 1331-1337.
34. Duchet, J., R. Legras, and S. Demoustier-Champagne, *Chemical synthesis of polypyrrole: structure-properties relationship.* Synthetic Metals, 1998. **98**(2): p. 113-122.
35. Martina, S., et al., *Polypyrrole - Towards the Development of a Chemical Synthesis.* Synthetic Metals, 1991. **41**(1-2): p. 403-406.
36. Omastova, M., M. Lazar, and S. Kosina, *Combined Electrochemical and Chemical Synthesis of Thick Polypyrrole Layers and Their Characterization.* Polymer International, 1994. **34**(2): p. 151-156.
37. Ramanavicius, A., A. Kausaite, and A. Ramanaviciene, *Self-encapsulation of oxidases as a basic approach to tune the upper detection limit of amperometric biosensors.* Analyst, 2008. **133**(8): p. 1083-1089.
38. Ramanavicius, A., et al., *Fluorescence study of glucose oxidase self-encapsulated within polypyrrole.* Sensors and Actuators B: Chemical, 2012. **171–172**(0): p. 753-759.
39. Fang, Q., D.G. Chetwynd, and J.W. Gardner, *Conducting polymer films by UV-photo processing.* Sensors and Actuators a-Physical, 2002. **99**(1-2): p. 74-77.
40. Zhang, Z.H., et al., *Plasma Polymerized Pyrrole Films for Biological Applications: Correlation Between Protein Adsorption Properties and Characteristics.* Plasma Processes and Polymers, 2011. **8**(10): p. 923-931.
41. Zhang, Z.H., et al., *DNA Detection and Cell Adhesion on Plasma-Polymerized Pyrrole.* Biopolymers, 2014. **101**(5): p. 496-503.
42. Vernitskaya, T.V. and O.N. Efimov, *Polypyrrole: A conducting polymer (synthesis, properties, and applications).* USPEKHI KHIMII, 1997. **66**(5): p. 489-505.
43. Genies, E.M., G. Bidan, and A.F. Diaz, *Spectroelectrochemical study of polypyrrole films.* Journal of Electroanalytical Chemistry and Interfacial Electrochemistry, 1983. **149**(1–2): p. 101-113.
44. Waltman, R.J., *Reactivity/structure correlations for the electropolymerization of pyrrole: An INDO/CNDO study of the reactive sites of oligomeric radical cations.* Tetrahedron, 1984. **40**(20): p. 3963-3970.
45. Andrieux, C.P., et al., *Identification of the 1st Steps of the Electrochemical Polymerization of Pyrroles by Means of Fast Potential Step Techniques.* Journal of Physical Chemistry, 1991. **95**(24): p. 10158-10164.
46. Diaz, A.F., et al., *Electrooxidation of aromatic oligomers and conducting polymers.* Journal of Electroanalytical Chemistry and Interfacial Electrochemistry, 1981. **121**(0): p. 355-361.
47. Diaz, A.F. and J. Bargon, *Handbook of conducting polymers*. Vol. 1. 1986: Marcel Dekker Inc.
48. Wei, Y., J. Tian, and D. Yang, *A new method for polymerization of pyrrole and derivatives.* Die Makromolekulare Chemie, Rapid Communications, 1991. **12**(11): p. 617-623.

49. Yen, W., et al., *Electrochemical Polymerization of Thiophenes in the Presence of Bithiophene or Terthiophene - Kinetics and Mechanism of the Polymerization.* Chemistry of Materials, 1991. **3**(5): p. 888-897.
50. Bloor, D., et al., *Structure-Property Relationships in Conductive Polymers.* Molecular Crystals and Liquid Crystals, 1990. **187**: p. 231-239.
51. Ansari, R., *Polypyrrole Conducting Electroactive Polymers: Synthesis and Stability Studies.* E-Journal of Chemistry, 2006. **3**(4): p. 186-201.
52. Machida, S., S. Miyata, and A. Techagumpuch, *Chemical synthesis of highly electrically conductive polypyrrole.* Synthetic Metals, 1989. **31**(3): p. 311-318.
53. Rapi, S., V. Bocchi, and G.P. Gardini, *Conducting polypyrrole by chemical synthesis in water.* Synthetic Metals, 1988. **24**(3): p. 217-221.
54. Armes, S.P., *Optimum reaction conditions for the polymerization of pyrrole by iron(III) chloride in aqueous solution.* Synthetic Metals, 1987. **20**(3): p. 365-371.
55. Chao, T.H. and J. March, *A study of polypyrrole synthesized with oxidative transition metal ions.* Journal of Polymer Science Part A: Polymer Chemistry, 1988. **26**(3): p. 743-753.
56. Mohammadi, A., et al., *Polypyrrole prepared by chemical vapour deposition using hydrogen peroxide and hydrochloric acid.* Synthetic Metals, 1987. **21**(1–3): p. 169-173.
57. Neoh, K.G., E.T. Kang, and T.C. Tan, *Effects of acceptor level on chemically synthesized polypyrrole-halogen complexes.* Journal of Applied Polymer Science, 1989. **37**(8): p. 2169-2180.
58. Chan, H.S.O., et al., *XPS studies of chemically synthesized polypyrrole-halogen charge transfer complexes.* Synthetic Metals, 1988. **22**(4): p. 365-370.
59. Dhawan, S.K. and D.C. Trivedi, *Thin conducting polypyrrole film on insulating surface and its applications.* Bulletin of Materials Science, 1993. **16**(5): p. 371-380.
60. Whang, Y.E., et al., *Polypyrroles prepared by chemical oxidative polymerization at different oxidation potentials.* Synthetic Metals, 1991. **45**(2): p. 151-161.
61. Bocchi, V. and G.P. Gardini, *Chemical synthesis of conducting polypyrrole and some composites.* Journal of the Chemical Society, Chemical Communications, 1986(2): p. 148a-148a.
62. Bocchi, V., G.P. Gardini, and S. Rapi, *Highly electroconductive polypyrrole composites.* Journal of Materials Science Letters, 1987. **6**(11): p. 1283-1284.
63. Leonavicius, K., A. Ramanaviciene, and A. Ramanavicius, *Polymerization Model for Hydrogen Peroxide Initiated Synthesis of Polypyrrole Nanoparticles.* Langmuir, 2011. **27**(17): p. 10970-10976.
64. Heinze, J., *Electrochemistry of conducting polymers.* Synthetic Metals, 1991. **43**(1–2): p. 2805-2823.
65. Kupila, E.L. and J. Kankare, *Electropolymerization of pyrrole: Effects of pH and anions on the conductivity and growth kinetics of polypyrrole.* Synthetic Metals, 1993. **55**(2–3): p. 1402-1405.
66. Beck, F. and M. Oberst, *Electrodeposition and cycling of polypyrrole.* Makromolekulare Chemie. Macromolecular Symposia, 1987. **8**(1): p. 97-125.
67. West, K., et al., *Electrochemical synthesis of polypyrrole: Influence of current density on structure.* Synthetic Metals, 1993. **55**(2–3): p. 1412-1417.
68. Ko, J.M., et al., *Morphology and Electrochemical Properties of Polypyrrole Films Prepared in Aqueous and Nonaqueous Solvents.* Journal of the Electrochemical Society, 1990. **137**(3): p. 905-909.
69. Kim, B.-S., et al., *Electrochemistry of conductive polymers XVI. Growth mechanism of polypyrrole studied by kinetic and spectroelectrochemical measurements.* Synthetic Metals, 1995. **69**(1–3): p. 455-458.
70. Kiani, M.S. and G.R. Mitchell, *The role of the counter-ion in the preparation of polypyrrole films with enhanced properties using a pulsed electrochemical potential.* Synthetic Metals, 1992. **48**(2): p. 203-218.

71. Witkowski, A., M.S. Freund, and A. Brajter-Toth, *Effect of electrode substrate on the morphology and selectivity of overoxidized polypyrrole films.* Analytical Chemistry, 1991. **63**(6): p. 622-626.
72. Asavapiriyanont, S., et al., *The electrodeposition of polypyrrole films from aqueous solutions.* Journal of Electroanalytical Chemistry and Interfacial Electrochemistry, 1984. **177**(1–2): p. 229-244.
73. Scharifker, B.R., E. García-Pastoriza, and W. Marino, *The growth of polypyrrole films on electrodes.* Journal of Electroanalytical Chemistry and Interfacial Electrochemistry, 1991. **300**(1–2): p. 85-98.
74. Rodriguez, I., M.L. Marcos, and J. González-Velasco, *Mechanism of electrochemical growth of polypyrrole on a glass electrode doped with SnO2 (ITO) from aqueous solutions.* Electrochimica Acta, 1987. **32**(8): p. 1181-1185.
75. Penner, R.M., L.S. Van Dyke, and C.R. Martin, *Electrochemical evaluation of charge-transport rates in polypyrrole.* The Journal of Physical Chemistry, 1988. **92**(18): p. 5274-5282.
76. Grunden, B. and J.O. Iroh, *Formation of graphite fibre-polypyrrole coatings by aqueous electrochemical polymerization.* Polymer, 1995. **36**(3): p. 559-563.
77. John, R. and G.G. Wallace, *Factors influencing the rate of the electrochemical oxidation of heterocyclic monomers.* Polymer International, 1992. **27**(3): p. 255-260.
78. Diaz, A.F., et al., *Electrochemistry of conducting polypyrrole films.* Journal of Electroanalytical Chemistry and Interfacial Electrochemistry, 1981. **129**(1–2): p. 115-132.
79. Salmon, M., et al., *Chemical modification of conducting polypyrrole films.* Molecular Crystals and Liquid Crystals, 1982. **83**(1): p. 265-276.
80. Angeli, A., *Sopra i neri di pirrolo.* Gazzetta Chimica Italiana, 1916. **46**: p. 279.
81. Dall'Olio, A., et al., *Resonance paramagnetique electronique et conductivité d'un noir d'oxypyrrole electrolytique.* Comptes Rendus de l'Académie des Sciences - Series IIC - Chemistry, 1968. **267**: p. 433-435.
82. Xiao, R., et al., *Controlled Electrochemical Synthesis of Conductive Polymer Nanotube Structures.* Journal of the American Chemical Society, 2007. **129**(14): p. 4483-4489.
83. Salmón, M., et al., *A chemical route to pyrrole polymer films.* Journal of Polymer Science: Polymer Letters Edition, 1982. **20**(3): p. 187-193.
84. Shimidzu, T., et al., *A functionalized polypyrrole film prepared by chemical polymerization at a vapour-liquid interface.* Journal of the Chemical Society, Chemical Communications, 1986(18): p. 1414-1415.
85. John, R. and G.G. Wallace, *The use of microelectrodes to probe the electropolymerization mechanism of heterocyclic conducting polymers.* Journal of Electroanalytical Chemistry and Interfacial Electrochemistry, 1991. **306**(1–2): p. 157-167.
86. Wei, Y. and J. Tian, *Effect of oligomeric additives and applied potential on the molecular weight and structure of electrochemically synthesized poly(3-alkylthiophenes).* Macromolecules, 1993. **26**(3): p. 457-463.
87. Mitchell, G.R., F.J. Davis, and C.H. Legge, *The effect of dopant molecules on the molecular order of electrically-conducting films of polypyrrole.* Synthetic Metals, 1988. **26**(3): p. 247-257.
88. Suarez-Herrera, M.F., *Conducting polymers*, in *Electrochemistry*, j.M. Feliu-Martinez and V.C. Payáa, Editors. 2010, EOLSS. p. 450.
89. Somani, P. and S. Radhakrishnan, *Electrochromic response in polypyrrole sensitized by Prussian blue.* Chemical Physics Letters, 1998. **292**(1-2): p. 218-222.
90. Rowley, N.M. and R.J. Mortimer, *New electrochromic materials.* Science Progress, 2002. **85**(3): p. 243-262.
91. Talaie, A., et al., *Dynamic sensing using intelligent composite: an investigation to development of new pH sensors and electrochromic devices.* Thin Solid Films, 2000. **363**(1-2): p. 163-166.

92. Facchetti, A., M.H. Yoon, and T.J. Marks, *Gate dielectrics for organic field-effect transistors: New opportunities for organic electronics.* Advanced Materials, 2005. **17**(14): p. 1705-1725.
93. Park, J.W., C. Lee, and J. Jang, *High-performance field-effect transistor-type glucose biosensor based on nanohybrids of carboxylated polypyrrole nanotube wrapped graphene sheet transducer.* Sensors and Actuators B-Chemical, 2015. **208**: p. 532-537.
94. Krings, L.H.M., et al., *The Application of Polypyrrole as Counterelectrode in Electrolytic Capacitors.* Synthetic Metals, 1993. **54**(1-3): p. 453-459.
95. Adeloju, S.B., S.J. Shaw, and G.G. Wallace, *Polypyrrole-Based Potentiometric Biosensor for Urea .1. Incorporation of Urease.* Analytica Chimica Acta, 1993. **281**(3): p. 611-620.
96. Lange, U., N.V. Roznyatouskaya, and V.M. Mirsky, *Conducting polymers in chemical sensors and arrays.* Analytica Chimica Acta, 2008. **614**(1): p. 1-26.
97. Forzani, E.S., et al., *A conducting polymer nanojunction sensor for glucose detection.* Nano Letters, 2004. **4**(9): p. 1785-1788.
98. Xue, K.W., et al., *A novel amperometric glucose biosensor based on ternary gold nanoparticles/polypyrrole/reduced graphene oxide nanocomposite.* Sensors and Actuators B-Chemical, 2014. **203**: p. 412-416.
99. Hamilton, A. and C.B. Breslin, *The development of a novel urea sensor using polypyrrole.* Electrochimica Acta, 2014. **145**: p. 19-26.
100. Chriswanto, H., H. Ge, and G.G. Wallace, *Polypyrrole-Coated Silica as a New Stationary-Phase for Liquid-Chromatography.* Chromatographia, 1993. **37**(7-8): p. 423-428.
101. Mermilliod, N. and J. Tanguy, *A Study of Chemically Synthesized Polypyrrole as Electrode Material for Battery Applications.* Journal of The Electrochemical Society, 1986. **133**(6): p. 1073-1079.
102. Priyadharshni, L.S. and M. Selvaraj, *Polypyrrole Sulfonate as a Transparent Conducting Film for Photovoltaic Applications.* International Journal of Polymeric Materials and Polymeric Biomaterials, 2015. **64**(1): p. 47-53.
103. Mirmohseni, A., et al., *Adaptive Membrane Systems Based on Conductive Electroactive Polymers.* Journal of Intelligent Material Systems and Structures, 1993. **4**(1): p. 43-49.
104. Sathiyanarayanan, S., S.S. Azim, and G. Venkatachari, *A new corrosion protection coating with polyaniline-TiO2 composite for steel.* Electrochimica Acta, 2007. **52**(5): p. 2068-2074.
105. Wang, X., et al., *Evaluation of biocompatibility of polypyrrole in vitro and in vivo.* J Biomed Mater Res A, 2004. **68**(3): p. 411-22.
106. Ramanaviciene, A., et al., *Biocompatibility of polypyrrole particles: an in-vivo study in mice.* J Pharm Pharmacol, 2007. **59**(2): p. 311-5.
107. Zhang, L., et al., *Enhanced differentiation of embryonic and neural stem cells to neuronal fates on laminin peptides doped polypyrrole.* Macromol Biosci, 2010. **10**(12): p. 1456-64.
108. Collier, J.H., et al., *Synthesis and characterization of polypyrrole-hyaluronic acid composite biomaterials for tissue engineering applications.* J Biomed Mater Res, 2000. **50**(4): p. 574-84.
109. Broda, C.R., et al., *A chemically polymerized electrically conducting composite of polypyrrole nanoparticles and polyurethane for tissue engineering.* J Biomed Mater Res A, 2011. **98**(4): p. 509-16.
110. Lakard, S., et al., *Adhesion and proliferation of cells on new polymers modified biomaterials.* Bioelectrochemistry, 2004. **62**(1): p. 19-27.
111. Stauffer, W.R. and X.T. Cui, *Polypyrrole doped with 2 peptide sequences from laminin.* Biomaterials, 2006. **27**(11): p. 2405-13.
112. Garner, B., et al., *Human endothelial cell attachment to and growth on polypyrrole-heparin is vitronectin dependent.* J Mater Sci Mater Med, 1999. **10**(1): p. 19-27.
113. Ateh, D.D., P. Vadgama, and H.A. Navsaria, *Culture of human keratinocytes on polypyrrole-based conducting polymers.* Tissue Eng, 2006. **12**(4): p. 645-55.

114. Gilmore, K.J., et al., *Skeletal muscle cell proliferation and differentiation on polypyrrole substrates doped with extracellular matrix components.* Biomaterials, 2009. **30**(29): p. 5292-304.
115. Lee, J.Y., et al., *Polypyrrole-coated electrospun PLGA nanofibers for neural tissue applications.* Biomaterials, 2009. **30**(26): p. 4325-35.
116. Bechara, S., L. Wadman, and K.C. Popat, *Electroconductive polymeric nanowire templates facilitates in vitro C17.2 neural stem cell line adhesion, proliferation and differentiation.* Acta Biomater, 2011. **7**(7): p. 2892-901.
117. Lundin, V., et al., *Control of neural stem cell survival by electroactive polymer substrates.* PLoS One, 2011. **6**(4): p. e18624.
118. Ghasemi-Mobarakeh, L., et al., *Application of conductive polymers, scaffolds and electrical stimulation for nerve tissue engineering.* J Tissue Eng Regen Med, 2011. **5**(4): p. e17-35.
119. Gensler, R., et al., *Application of nanoparticles in polymers for electronics and electrical engineering.* Particle & Particle Systems Characterization, 2002. **19**(5): p. 293-299.
120. Paquet, C. and E. Kumacheva, *Nanostructured polymers for photonics.* Materials Today, 2008. **11**(4): p. 48-56.
121. Kumar, P., et al., *Narrow-bandwidth spontaneous luminescence from oriented semiconducting polymer nanostructures.* Journal of Physical Chemistry B, 2003. **107**(26): p. 6252-6257.
122. Dersch, R., et al., *Nanoprocessing of polymers: applications in medicine, sensors, catalysis, photonics.* Polymers for Advanced Technologies, 2005. **16**(2-3): p. 276-282.
123. Prasad, P.N., *Polymer science and technology for new generation photonics and biophotonics.* Current Opinion in Solid State & Materials Science, 2004. **8**(1): p. 11-19.
124. Zhang, P., et al., *One-pot fabrication of polymer nanoparticle-based chemosensors for Cu2+ detection in aqueous media.* Polymer Chemistry, 2013. **4**(7): p. 2325-2332.
125. Vanderhoff, J.W., M.S. El-Aasser, and J. Ugelstad, *Polymer emulsification process*, 1979, Google Patents.
126. Rao, J.P. and K.E. Geckeler, *Polymer nanoparticles: Preparation techniques and size-control parameters.* Progress in Polymer Science, 2011. **36**(7): p. 887-913.
127. Bakshi, M.S., et al., *Effect of sodium dodecylsulfate and dodecyltrimethyl ammonium bromide on the morphologies of gold nanoparticles in the presence of poly(amidoamine) dendrimers.* J Nanosci Nanotechnol, 2006. **6**(3): p. 644-50.
128. Jana, N.R., *Gram-scale synthesis of soluble, near-monodisperse gold nanorods and other anisotropic nanoparticles.* Small, 2005. **1**(8-9): p. 875-882.
129. Jana, N.R., L. Gearheart, and C.J. Murphy, *Evidence for Seed-Mediated Nucleation in the Chemical Reduction of Gold Salts to Gold Nanoparticles.* Chemistry of Materials, 2001. **13**(7): p. 2313-2322.
130. Sakai, T. and P. Alexandridis, *Single-step synthesis and stabilization of metal nanoparticles in aqueous pluronic block copolymer solutions at ambient temperature.* Langmuir, 2004. **20**(20): p. 8426-8430.
131. Sakai, T. and P. Alexandridis, *Mechanism of gold metal ion reduction, nanoparticle growth and size control in aqueous amphiphilic block copolymer solutions at ambient conditions.* Journal of Physical Chemistry B, 2005. **109**(16): p. 7766-7777.
132. Sakai, T. and P. Alexandridis, *Spontaneous formation of gold nanoparticles in poly(ethylene oxide)-poly(propylene oxide) solutions: Solvent quality and polymer structure effects.* Langmuir, 2005. **21**(17): p. 8019-8025.
133. Ray, D. and V.K. Aswal, *Step-addition Method for Enhancing the Yield of Gold Nanoparticles in Block Copolymer Solution.* Journal of Macromolecular Science Part B-Physics, 2010. **49**(4): p. 810-820.
134. Pelaz, B., et al., *Tailoring the Synthesis and Heating Ability of Gold Nanoprisms for Bioapplications.* Langmuir, 2012. **28**(24): p. 8965-8970.

135. Saberi, R.S., S. Shahrokhian, and G. Marrazza, *Amplified Electrochemical DNA Sensor Based on Polyaniline Film and Gold Nanoparticles.* Electroanalysis, 2013. **25**(6): p. 1373-1380.
136. Zawadzka, M., et al., *In situ polymerised polypyrrole films for sensors application.* Microelectronics International, 2014. **31**(3): p. 158-162.
137. Sadrolhosseini, A.R., et al., *Application of Polypyrrole Multi-Walled Carbon Nanotube Composite Layer for Detection of Mercury, Lead and Iron Ions Using Surface Plasmon Resonance Technique.* Plos One, 2014. **9**(4).
138. Karadas, N. and S.A. Ozkan, *Electrochemical preparation of sodium dodecylsulfate doped over-oxidized polypyrrole/multi-walled carbon nanotube composite on glassy carbon electrode and its application on sensitive and selective determination of anticancer drug: Pemetrexed.* Talanta, 2014. **119**: p. 248-254.
139. Ashraf, R., A. Kausar, and M. Siddiq, *High-performance polymer/nanodiamond composites: synthesis and properties.* Iranian Polymer Journal, 2014. **23**(7): p. 531-545.
140. Endrodi, B., et al., *Fixation of laccase enzyme into polypyrrole, assisted by chemical interaction with modified magnetite nanoparticles: A facile route to synthesize stable electroactive bionanocomposite catalysts.* Electrochimica Acta, 2014. **122**: p. 282-288.
141. Nowicka, A.M., et al., *Polypyrrole-Au Nanoparticles Composite as Suitable Platform for DNA Biosensor with Electrochemical Impedance Spectroscopy Detection.* Electrochimica Acta, 2014. **140**: p. 65-71.
142. Ciobotaru, I.C., et al., *Embedding of IrQ(ppy)(2) organometallic compounds in polypyrrole conducting polymer for OLED's applications.* Synthetic Metals, 2014. **198**: p. 323-328.
143. Sadrolhosseini, A.R., et al., *Application of Conducting Polymer Layer for Measurement of Ag Nanoparticle Concentration Using Surface Plasmon Resonance.* Polymer-Plastics Technology and Engineering, 2014. **53**(5): p. 520-525.
144. Ruhparwar, A., et al., *Electrically Contractile Polymers Augment Right Ventricular Output in the Heart.* Artificial Organs, 2014. **38**(12): p. 1034-1039.
145. Jager, E.W.H., et al., *Biomedical applications of polypyrrole microactuators: From single-cell clinic to microrobots.* 1st Annual International Ieee-Embs Special Topic Conference on Microtechnologies in Medicine & Biology, Proceedings, 2000: p. 58-61.
146. Flamini, D.O., M. Saugo, and S.B. Saidman, *Electrodeposition of polypyrrole on Nitinol alloy in the presence of inhibitor ions for corrosion protection.* Corrosion Science, 2014. **81**: p. 36-44.
147. Kalendova, A., et al., *Anticorrosion efficiency of zinc-filled epoxy coatings containing conducting polymers and pigments.* Progress in Organic Coatings, 2015. **78**: p. 1-20.
148. Tonelli, D., et al., *A novel potentiometric sensor for L-ascorbic acid based on molecularly imprinted polypyrrole.* Electrochimica Acta, 2011. **56**(20): p. 7149-7154.
149. Ebarvia, B.S., S. Cabanilla, and F. Sevilla, *Biomimetic properties and surface studies of a piezoelectric caffeine sensor based on electro synthesized polypyrrole.* Talanta, 2005. **66**(1): p. 145-152.
150. Horemans, F., et al., *MIP-based sensor platforms for the detection of histamine in the nano- and micromolar range in aqueous media.* Sensors and Actuators B-Chemical, 2010. **148**(2): p. 392-398.
151. Piletsky, S.A., et al., *Recognition of ephedrine enantiomers by molecularly imprinted polymers designed using a computational approach.* Analyst, 2001. **126**(10): p. 1826-1830.
152. Jiang, M. and J. Wang, *Recognition and detection of oligonucleotides in the presence of chromosomal DNA based on entrapment within conducting-polymer networks.* Journal of Electroanalytical Chemistry, 2001. **500**(1-2): p. 584-589.
153. Szunerits, S., et al., *Comparison of different strategies on DNA chip fabrication and DNA-sensing: Optical and electrochemical approaches.* Electroanalysis, 2005. **17**(22): p. 2001-2017.

154. Booth, M.A., S. Harbison, and J. Travas-Sejdic, *Effects of Redox Couple on the Response of Polypyrrole-Based Electrochemical DNA Sensors.* Electroanalysis, 2012. **24**(6): p. 1311-1317.
155. Zhang, Z.H., et al., *Highly Sensitive Functionalized Conducting Copolypyrrole Film for DNA Sensing and Protein-resistant.* Chinese Journal of Chemistry, 2012. **30**(2): p. 259-266.
156. Ghanbari, K., S.Z. Bathaie, and M.F. Mousavi, *Electrochemically fabricated polypyrrole nanofiber-modified electrode as a new electrochemical DNA biosensor.* Biosensors & Bioelectronics, 2008. **23**(12): p. 1825-1831.
157. Ramanaviciene, A., A. Finkelsteinas, and A. Ramanavicius, *Basic electrochemistry meets nanotechnology: electrochemical preparation of artificial receptors based on a nanostructured conducting polymer, polypyrrole.* Journal of Chemical Education, 2006. **83**(8): p. 1212-1214.
158. Ozcan, L., M. Sahin, and Y. Sahin, *Electrochemical preparation of a molecularly imprinted polypyrrole-modified pencil graphite electrode for determination of ascorbic acid.* Sensors, 2008. **8**(9): p. 5792-5805.
159. Ozcan, L. and Y. Sahin, *Determination of paracetamol based on electropolymerized-molecularly imprinted polypyrrole modified pencil graphite electrode.* Sensors and Actuators B-Chemical, 2007. **127**(2): p. 362-369.
160. Ramanaviciene, A. and A. Ramanavicius, *Molecularly imprinted polypyrrole-based synthetic receptor for direct detection of bovine leukemia virus glycoproteins.* Biosensors & Bioelectronics, 2004. **20**(6): p. 1076-1082.
161. Castano, H., et al., *Polypyrrole thin films formed by admicellar polymerization support the osteogenic differentiation of mesenchymal stem cells.* Macromol Biosci, 2004. **4**(8): p. 785-94.
162. Henry, S.A. and J.L. Patton-Vogt, *Genetic Regulation of Phospholipid Metabolism: Yeast as a Model Eukaryote*, in *Progress in Nucleic Acid Research and Molecular Biology*, M. Kivie, Editor. 1998, Academic Press. p. 133-179.
163. Valimaa, A.L., et al., *Real-time Monitoring of Non-specific Toxicity Using a Saccharomyces cerevisiae Reporter System.* Sensors, 2008. **8**(10): p. 6433-6447.
164. Gonchar, M., et al., *New Approaches for Formaldehyde Assay Based on Use of Enzymatic Kit or pH-Sensitive Field Effect Transistor Biosensor*, in *Environmental Biotechnology*, M. Moo-Young, W.A. Anderson, and A.M. Chakrabarty, Editors. 1996, Springer Netherlands. p. 689-700.
165. Endo, H., et al., *Microbial Biosensor System for Rapid Determination of Vitamin B6.* Journal of Food Science, 1995. **60**(3): p. 554-557.
166. Hollis, R.P., K. Killham, and L.A. Glover, *Design and Application of a Biosensor for Monitoring Toxicity of Compounds to Eukaryotes.* Applied and Environmental Microbiology, 2000. **66**(4): p. 1676-1679.
167. Ikebukuro, K., et al., *Flow-type cyanide sensor using an immobilized microorganism.* Electroanalysis, 1996. **8**(10): p. 876-879.
168. F, N. and M.-R. LA, *A microbial biosensor for the microscale measurement of bioavailable organic carbon in oxic sediments.* Marine Ecology Progress Series, 1997. **147**: p. 295-300.
169. Tag, K., et al., *Measurement of biodegradable substances with a mycelia-sensor based on the salt tolerant yeast Arxula adeninivorans LS3.* Sensors and Actuators B: Chemical, 2000. **67**(1–2): p. 142-148.
170. Svitel, J., O. Curilla, and J. Tkac, *Microbial cell-based biosensor for sensing glucose, sucrose or lactose.* Biotechnology and Applied Biochemistry, 1998. **27**: p. 153-158.
171. Chen, D., et al., *A BOD biosensor based on a microorganism immobilized on an Al2O3 sol-gel matrix.* Anal Bioanal Chem, 2002. **372**(5-6): p. 737-9.
172. Trosok, S.P., B.T. Driscoll, and J.H. Luong, *Mediated microbial biosensor using a novel yeast strain for wastewater BOD measurement.* Appl Microbiol Biotechnol, 2001. **56**(3-4): p. 550-4.

173. Rotariu, L., C. Bala, and V. Magearu, *Yeast cells sucrose biosensor based on a potentiometric oxygen electrode.* Analytica Chimica Acta, 2002. **458**(1): p. 215-222.
174. Ikebukuro, K., et al., *Microbial cyanide sensor for monitoring river water.* J Biotechnol, 1996. **48**(1-2): p. 73-80.
175. Nakanishi, K., K. Ikebukuro, and I. Karube, *Determination of cyanide using a microbial sensor.* Appl Biochem Biotechnol, 1996. **60**(2): p. 97-106.
176. Lehmann, M., et al., *Amperometric measurement of copper ions with a deputy substrate using a novel Saccharomyces cerevisiae sensor.* Biosensors & Bioelectronics, 2000. **15**(3-4): p. 211-219.
177. Selvakumar, R., et al., *Screening of silver nanoparticles containing carbonized yeast cells for adsorption of few long-lived active radionuclides.* Journal of Radioanalytical and Nuclear Chemistry, 2011. **288**(2): p. 629-633.
178. Lauterbach, T., et al., *Weak Glycolipid Binding of a Microdomain-Tracer Peptide Correlates with Aggregation and Slow Diffusion on Cell Membranes.* Plos One, 2012. **7**(12).
179. Cheng, N.C., et al., *Cell death detection by quantitative three-dimensional single-cell tomography.* Biomedical Optics Express, 2012. **3**(9): p. 2111-2120.
180. Bago, J.R., et al., *In Vivo Bioluminescence Imaging of Cell Differentiation in Biomaterials: A Platform for Scaffold Development.* Tissue Engineering Part A, 2013. **19**(5-6): p. 593-603.
181. Murata, K., et al., *Whole-cell imaging of the budding yeast Saccharomyces cerevisiae by high-voltage scanning transmission electron tomography.* Ultramicroscopy, 2014. **146**(0): p. 39-45.
182. Antonio, K.A. and Z.D. Schultz, *Advances in Biomedical Raman Microscopy.* Analytical Chemistry, 2014. **86**(1): p. 30-46.
183. Baniukevic, J., et al., *Magnetic gold nanoparticles in SERS-based sandwich immunoassay for antigen detection by well oriented antibodies.* Biosensors & Bioelectronics, 2013. **43**: p. 281-288.
184. Matousek, P. and N. Stone, *Recent advances in the development of Raman spectroscopy for deep non-invasive medical diagnosis.* Journal of Biophotonics, 2013. **6**(1): p. 7-19.
185. Ferrari, A.C. and D.M. Basko, *Raman spectroscopy as a versatile tool for studying the properties of graphene.* Nature nanotechnology, 2013. **8**(4): p. 235-246.
186. Huang, C.K., H. Hamaguchi, and S. Shigeto, *In vivo multimode Raman imaging reveals concerted molecular composition and distribution changes during yeast cell cycle.* Chemical Communications, 2011. **47**(33): p. 9423-9425.
187. Huang, Y.S., et al., *Molecular-level investigation of the structure, transformation, and bioactivity of single living fission yeast cells by time- and space-resolved Raman spectroscopy.* Biochemistry, 2005. **44**(30): p. 10009-10019.
188. Matthaus, C., et al., *Label-free detection of mitochondrial distribution in cells by nonresonant Raman microspectroscopy.* Biophysical Journal, 2007. **93**(2): p. 668-673.
189. Notingher, I., et al., *Spectroscopic study of human lung epithelial cells (A549) in culture: Living cells versus dead cells.* Biopolymers, 2003. **72**(4): p. 230-240.
190. Chiu, L., M. Ando, and H. Hamaguchi, *Study of the 'Raman spectroscopic signature of life' in mitochondria isolated from budding yeast.* Journal of Raman Spectroscopy, 2010. **41**(1): p. 2-3.
191. Onogi, C. and H.O. Hamaguchi, *Photobleaching of the "Raman Spectroscopic Signature of Life" and Mitochondrial Activity in Rho(-) Budding Yeast Cells.* Journal of Physical Chemistry B, 2009. **113**(31): p. 10942-10945.
192. Brauchle, E., et al., *Cell death stages in single apoptotic and necrotic cells monitored by Raman microspectroscopy.* Sci. Rep., 2014. **4**.
193. Huang, Y.S., et al., *Molecular-level pursuit of yeast mitosis by time- and space-resolved Raman spectroscopy.* Journal of Raman Spectroscopy, 2003. **34**(1): p. 1-3.
194. Cheng, H.W., et al., *Surface-enhanced Raman spectroscopic detection of Bacillus subtilis spores using gold nanoparticle based substrates.* Analytica Chimica Acta, 2011. **707**(1): p. 155-163.

195. Alexander, K.D. and Z.D. Schultz, *Tip-Enhanced Raman Detection of Antibody Conjugated Nanoparticles on Cellular Membranes.* Analytical Chemistry, 2012. **84**(17): p. 7408-7414.
196. Deckert-Gaudig, T., E. Bailo, and V. Deckert, *Perspectives for spatially resolved molecular spectroscopy - Raman on the nanometer scale*. Journal of Biophotonics, 2008. **1**(5): p. 377-389.
197. Rosch, P., et al., *Raman spectroscopic identification of single yeast cells.* Journal of Raman Spectroscopy, 2005. **36**(5): p. 377-379.
198. Kniggendorf, A.K., T.W. Gaul, and M. Meinhardt-Wollweber, *Effects of Ethanol, Formaldehyde, and Gentle Heat Fixation in Confocal Resonance Raman Microscopy of Purple NonSulfur Bacteria.* Microscopy Research and Technique, 2011. **74**(2): p. 177-183.
199. Draux, F., et al., *Raman spectral imaging of single living cancer cells: a preliminary study.* Analyst, 2009. **134**(3): p. 542-548.
200. Novikov, S.M., et al., *Raman microscopy of individual living human embryonic stem cells.* Biophotonics: Photonic Solutions for Better Health Care Ii, 2010. **7715**.
201. German, N., et al., *Glucose biosensor based on glucose oxidase and gold nanoparticles of different sizes covered by polypyrrole layer.* Colloids and Surfaces a-Physicochemical and Engineering Aspects, 2012. **413**: p. 224-230.
202. Ratner, B.D., A.S. Hoffman, F.J. Schoen, J.E. Lemons (Eds), *Biomaterials Sciences: An Introduction to Materials in Medicine*. 2nd ed. 2004, Amsterdam: Elsevier.
203. Karadeniz, H., et al., *Disposable electrochemical biosensor for the detection of the interaction between DNA and lycorine based on guanine and adenine signals.* Journal of Pharmaceutical and Biomedical Analysis, 2003. **33**(2): p. 295-302.
204. Maquelin, K., et al., *Identification of medically relevant microorganisms by vibrational spectroscopy.* Journal of Microbiological Methods, 2002. **51**(3): p. 255-271.
205. Kara, P., et al., *Electrochemical genoassay design for allele-specific detection of toll-like receptor-2 gene polymorphism.* Electroanalysis, 2007. **19**(18): p. 1875-1882.
206. Coplen, T.B., et al., *New guidelines for δ 13C measurements.* Analytical Chemistry, 2006. **78**(7): p. 2439-2441.
207. Polyanskiy, M., *Refractive index database*, 2015, RefractiveIndex.
208. *Series Page*, in *International Review of Cell and Molecular Biology*, H. Ronald and W.J. Kwang, Editors. 2014, Academic Press. p. ii.
209. Liang, X.J., et al., *Determining refractive index of single living cell using an integrated microchip.* Sensors and Actuators A: Physical, 2007. **133**(2): p. 349-354.
210. Oztekin, Y., et al., *Direct electron transfer from glucose oxidase immobilized on polyphenanthroline-modified glassy carbon electrode.* Biosensors & Bioelectronics, 2011. **26**(5): p. 2541-2546.
211. Lu, H., et al., *Pyridine-Coated Lead Sulfide Quantum Dots for Polymer Hybrid Photovoltaic Devices.* Advanced Science Letters, 2010. **3**(2): p. 101-109.
212. Ramanavicius, A., et al., *Stabilization of (CdSe)ZnS quantum dots with polypyrrole formed by UV/VIS irradiation initiated polymerization.* J Nanosci Nanotechnol, 2009. **9**(3): p. 1909-15.
213. Shi, J.H., et al., *One-Pot Synthesis and Electrical Characterization of Monodisperse Solid Polyaniline Sub-Microspheres.* Advanced Science Letters, 2011. **4**(2): p. 449-457.
214. Ren, Q., et al., *Interface synthesis, assembly and characterization of close-packed monolayer of prussian blue/polypyrrole nanocomposites.* J Nanosci Nanotechnol, 2012. **12**(3): p. 2049-53.
215. Ramanaviciene, A. and A. Ramanavicius, *Pulsed amperometric detection of DNA with an ssDNA/polypyrrole-modified electrode.* Analytical and Bioanalytical Chemistry, 2004. **379**(2): p. 287-293.
216. Abdi, M.M., et al., *Physical, optical, and electrical properties of a new conducting polymer.* Journal of Materials Science, 2009. **44**(14): p. 3682-3686.

217. Garfias-Garcia, E., et al., *Mechanism and kinetics of the electrochemical formation of polypyrrole under forced convection conditions.* Journal of Electroanalytical Chemistry, 2008. **613**(1): p. 67-79.
218. Chen, W., et al., *In situ AFM study of electrochemical synthesis of polypyrrole/Au nanocomposite.* Electrochemistry Communications, 2008. **10**(9): p. 1340-1343.
219. Martin, S.J., V.E. Granstaff, and G.C. Frye, *Characterization of a Quartz Crystal Microbalance with Simultaneous Mass and Liquid Loading.* Analytical Chemistry, 1991. **63**(20): p. 2272-2281.
220. Muramatsu, H., E. Tamiya, and I. Karube, *Computation of equivalent circuit parameters of quartz crystals in contact with liquids and study of liquid properties.* Analytical Chemistry, 1988. **60**(19): p. 2142-2146.
221. Christie, J.H., G. Laurer, and R.A. Osteryoung, *Measurement of charge passed following application of a potential step-application to the study of electrode reactions and adsorption.* Journal of Electroanalytical Chemistry (1959), 1964. **7**(1): p. 60-72.
222. Daniel, M.C. and D. Astruc, *Gold nanoparticles: Assembly, supramolecular chemistry, quantum-size-related properties, and applications toward biology, catalysis, and nanotechnology*. Chemical Reviews, 2004. **104**(1): p. 293-346.
223. Shumyantseva, V., et al., *Electrochemical Methods for the Investigation of Bioaffinity Interactions Based on Gold Nanoparticles Modified Sensors.* Electroanalysis, 2009. **21**(3-5): p. 530-535.
224. Nicol, M.J., *The anodic behaviour of gold. Part II — Oxidation in alkaline solutions.* Gold Bulletin, 1980. **13**(3): p. 105-106.
225. Nicol, M.J., *The anodic behaviour of gold Part I — Oxidation in acidic solutions.* Gold Bulletin, 1980. **13**(2): p. 46-55, DOI: 10.1007/BF03215452.
226. Senanayake, G., *Kinetic model for anodic oxidation of gold in thiosulfate media based on the adsorption of MS2O3- ion-pair*. Hydrometallurgy, 2005. **76**(3-4): p. 233-238.
227. Rahman, S.U., M.A. Abul-Hamayel, and B.J.A. Aleem, *Electrochemically synthesized polypyrrole films as primer for protective coatings on carbon steel.* Surface & Coatings Technology, 2006. **200**(9): p. 2948-2954.
228. Rahman, S.U., *Corrosion protection of steel by catalyzed polypyrrole films.* Surface & Coatings Technology, 2011. **205**(8-9): p. 3035-3042.
229. Machnikova, E., et al., *Corrosion study of PVD coatings and conductive polymer deposited on mild steel 14 Part I: Polypyrrole.* Surface & Coatings Technology, 2008. **202**(8): p. 1543-1550.
230. Idla, K., O. Inganas, and M. Strandberg, *Good adhesion between chemically oxidised titanium and electrochemically deposited polypyrrole.* Electrochimica Acta, 2000. **45**(13): p. 2121-2130.
231. Li, C.M., et al., *Electrochemical thin film deposition of polypyrrole on different substrates.* Surface & Coatings Technology, 2005. **198**(1-3): p. 474-477.
232. Wang, J., et al., *DNA electrochemical biosensors for environmental monitoring. A review.* Analytica Chimica Acta, 1997. **347**(1–2): p. 1-8.
233. Wang, J., G. Rivas, and X.H. Cai, *Screen-printed electrochemical hybridization biosensor for the detection of DNA sequences from the Escherichia coli pathogen.* Electroanalysis, 1997. **9**(5): p. 395-398.
234. Prance, A., et al., *Biosensors for the Detection of DNA Damage by Toxicants*, in *Chemical Sensors 9 -and- Mems/Nems 9*, G. Hunter, et al., Editors. 2010, Electrochemical Soc Inc: Pennington. p. 3-15.
235. Stobiecka, M., et al., *Novel DNA-Hybridization Biosensors for Studies of DNA Underwinding Caused by Herbicides and Pesticides*, in *Electrochemical Nano/Bio Sensors 2*, B. Chin, Editor. 2010, Electrochemical Soc Inc: Pennington. p. 1-12.
236. Wang, J., et al., *Stripping potentiometric transduction of DNA hybridization processes.* Analytica Chimica Acta, 1996. **326**(1–3): p. 141-147.

237. Jin, J.H., E.C. Alocilja, and D.L. Grooms, *Fabrication and electroanalytical characterization of label-free DNA sensor based on direct electropolymerization of pyrrole on p-type porous silicon substrates.* Journal of Porous Materials, 2010. **17**(2): p. 169-176.
238. Riccardi, C.D., et al., *Label-free DNA detection based on modified conducting polypyrrole films at microelectrodes.* Analytical Chemistry, 2006. **78**(4): p. 1139-1145.
239. Eftekhari, A. and I. Ahmadi, *Electrodeposition of smooth and adherent film of polypyrrole on lead electrode.* Progress in Organic Coatings, 2006. **57**(4): p. 371-375.
240. Ozsoz, M., et al., *Electrochemical genosensor based on colloidal gold nanoparticles for the detection of Factor V Leiden mutation using disposable pencil graphite electrodes.* Analytical Chemistry, 2003. **75**(9): p. 2181-2187.
241. Ozcan, A., et al., *Electrochemical oxidation of ds-DNA on polypyrrole nanofiber modified pencil graphite electrode.* Electroanalysis, 2007. **19**(21): p. 2208-2216.
242. Özcan, L., M. Sahin, and Y. Sahin, *Electrochemical Preparation of a Molecularly Imprinted Polypyrrole-modified Pencil Graphite Electrode for Determination of Ascorbic Acid.* Sensors, 2008. **8**(9): p. 5792-5805.
243. Marx, K.A., *Quartz crystal microbalance: A useful tool for studying thin polymer films and complex biomolecular systems at the solution-surface interface.* Biomacromolecules, 2003. **4**(5): p. 1099-1120.
244. Feldötö, Z., T. Pettersson, and A. Dėdinaitė, *Mucin−Electrolyte Interactions at the Solid−Liquid Interface Probed by QCM-D.* Langmuir, 2008. **24**(7): p. 3348-3357.
245. Syritski, V., et al., *Electrosynthesized molecularly imprinted polypyrrole films for enantioselective recognition of L-aspartic acid.* Electrochimica Acta, 2008. **53**(6): p. 2729-2736.
246. Shiigi, H., et al., *Molecular Recognition for Bile Acids Using a Molecularly Imprinted Overoxidized Polypyrrole Film.* Journal of The Electrochemical Society, 2005. **152**(8): p. H129-H134.
247. Shiigi, H., et al., *Fabrication Process and Characterization of a Novel Structural Isomer Sensor: Molecularly Imprinted Overoxidized Polypyrrole Film.* Electrochemical and Solid-State Letters, 2003. **6**(1): p. H1-H3.
248. Chen, Z., et al., *Enantioselective uptake of amino acid with overoxidized polypyrrole colloid templated with L-lactate.* Analyst, 2000. **125**(12): p. 2249-54.
249. Deore, B., Z. Chen, and T. Nagaoka, *Potential-induced enantioselective uptake of amino acid into molecularly imprinted overoxidized polypyrrole.* Anal Chem, 2000. **72**(17): p. 3989-94.
250. Segawa, H., T. Shimidzu, and K. Honda, *A novel photo-sensitized polymerization of pyrrole.* Journal of the Chemical Society, Chemical Communications, 1989(2): p. 132-133.
251. Sargent, A., et al., *The electrochemistry of antibody-modified conducting polymer electrodes.* J Electroanal Chem, 1999. **470**(2): p. 144-156.
252. Kern, J.-M. and J.-P. Sauvage, *Photochemical deposition of electrically conducting polypyrrole.* Journal of the Chemical Society, Chemical Communications, 1989(10): p. 657-658.
253. Wilson, J., et al., *Polypyrrole-polyaniline-Au (PPy-PANi-Au) nano composite films for label-free electrochemical DNA sensing.* Sensors and Actuators B-Chemical, 2012. **171**: p. 216-222.
254. Njagi, J. and S. Andreescu, *Stable enzyme biosensors based on chemically synthesized Au-polypyrrole nanocomposites.* Biosensors & Bioelectronics, 2007. **23**(2): p. 168-175.
255. German, N., et al., *Gold nanoparticles and polypyrrole for glucose biosensor design.* 26th European Conference on Solid-State Transducers, Eurosensor 2012, 2012. **47**: p. 482-485.
256. Babu, T.G.S., et al., *Gold nanoparticle-polypyrrole composite modified TiO2 nanotube array electrode for the amperometric sensing of ascorbic acid.* Journal of Applied Electrochemistry, 2012. **42**(6): p. 427-434.

257. Haghighi, B. and M.A. Tabrizi, *Direct electron transfer from glucose oxidase immobilized on an overoxidized polypyrrole film decorated with Au nanoparticles.* Colloids and Surfaces B-Biointerfaces, 2013. **103**: p. 566-571.
258. Kesik, M., et al., *A functional immobilization matrix based on a conducting polymer and functionalized gold nanoparticles: Synthesis and its application as an amperometric glucose biosensor.* Polymer, 2013. **54**(17): p. 4463-4471.
259. Qu, L., et al. *Electrochemical Synthesis of Gold Nanoparticles in Polypyrrole for Antibody Immobilization*. in *2009 4th Ieee International Conference on Nano/Micro Engineered and Molecular Systems, Vols 1 and 2*. 2009. Shenzhen IEEE Xplore.
260. Li, J., et al., *Coating Urchinlike Gold Nanoparticles with Polypyrrole Thin Shells To Produce Photothermal Agents with High Stability and Photothermal Transduction Efficiency.* Langmuir, 2013. **29**(23): p. 7102-7110.
261. Vijaya Sarathy, K., et al., *Novel fluorescence and morphological structures in gold nanoparticle–polyoctylthiophene based thin films.* Chemical Physics Letters, 2000. **318**(6): p. 543-548.
262. Hertel, T., et al., *Ultrafast electron dynamics at Cu(111): Response of an electron gas to optical excitation.* Phys Rev Lett, 1996. **76**(3): p. 535-538.
263. Shin, H.J., et al., *Comparative investigation of energy relaxation dynamics of gold nanoparticles and gold-polypyrrole encapsulated nanoparticles.* Journal of Physical Chemistry B, 2003. **107**(20): p. 4699-4704.
264. Millstone, J.E., et al., *Observation of a quadrupole plasmon mode for a colloidal solution of gold nanoprisms.* Journal of the American Chemical Society, 2005. **127**(15): p. 5312-5313.
265. Selvan, S.T. and M. Nogami, *Novel gold-polypyrrole anisotropic colloids: a TEM investigation.* Journal of Materials Science Letters, 1998. **17**(16): p. 1385-1388.
266. Cosnier, S., et al., *A glucose biosensor based on enzyme entrapment within polypyrrole films electrodeposited on mesoporous titanium dioxide.* Journal of Electroanalytical Chemistry, 1999. **469**(2): p. 176-181.
267. Doretti, L., et al., *PEG-modified glucose oxidase immobilized on a PVA cryogel membrane for amperometric biosensor applications.* Talanta, 1998. **45**(5): p. 891-898.
268. Chen, S.J., W. Chen, and G. Xue, *Electrogeneration of polypyrrole/alginate films for immobilization of glucose oxidase*. Macromolecular Bioscience, 2008. **8**(6): p. 478-483.
269. Olea, D., O. Viratelle, and C. Faure, *Polypyrrole-glucose oxidase biosensor - Effect of enzyme encapsulation in multilamellar vesicles on analytical properties.* Biosensors & Bioelectronics, 2008. **23**(6): p. 788-794.
270. Dumont, J. and G. Fortier, *Behavior of glucose oxidase immobilized in various electropolymerized thin films.* Biotechnology and Bioengineering, 1996. **49**(5): p. 544-552.
271. Street, G.B., et al., *Preparation and characterization of neutral and oxidized polypyrrole films.* Molecular Crystals and Liquid Crystals, 1982. **83**(1): p. 253-264.
272. Raba, J. and H.A. Mottola, *Glucose Oxidase as an Analytical Reagent.* Critical Reviews in Analytical Chemistry, 1995. **25**(1): p. 1-42.
273. Wilkening, S., F. Stahl, and A. Bader, *Comparison of primary human hepatocytes and hepatoma cell line Hepg2 with regard to their biotransformation properties.* Drug Metab Dispos, 2003. **31**(8): p. 1035-42.
274. Soleimani, M. and S. Nadri, *A protocol for isolation and culture of mesenchymal stem cells from mouse bone marrow*. Nat Protoc, 2009. **4**(1): p. 102-6.
275. Lakard, B., et al., *Effect of ultrasounds on the electrochemical synthesis of polypyrrole, application to the adhesion and growth of biological cells.* Bioelectrochemistry, 2009. **75**(2): p. 148-57.
276. Ateh, D.D., H.A. Navsaria, and P. Vadgama, *Polypyrrole-based conducting polymers and interactions with biological tissues.* J R Soc Interface, 2006. **3**(11): p. 741-52.
277. Aznar-Cervantes, S., et al., *Fabrication of conductive electrospun silk fibroin scaffolds by coating with polypyrrole for biomedical applications.* Bioelectrochemistry, 2012. **85**: p. 36-43.

278. Ring, J., et al., *The metabolism beyond programmed cell death in yeast.* Experimental cell research, 2012. **318**(11): p. 1193-1200.
279. Ocampo, A., et al., *Mitochondrial Respiratory Thresholds Regulate Yeast Chronological Life Span and its Extension by Caloric Restriction.* Cell Metabolism, 2012. **16**(1): p. 55-67.
280. Fontana, L., L. Partridge, and V.D. Longo, *Extending Healthy Life Span-From Yeast to Humans.* Science, 2010. **328**(5976): p. 321-326.
281. Xie, C.G., et al., *Study of dynamical process of heat denaturation in optically trapped single microorganisms by near-infrared Raman spectroscopy.* Journal of Applied Physics, 2003. **94**(9): p. 6138-6142.
282. Rosch, P., et al., *Identification of single eukaryotic cells with micro-Raman spectroscopy.* Biopolymers, 2006. **82**(4): p. 312-316.
283. Zinin, P.V., et al., *Visible, near-infrared, and ultraviolet laser-excited Raman spectroscopy of the monocytes/macrophages (U937) cells.* Journal of Raman Spectroscopy, 2010. **41**(3): p. 268-274.
284. Neugebauer, U., et al., *Towards a detailed understanding of bacterial metabolism - Spectroscopic characterization of Staphylococcus epidermidis.* Chemphyschem, 2007. **8**(1): p. 124-137.
285. Bhowmick, T.K., et al., *A study of the effect of JB particles on Saccharomyces cerevisiae (yeast) cells by Raman spectroscopy.* Journal of Raman Spectroscopy, 2008. **39**(12): p. 1859-1868.
286. Edwards, H.G.M., et al., *Fourier-Transform Raman-Spectroscopic Study of Fungi.* Journal of Raman Spectroscopy, 1995. **26**(8-9): p. 911-916.
287. Wood, B.R. and D. McNaughton, *Raman excitation wavelength investigation of single red blood cells in vivo.* Journal of Raman Spectroscopy, 2002. **33**(7): p. 517-523.
288. Socrates, G., *Infrared and Raman Characteristic Group Frequencies*. 2001, Chichester: John Wiley & Sons Ltd.
289. Luo, S.C., et al., *Nanofabricated SERS-active substrates for single-molecule to virus detection in vitro: A review.* Biosensors & Bioelectronics, 2014. **61**: p. 232-240.
290. Kleinman, S.L., et al., *Creating, characterizing, and controlling chemistry with SERS hot spots.* Physical Chemistry Chemical Physics, 2013. **15**(1): p. 21-36.
291. Kalbacova, J., et al., *Chemical stability of plasmon-active silver tips for tip-enhanced Raman spectroscopy.* Nanospectroscopy, 2015. **1**(1): p. 2300-3537.
292. Rai, M., A. Yadav, and A. Gade, *Silver nanoparticles as a new generation of antimicrobials.* Biotechnology Advances, 2009. **27**(1): p. 76-83.
293. Nosoh, Y., *Absorption spectrum of actively respiring yeast cells.* Archives of Biochemistry and Biophysics, 1964. **105**(2): p. 439-445.
294. Ganguli, R. and B.S. Dunn, *Kinetics of Anode Reactions for a Yeast-Catalysed Microbial Fuel Cell.* Fuel Cells, 2009. **9**(1): p. 44-52.
295. Rawson, F.J., A.J. Downard, and K.H. Baronian, *Electrochemical detection of intracellular and cell membrane redox systems in Saccharomyces cerevisiae.* Scientific Reports, 2014. **4**: p. 9.
296. Asami, K., T. Hanai, and N. Koizumi, *Dielectric properties of yeast cells.* The Journal of Membrane Biology, 1976. **28**(1): p. 169-180.